A PETROLOGIC AND GEOCHEMICAL STUDY OF GRANOPHYRIC GRANITE IN THE ROOF OF THE KEWEENAWAN DULUTH COMPLEX, EAGLE MOUNTAIN, COOK COUNTY, MINNESOTA

A Thesis
Submitted to the Faculty of the Graduate School
of the University of Minnesota

By
Nancy Nelson

In Partial Fulfillment of the Requirements for
the Degree of
Master of Science

April, 1991

ABSTRACT

Field work in the roof zone of the Keweenawan (1.1 b.y.) Duluth Complex in the area of Eagle Mountain, Cook County, Minnesota, resulted in the identification of eight major rock units. These are metabasalt, metagabbro, ophitic diabase, syenogabbro, ferrodiorite, rhyolite, and two distinct granophyre units.

On the basis of field relations and petrography, the rhyolite appears to be the oldest unit in the area and to have formed the roof rocks below which the intrusive units were emplaced. The metabasalt unit is composed of xenoliths of basalt that were carried and slightly metamorphosed by the magma now represented by the metagabbro unit. This metagabbro was emplaced beneath the rhyolite and later slightly metamorphosed by the intrusion of the magma that formed the Eagle Mountain granophyre. The Eagle Mountain granophyre shares a gradational contact with the ferrodiorite, and these two units appear to be genetically related. The relationship of the syenogabbro to other units is unknown. The miarolitic granophyre was intruded beneath the rhyolite, but its age relation to other units is ambiguous. The ophitic diabase crosscuts other units and appears to be the youngest unit in the field area.

The Eagle Mountain granophyre (EMG) is red-brown, fine-grained, porphyritic, and locally granophyric and spherulitic. It is composed of 60-75% feldspars, 20-30% quartz, 5-10% ferroaugite and hornblende, and <5% Fe-Ti oxides. Probe analysis shows average compositions of $An_{40}Ab_{52}Or_8$ for andesine phenocrysts and $Mg_{16}Fe_{41}Ca_{43}$ for ferroaugite phenocrysts. Chemically the EMG contains 69-71 wt% SiO_2, 1.4-1.8 wt% CaO, and $K_2O/Na_2O \approx 1.1$.

The miarolitic granophyre (MG) is brick-red, medium-grained, and contains approximately 5% miarolitic cavities. It is composed almost entirely of feldspar and quartz in well-developed granophyric intergrowths that radiate outward from phenocrysts of nearly pure albite ($An_2Ab_{95}Or_3$) and pure orthoclase ($An_0Ab_5Or_{95}$). Chemically the MG contains 73-74 wt% SiO_2, 0.2-0.4 wt% CaO, and $K_2O/Na_2O \approx 2.3$. The MG has an unusual REE pattern, with HREEs enriched over LREEs.

Mass balance calculations and trace element models support formation of the EMG by fractional crystallization of a tholeiitic parent liquid comparable to local basaltic andesites. Chemical and mineralogical evidence also supports silicate liquid immiscibility as a possible fractionation mechanism. For the formation of the MG, mass balance calculations and trace element models do not clearly support either fractional crystallization or partial melting as a mode of origin. This unit may have undergone deuteric or metasomatic alteration that makes modeling impossible.

Based on the estimated total thickness of the overlying volcanic pile, the granophyres crystallized at a maximum pressure of 2.0 kb; pressure could have been much lower, depending on the thickness of the volcanic pile at the time of intrusion. Based on experimental work on the granite system, both units crystallized at temperatures near the 990° C thermal minimum for the Ab-Or-Qz system at 1 kb pressure.

ACKNOWLEDGEMENTS

Financial assistance for this study was provided by the Minnesota Geological Survey, the University of Minnesota Graduate School, and Sigma Xi, The Scientific Research Society. Thanks go to committee members John Green, Penny Morton, James Grant, and J. C. Nichol of UMD for their advice and assistance, to Jon Berg and Neil Dickey of Northern Illinois University for making the XRF analyses possible, to Jayne Reichhoff and Mark Severson of NRRI for microprobe support, to Jim Miller of the MGS for inspiration, to Eric Jerde of UCLA for REE analysis and field assistance, and to Tracey Felger of UMD for field assistance and a willing ear.

TABLE OF CONTENTS

Abstract. i

Acknowledgements. ii

Table of Contents. iii

Introduction. 1
Location 3
Regional Geology. 3
Previous Work. 6
Methods. 11

Lithology and Petrography. 12
Introduction. 12
Field Relations. 13
Description of Units. 20
Syenogabbro. 20
Ferrodiorite. 23
Eagle Mountain Granophyre. 26
Metagabbro. 34
Metabasalt. 36
Miarolitic Granophyre. 38
Rhyolite. 42
Ophitic Diabase. 44

Geochemistry. 47
Introduction. 47
Description of Units. 52
Metabasalt and Metagabbro. 52
Ophitic Diabase. 53
Syenogabbro and Ferrodiorite. 53
Rhyolite, Eagle Mountain Granophyre,
and Miarolitic Granophyre. 54
Comparison with A-type Granites. 57

Petrogenesis. 63
Introduction. 63
Fractional Crystallization vs. Partial Melting. 65
Variation Diagrams. 65
Mass Balance Calculations. 72
Trace Element Modeling. 78
Silicate Liquid Immiscibility. 85
Physical Conditions of Crystallization. 90
Pressure. 90
Granite Phase Diagram. 90
Spherulites. 92

Summary and Conclusions. 94

References. 99

Appendix I: Whole Rock Analyses. 107

Appendix II: CIPW Norms. 113

Appendix III: Mineral Chemistry. 116

Appendix IV: Mass Balance Calculations. 142

Appendix V: Distribution Coefficients. 148

FIGURES

Fig. 1. Location map. 2

Fig. 2. Eagle Mountain topographic quadrangle. 4

Fig. 3. Bedrock geology, Eagle Mountain area. 13

Fig. 4. Cross-section, Eagle Mountain area. 15

Fig. 5. Sample locations. 16

Fig. 6. Feldspar compositions. 17

Fig. 7. Pyroxene and olivine compositions. 18

Fig. 8. Oxide compositions. 19

Fig. 9. Photo of cut slab of syenogabbro. 21

Fig. 10. Photo of thin section of ferrodiorite. 24

Fig. 11. Photo of thin section of Eagle Mountain granophyre. 28

Fig. 12. Photomicrograph of andesine phenocryst. 30

Fig. 13. Photomicrograph of spherulite 31

Fig. 14. Photomicrograph of granophyric texture. 33

Fig. 15. Photomicrograph of granophyric texture. 40

Fig. 16. Photo of entire thin section of rhyolite. 43

Fig. 17. A=AFM diagram; B=Jensen cation plot. 51

Fig. 18. REE plot for metabasalt and metagabbro. 52

Fig. 19. REE plot for ophitic diabase. 53

Fig. 20. REE plot for syenogabbro. 54

Fig. 21. REE plot for granophyres and rhyolite. 55

Fig. 22. Comparison of chemistry of granophyre units. 57

Fig. 23. Ga/Al ratios for A-type granites. 59

Fig. 24. Granite discrimination diagrams. 61

Fig. 25. Major elements vs. SiO_2 for Eagle Mountain units. 67

Fig. 26. Compatible and incompatible elements vs. SiO_2. 69

Fig. 27. Ratios of incompatible elements. 70

Fig. 28. REE plot for all Eagle Mountain units. 71

Fig. 29. Plot illustrating liquid immiscibility. 89

Fig. 30. Granite phase diagram. 92

TABLES

Table 1 List of analyzed samples. 48

Table 2 Average compositions of units. 49

Table 3 CIPW norms for average compositions. 50

Table 4 Compositions of NSVG andesites and a hypothetical liquid. 75

Table 5 Results of trace element modeling of fractional crystallization as a mode of formation of Eagle Mountain granophyre. 80

Table 6 Results of trace element modeling of fractional crystallization as a mode of formation of miarolitic granophyre. 81

Table 7 Results of trace element modeling of partial melting as a mode of formation of miarolitic granophyre. 83

INTRODUCTION

The Keweenawan Duluth Complex of northeastern Minnesota is a large intrusive body that was emplaced about 1.1 billion years ago during a major episode of continental rifting (Green, 1972; Phinney, 1972; Weiblen and Morey, 1980; Green, 1983). The complex is primarily mafic, consisting of an early anorthositic series and a later, layered troctolitic series (Taylor, 1964; Weiblen and Morey, 1980; Weiblen, 1982). Felsic rocks form a discontinuous zone near the roof of the complex; rocks of intermediate composition are relatively rare.

Within the zone of felsic rocks, granophyric granite is the most common rock type. It is characterized by its brick-red color and granophyric intergrowths; the granite is known locally as "red rock" or granophyre. Although the origin of the Keweenawan granophyre is a question that has intrigued geologists for nearly 100 years, it has been studied only in the Pigeon Point Sill, the Beaver Bay Complex, and in the Duluth area. Little work has been done in Cook County where the Duluth Complex divides into two major sills with a much larger proportion of granophyre than in other areas (Fig. 1). Eagle Mountain, a prominent knob of granophyre that forms the highest elevation in Minnesota, lies in the southern half of T63N, R2W where two belts of granophyre, each nearly 2 km wide, are separated by a tongue of gabbro. The belt that includes Eagle Mountain continues for about 55 km along strike. For this reason Eagle Mountain was chosen as a field area for this study.

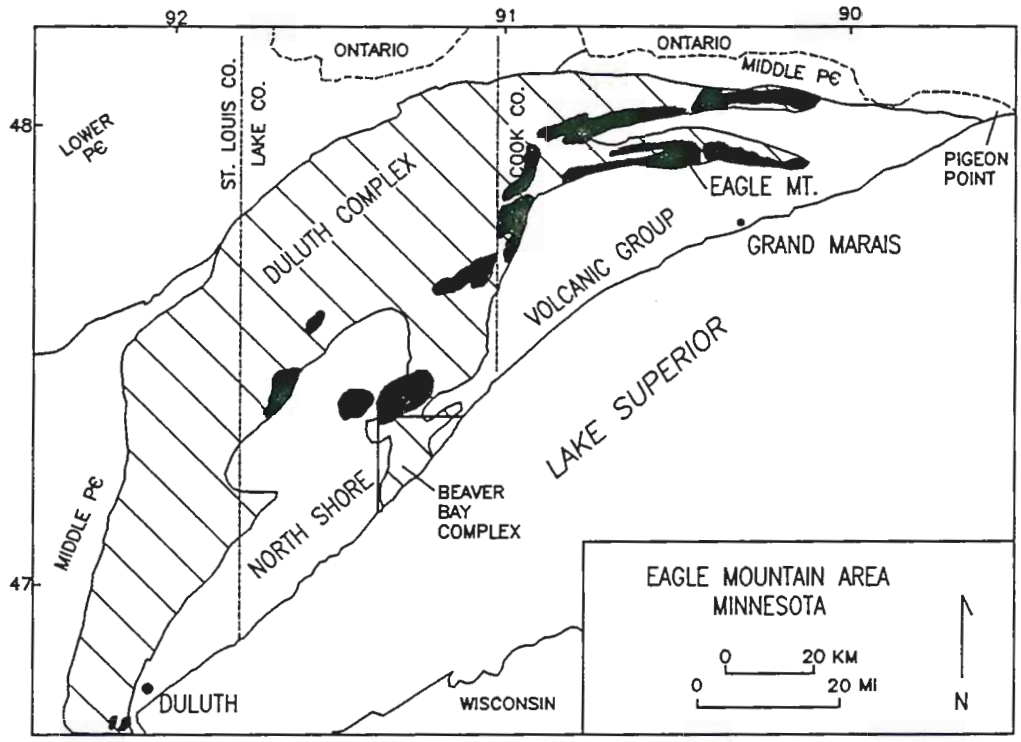

Figure 1: Location map. Hatched area represents extent of the Duluth Complex; solid areas represent mappable felsic bodies.

Many models have been proposed to explain the origin of the granophyre related to the Duluth Complex, including simple fractional crystallization (Schwartz & Sandberg, 1940; Davidson, 1972), partial melting (Davidson, 1972), liquid immiscibility (Grout, 1918), crustal assimilation, intrusion of a separate granitic magma (Taylor, 1964; Stevenson, 1974), and contact metamorphism of country rock (Mudrey, 1973). Fractional crystallization is the most widely accepted model of granophyre origin, but most geologists agree that another mechanism must also be involved to explain the disproportionately large volume of granophyre in the eastern Duluth Complex and the relative rarity of intermediate rock types. Because large volumes of hot mafic magma

were emplaced into the sialic crust here, it seems likely that some crustal assimilation and/or melting took place. The specific objectives of this study are 1) to establish contact relations of the granophyre with adjacent intrusive and extrusive rocks, 2) to establish the depth, temperature, and history of crystallization of the granophyre, and 3) to determine the mode of origin of the granophyre.

LOCATION

Eagle Mountain is located in Section 34, Township 63 North, Range 2 West, Cook County, Minnesota. It is approximately 28 km northwest of Grand Marais, Minnesota, and lies within the borders of the Boundary Waters Canoe Area Wilderness. Access is by foot, along the 4.8-km trail that begins from the parking area at the junction of Superior National Forest Roads 153 and 158. The field area for this study includes the southern portion of Section 27, the eastern portion of Section 34, and the western portion of Section 35, all in T63N, R2W, and portions of the north half of Sections 2 and 3, T62N, R2W (Fig. 2).

REGIONAL GEOLOGY

The Lake Superior basin is underlain by a thick mass of Upper Precambrian (Middle Proterozoic) igneous rocks that are interpreted as the product of a 1.2-1.1 b.y. major episode of abortive continental rifting, now referred to as the Midcontinent Rift System (Van Schmus and Hinze, 1985). Nicholson and Shirey (1990) have proposed a mantle plume as the most likely cause of the magmatism. The rocks, designated as Keweenawan (Morey and Green, 1982), are exposed along much of the present-day

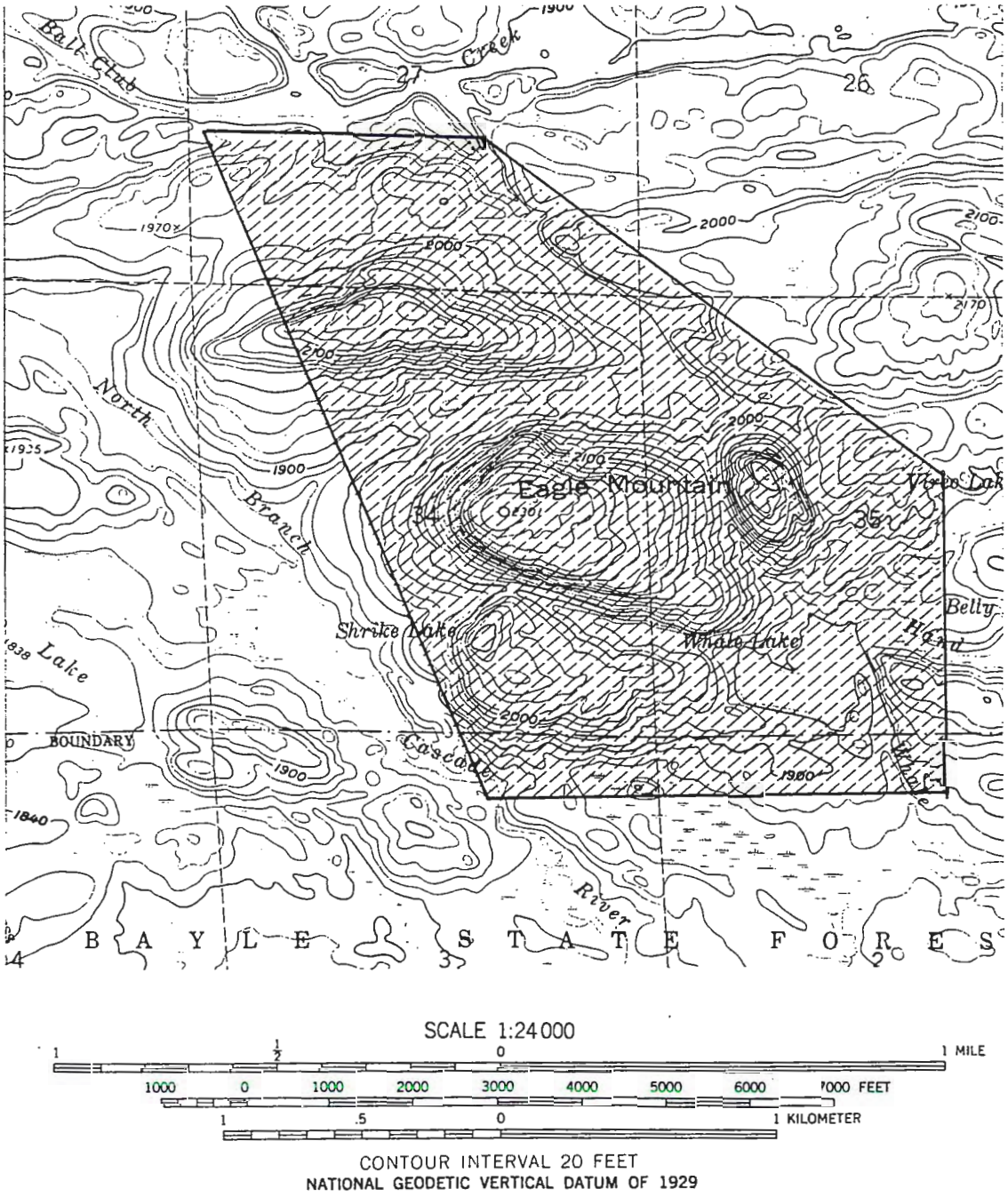

Figure 2: A portion of the Eagle Mountain 7.5' topographic quadrangle ; the hatching represents the field area for this study.

Lake Superior shoreline. In Wisconsin and Upper Michigan, the Keweenawan rocks are primarily lavas and volcanic-derived sediments. In northeastern Minnesota, however, the Keweenawan rocks are dominated by intrusions that underlie and crosscut the volcanic rocks (Green, 1972). According to Van Schmus et al. (1982), Keweenawan rifting and igneous activity began 1200-1225 m.y. ago, peaked at 1110 m.y. ago, and ceased shortly thereafter.

The structure of the region is controlled by the Lake Superior syncline, an asymmetric syncline with a steeply dipping south limb and gently dipping north limb (Davidson, 1982; Cannon et al., 1989). The syncline axis trends through western Lake Superior from southwest to northeast. In northeastern Minnesota the volcanic strata dip toward the lake at angles of 8-20°. The relatively low relief of most of the region combined with the gentle dip makes it difficult to develop a good three-dimensional model of the structural relations between the intrusive and extrusive rocks (Weiblen, 1982).

Exposed along the north shore of Lake Superior in northeastern Minnesota, the North Shore Volcanic Group (NSVG) forms a thick (4-7.5 km) bimodal sequence of plateau lavas dominated by olivine tholeiite and transitional basalt but also including some basaltic andesite and rhyolite (Green, 1982a). The lavas erupted from fissures controlled by spreading zones within the rift and accumulated as overlapping individual plateaus (Green, 1977, 1983, 1987, 1989).

The Duluth Complex is a 225 km long crescent-shaped intrusive complex that extends from Duluth north nearly to the Canadian border (Fig. 1). It has been dated at 1115 ± 14 m.y. using Rb/Sr isotopes (Faure et al., 1969) and at 1110 ± 10 m.y. using U-Pb from zircon (Silver and Green, 1963). The complex is composed of many separate intrusions that were emplaced both beneath and within the plateau lavas, mainly along the unconformity between the volcanic rocks and the underlying older Precambrian rocks (Phinney, 1972; Basaltic Volcanism Study Project, 1981); it may represent a series of magma chambers for some of the Keweenawan flows. Rocks of the complex are primarily mafic with an older "cap" of anorthositic rocks underlain by younger troctolitic rocks. Felsic rocks occur in irregular masses along a linear zone in the upper portion of the complex (Taylor, 1964; Weiblen and Morey, 1980; Weiblen, 1982).

Many Keweenawan mafic dikes and sills cross-cut both extrusive and intrusive rocks. The dikes generally have ophitic texture and chilled margins (Green et al., 1987). Many strike northeast, roughly parallel to the axis of the Lake Superior syncline.

PREVIOUS WORK

Layers or bodies of granophyric rocks are associated with upper levels of many layered mafic intrusions and diabasic sills throughout the world. Although no consensus has been reached concerning their origin, granophyres do form a distinctive

group of rocks within the granite family (Williams, Turner, and Gilbert, 1982). Granophyres share a number of important characteristics:

1) Granophyres are usually sodic rather than potassic, containing Na-rich mafic silicates (usually Na-rich amphiboles or pyroxenes) rather than K-rich mafic silicates (such as biotite).

2) FeO/(FeO + MgO) ratios are unusually high.

3) Mafic phases are very ferrous (usually hedenbergite and fayalite).

4) SiO_2 content is variable; it ranges from 64% to 72%.

5) Quartz is mostly intergrown with alkali feldspar.

6) Granophyres are common as streaks and lenses in the upper levels of thick differentiated sills of tholeiitic diabase and near the roof of major layered mafic intrusions.

Two of the best known examples of layered mafic intrusions with associated granophyre are the Bushveld Complex and the Skaergaard Intrusion. The Precambrian Bushveld Complex of South Africa includes the Rashoop Granophyre Suite, comprising layers of granophyre at various stratigraphic levels. Walraven (1985) distinguished three different types of granophyre based on field relations, textures, and geochemistry. He proposed that the Diepkloof granophyre formed by melting of the overlying Rooiberg felsites and that the Zwartbank granophyre formed by recrystallization of overlying Pretoria sediments with the basic magma of the intrusion acting as the heat source for both. The third unit, the Stavoren granophyre, represents the

shallow intrusive equivalent of the Rooiberg volcanics. Based on Sr concentrations, he concluded that the Stavoren granophyre formed from a primary magma that originated from the partial melting of felsic rocks, not from differentiation of a mafic magma.

The Tertiary Skaergaard Intrusion of Greenland also includes a significant proportion of granophyre in the upper levels. Wager and Brown (1967) describe melanogranophyres associated with the Upper Border Group as well as a transitional granophyre, the Sydtoppen, and the more felsic granophyre that forms the Tinden Sill. They concluded that all the granophyres were produced by filter-pressing of the partly solidified Upper Zone and Upper Border Group rocks, and thus the granophyre magmas are products of the crystal fractionation of the Skaergaard magma.

In the area of the Duluth Complex, the Pigeon Point Sill, forming the far northeastern point of Minnesota, is a mafic intrusion within the argillite and quartzite of the Lower Proterozoic Rove Formation. The sill includes a zone of granophyre beneath the upper chilled diabasic margin. Bayley (1893) was one of the first geologists to study the sill, and he described the zone of red rock and altered quartzites as the most interesting feature of the Point. He concluded that the red rock was secondary, a result of the melting and recrystallization of the slates and quartzites following the intrusion of the diabasic magma. Daly (1917) suggested that the red rock of the Pigeon Point Sill was the result of gravitative differentiation along with assimilation and contact fusion of the country rock. Grout (1928) and Grout and Schwartz (1933) thought the granophyre formed mainly by magmatic differentiation with only a small

amount of assimilation of country rock. Bastin (1938) believed the diabase and granophyre to be separate intrusions. Based mainly on oxygen isotope data and mass balance calculations, Mudrey (1973) proposed that the granophyre originated from partial fusion and contact metamorphism of overlying country rock when the diabasic magma was emplaced. The granitoid magma then migrated away from the areas where it formed to crystallize in its present locations.

Schwartz and Sandberg (1940) examined three sills in Duluth that have upper granophyric zones: the Endion Sill, the Northland Sill, and the Lester River Sill. They concluded that the granophyre formed from *in situ* differentiation of mafic magma. Ernst (1960) also studied the Endion Sill, but he was uncertain whether the granophyre was a product of magmatic differentiation or the result of a separate, unrelated intrusion.

Grout (1918) and Taylor (1964) studied numerous granophyre outcrops in the Duluth area. Grout concluded that separation of an immiscible granitic fraction from the mafic magma was responsible for the granophyre. Taylor felt that some of the granophyre formed from a magma and some by secondary replacement of the gabbroic rocks.

Gehman (1957), in a study of the gabbroic Beaver Bay Complex, noted the occurrence of many granophyric dikes, but he did not attempt to establish their genetic relationship to the gabbros. Stevenson (1974) conducted a detailed study of the Sonju

Lake Intrusion within the Beaver Bay Complex, and he concluded that the granophyre in this intrusion was the result of a late, separate magma.

Leighton (1954), in a study of the Keweenawan Mellen Complex of northern Wisconsin, concluded that the granophyre in this complex resulted from the crystallization of a separate granitic melt that was intruded after the gabbro solidified. Klewin (1987) found evidence for four groups of felsic rocks in the Mellen Complex. He recognized one group as late-stage differentiates of the main zone of the intrusions and the other three groups as products of a separate source, possibly partial melting of lower crust.

Davidson (1972) described two distinct structural habits for the granophyre in the eastern portion of the Duluth Complex. He found that small, local plutons associated with the anorthositic series lie above the projection of the buried portions of the Giants Range Granite and may have been derived from this granite by partial melting. Larger, flat-lying sheets overlying the margins of olivine gabbro units are probably differentiates from the gabbroic magma.

Weiblen and Morey's (1980) review of data concerning the Duluth Complex illustrates the lack of conclusive evidence for the origin of the granophyre. They concluded that petrogenetic relationships between the felsic and mafic rocks of the complex have not been established and that present data do not permit unequivocal assignment of the felsic series to specific intrusions.

METHODS

Field mapping, using the USGS Eagle Mountain 7.5' quadrangle map as a base, was completed during June, 1988. Approximately 80 thin sections were prepared and examined using a petrographic microscope. Ten polished thin sections were prepared for microprobe analysis to determine the composition of olivine, pyroxene, feldspar, and Fe-Ti oxide in each rock unit. Microprobe analyses were done using the semi-automated MAC probe at the Natural Resources Research Institute, Duluth, Minnesota, between March and September, 1989. Thirty-six rock samples were prepared for chemical analysis by removing all weathered surfaces from an aliquot, crushing, and powdering using a tungsten carbide shatter box. Major and trace element analyses were done in January, 1989, at Northern Illinois University using a Siemens SRS 300 XRF. REE analysis of sample EM64 was done using INAA by Eric Jerde of UCLA in June, 1989. Volatile analyses and all other rare earth element analyses were done by Nuclear Activation Service, Inc., in February, 1989. Norm calculations and mass balance calculations were prepared using the Geochemical Program Package (GPP) by Geist, Baker, and McBirney (1985).

LITHOLOGY AND PETROGRAPHY

INTRODUCTION

Previous reconnaissance mapping of the Eagle Mountain Quadrangle (Grout, Sharp, and Schwartz, 1959; Davidson, 1977) revealed only three rock types in the study area: olivine gabbro, granophyric granite, and metavolcanics. The current study focused on a small area of the Eagle Mountain Quadrangle, but in the course of field mapping, eight rock units were distinguished. The units were informally named metabasalt, metagabbro, ophitic diabase, syenogabbro, ferrodiorite, Eagle Mountain granophyre, rhyolite, and miarolitic granophyre. The units occur in roughly east/west strips with syenogabbro at the northern boundary of the area, succeeded to the south by ferrodiorite, Eagle Mountain granophyre, metagabbro, metabasalt, miarolitic granophyre, and rhyolite; ophitic diabase cross-cuts other units, occurring in a northwest/southeast-trending, discontinuous line (Fig. 3 and Plate 1). The metabasalt and metagabbro units are part of Davidson's (1977) metavolcanic unit. The syeno-gabbro and ferrodiorite are apparently both part of Davidson's olivine gabbro unit, which he later (1982) assigned to a troctolite-olivine gabbro series that he found had intruded older anorthositic series rocks of the region. He identified subhorizontal sheets of granophyric granite, which includes both the Eagle Mountain granophyre and the miarolitic granophyre, along both upper and lower contacts of the olivine gabbro unit, and he interpreted the granophyric granites as differentiates of the olivine gabbro unit.

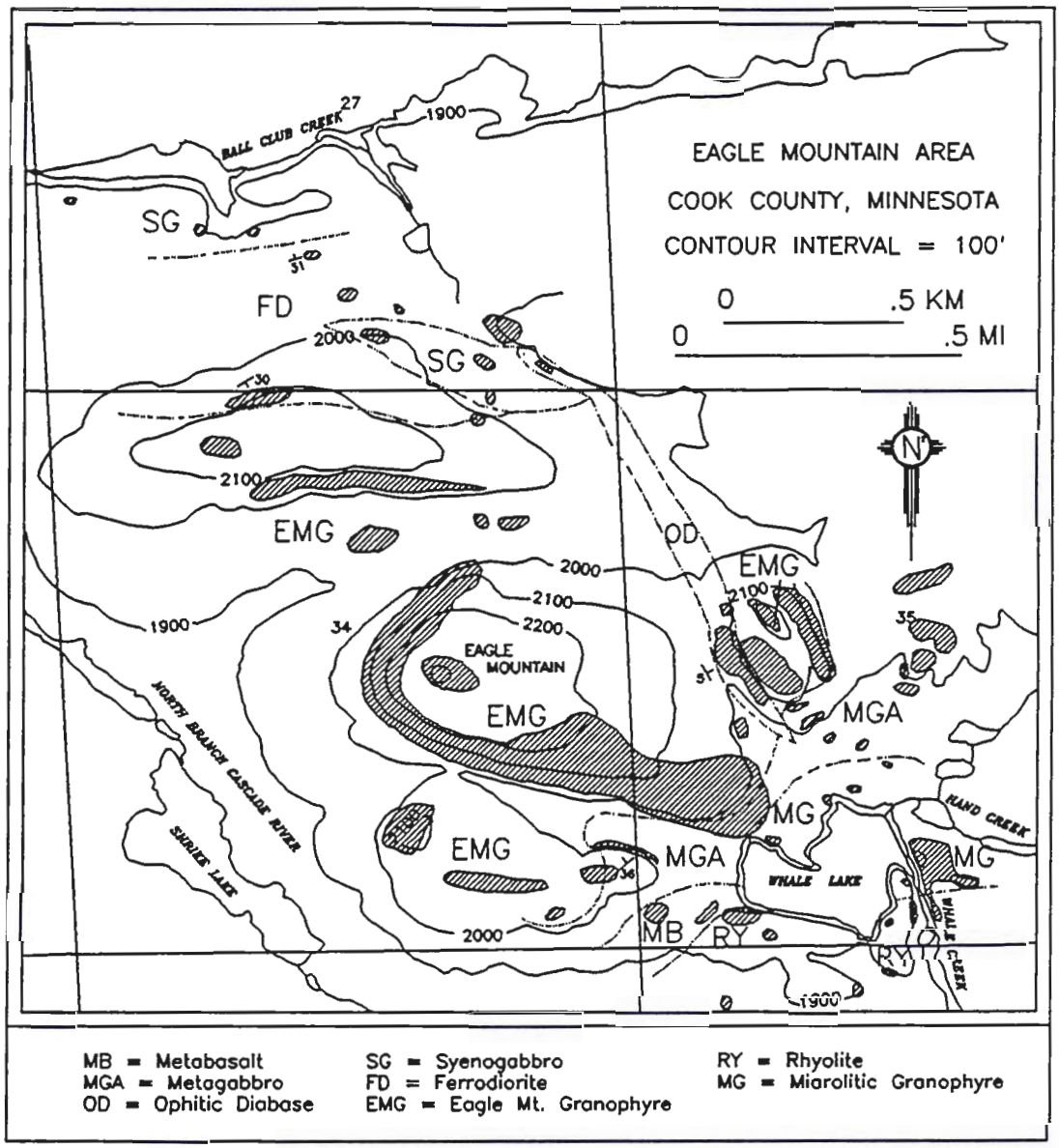

Figure 3: Bedrock geology, Eagle Mountain area. Hatching represents mapped outcrop.

FIELD RELATIONS

The rhyolite, which lies at the base of a sequence of NSVG lavas 4-5 km thick (Green, 1972b), appears to be the oldest unit in the area. The metabasalt, which underlies the rhyolite in the southern portion of the area, shows evidence of high

temperature metamorphism and could be as old as or older than the rhyolite. The boundaries of the unit are not well-defined and textures are variable; it may actually be made up of a number of separate xenoliths that were rafted to the present location. The rhyolite probably represents the base of the volcanic pile that formed the roof against which the xenoliths were impounded. The metagabbro, which shares an indistinct contact with the metabasalt, may represent the magma that carried the basalt xenoliths and provided the heat for metamorphism. This gabbro also shows signs of metamorphism; where it is in contact with the Eagle Mountain granophyre, the contact is very sharp with no chilled margin apparent in either unit. The granophyre occurs as veins within the metagabbro, indicating that the granophyre was emplaced after the gabbro; the granophyre magma probably provided the heat that caused the metamorphism seen in the metagabbro. The Eagle Mountain granophyre shares a gradational contact and similar mineral compositions with the ferrodiorite, and, thus, these two units appear to be genetically related and of the same age. The syenogabbro shows no clear genetic relationship to the ferrodiorite, and no contact between these two units was located in the field. The syenogabbro may represent a separate intrusion, but its age relationship to the other units is not known. In the southeastern portion of the field area, miarolitic granophyre is in contact with rhyolite; the contact between the units is gradational over a distance of about 2 m. Fragments of rhyolite occur within a matrix of quartz and feldspar similar to the granophyre, indicating that the miarolitic granophyre is younger than the rhyolite. The age relationship between the granophyre

and other units, however, is ambiguous. The ophitic diabase cross-cuts several units and probably is the youngest unit in the area.

A simplified, interpretive cross-section of the area is shown in Figure 4. Very few outcrops in the field area provided suitable measures of structural attitudes;

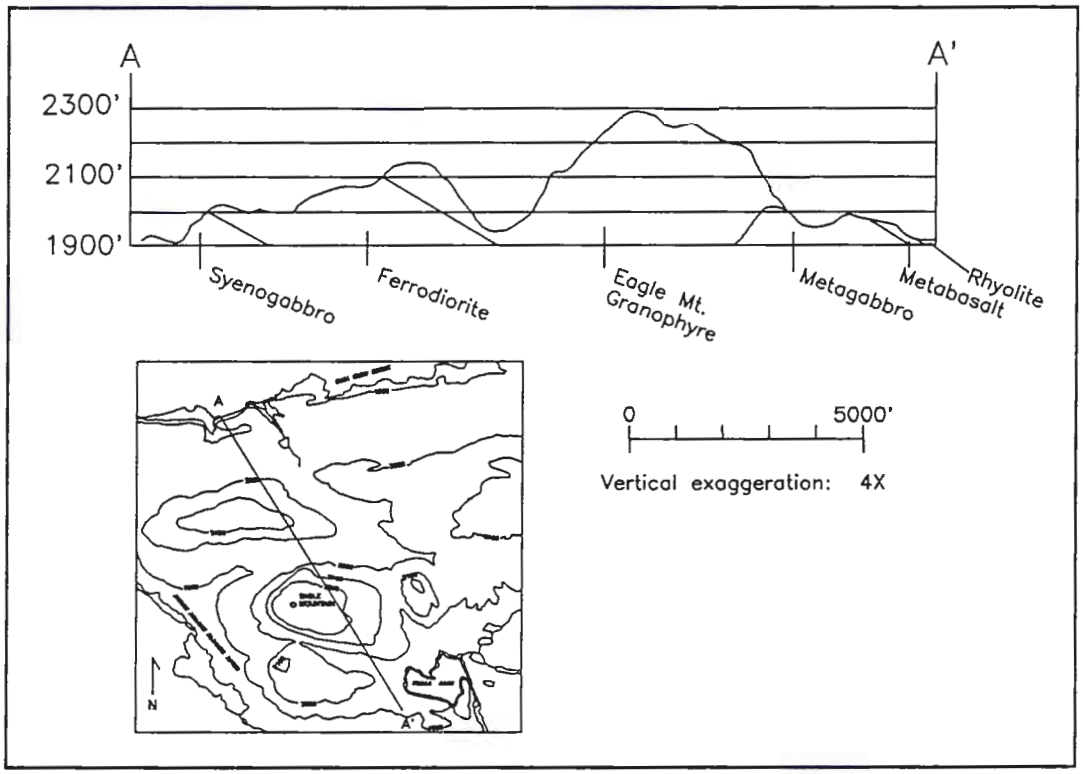

Figure 4: Cross-section, Eagle Mountain area, from northwest to southeast.

therefore, the attitudes used in the cross-section are based on a few field measurements and Davidson's (1982) interpretation of dips of 15-20° in the southern prong of the Duluth Complex and intercalated Keweenawan flows. Locations of outcrop samples taken for thin section examination and geochemical analysis are shown in Figure 5.

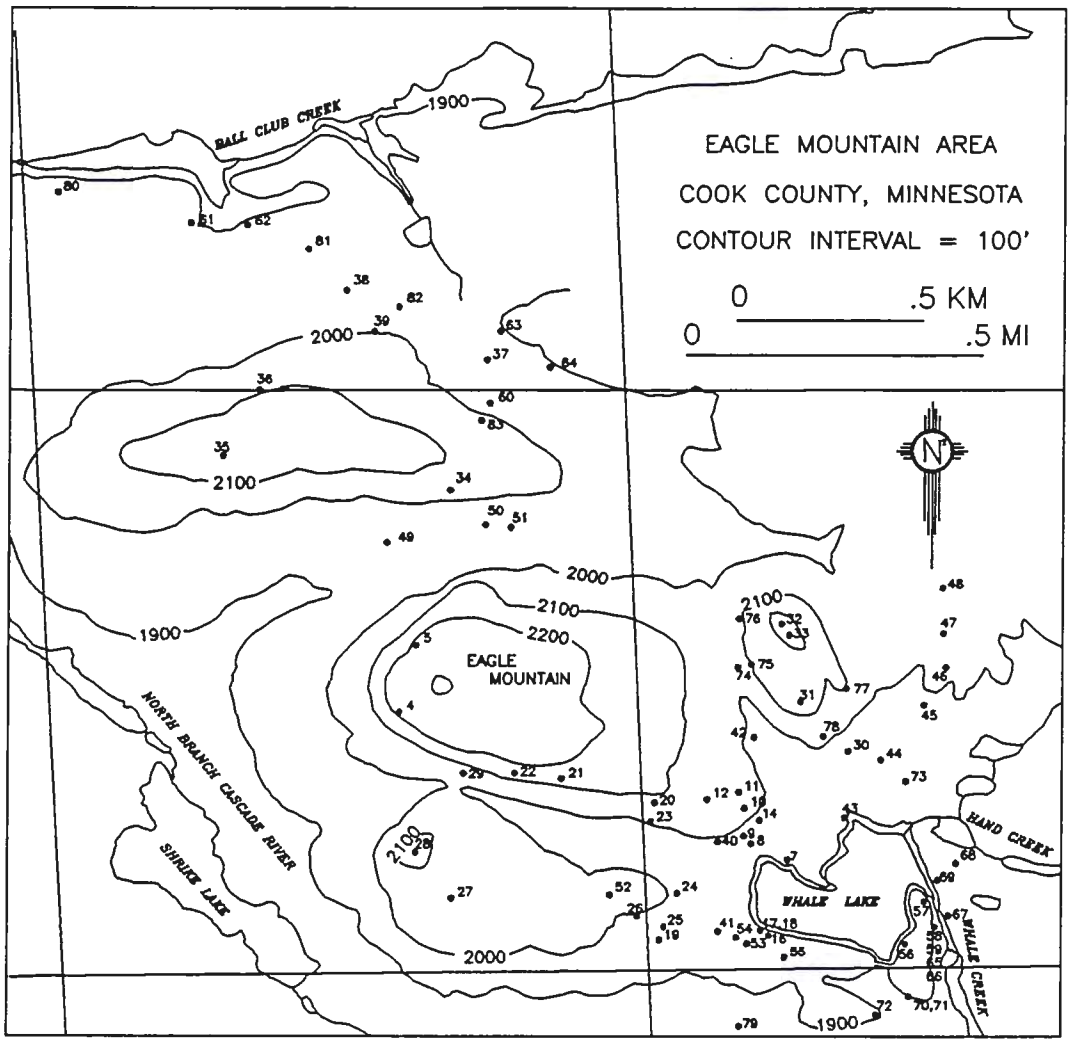

Figure 5: Sample locations.

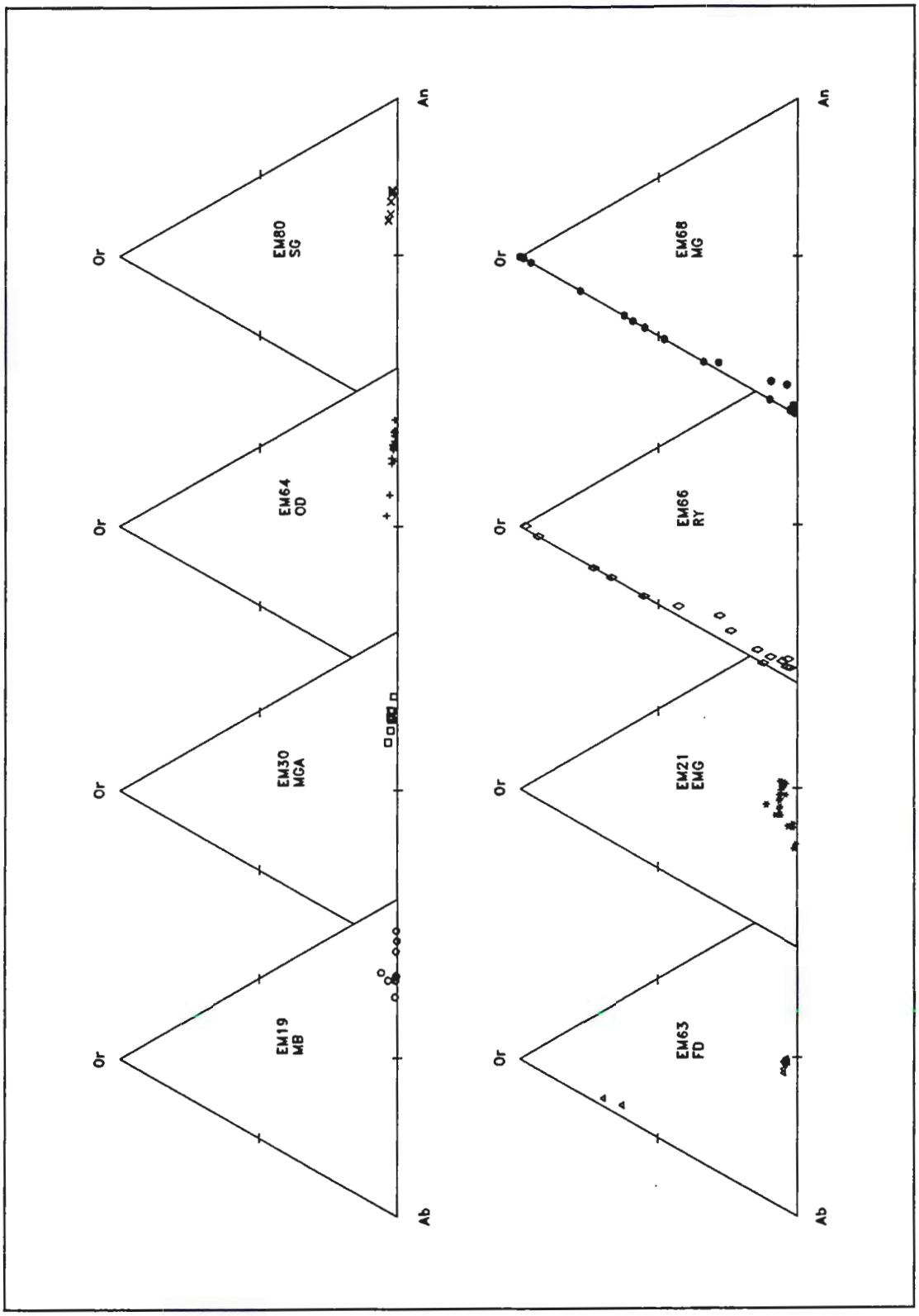

Figure 6: Feldspar compositions determined by microprobe analysis. (Mol%)

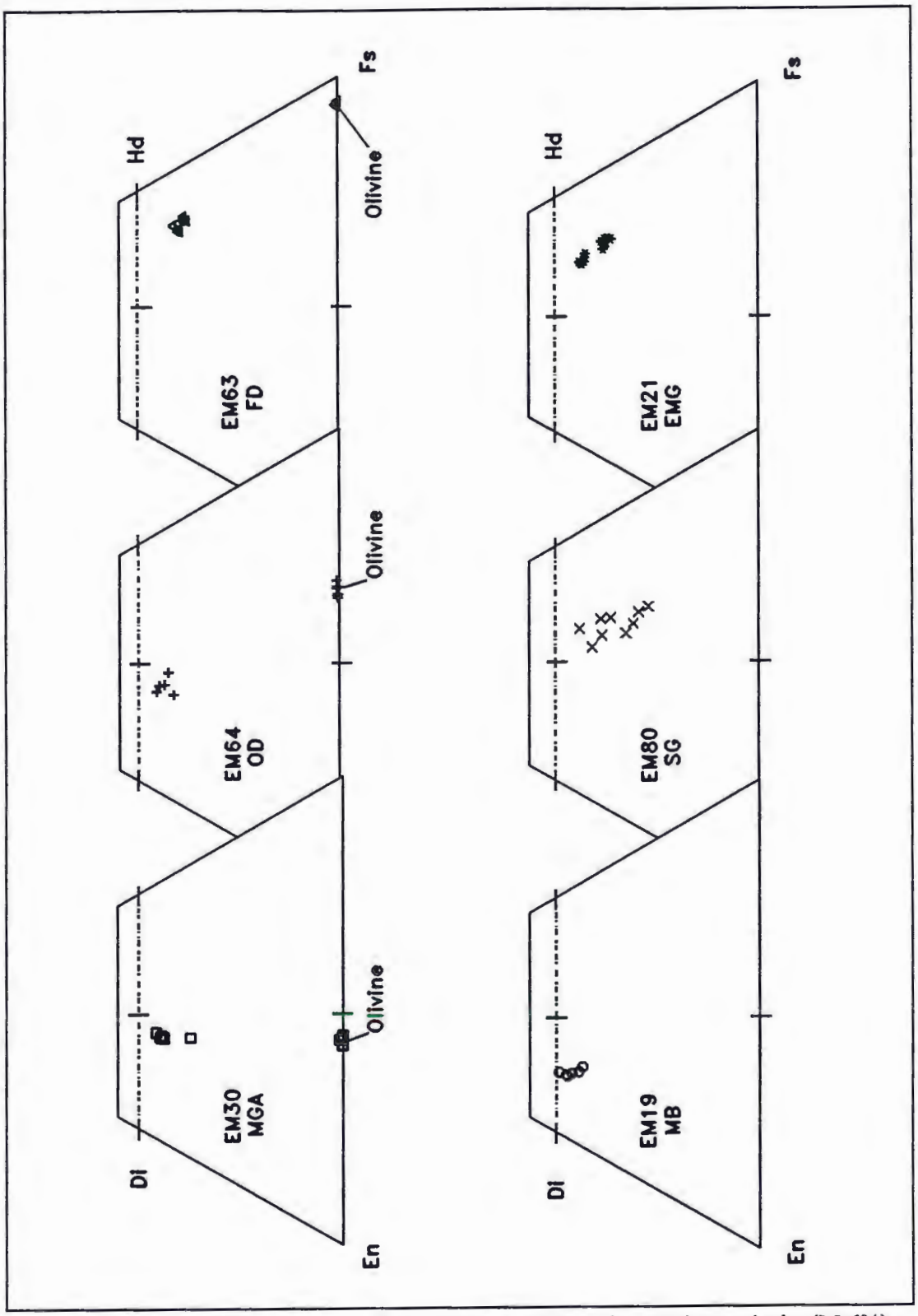

Figure 7: Pyroxene/olivine compositions determined by microprobe analysis. (Mol%)

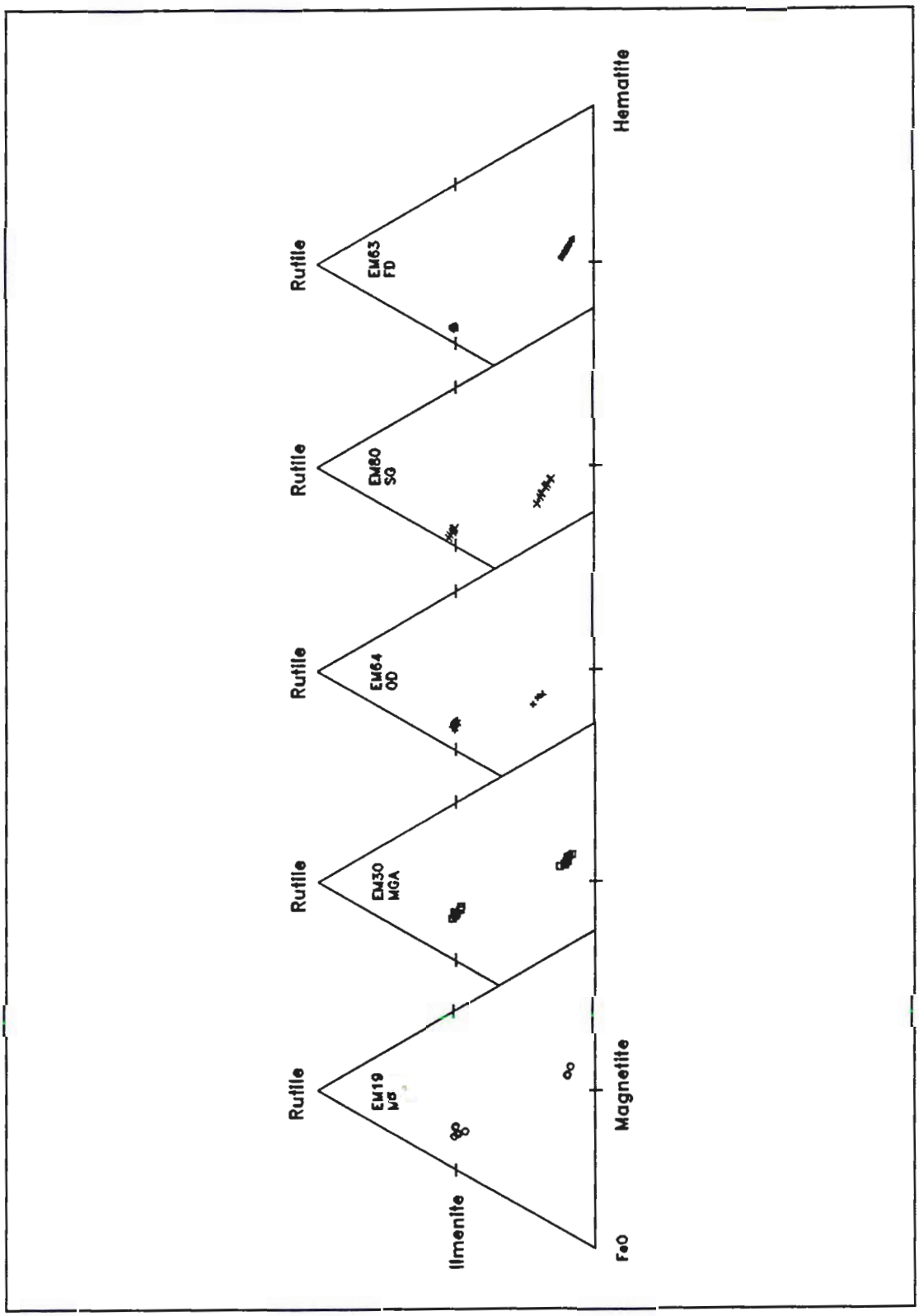

Figure 8: Oxide compositions determined by microprobe analysis. (Mol%)

DESCRIPTION OF UNITS

In the following lithologic descriptions, fine-grained indicates an average grain size <1 mm, medium-grained indicates an average grain size between 1 mm and 5 mm, and coarse-grained indicates an average grain size >5 mm. Complete microprobe analyses of individual minerals are contained in Appendix III; mineral analyses plotted on compositional triangles are shown in Figures 6, 7, and 8.

Syenogabbro: Syenogabbro occurs in a narrow strip south of Ball Club Creek and in a small zone to the southeast within the ferrodiorite. No outcrops were sampled north of Ball Club Creek, so the northern extent of the syenogabbro was not determined; however, Grout, Sharp, and Schwartz (1959) and Davidson (1977) indicate that it continues at least 0.5 km north of the creek. This unit is distinguished by its medium to coarse grain size, decussate texture, large plagioclase laths that are conspicuous in handsample, ophitic pyroxenes, and interstitial granophyric intergrowths that are visible in thin section.

In outcrop the syenogabbro is decussate and medium- to coarse-grained with plagioclase laths up to 1 cm long and interstitial oxide and pyroxene crystals up to 1 cm across. The rock is quite magnetic. Fresh surfaces show a mixture of coarse white feldspar, black pyroxene, and Fe-Ti oxides (Fig. 9). Weathered surfaces are brown to gray and generally rust-stained. Plagioclase weathers chalky white with some salmon-pink edges; some interstitial material also weathers salmon-pink. The exposed rock is very punky and crumbly, making it difficult to obtain fresh samples.

Figure 9: Photo of cut slab of syenogabbro (EM80).

In thin section, the syenogabbro (samples EM37, EM60, EM61, EM62, EM80) is made up of 60-75% plagioclase, 10-20% clinopyroxene, 5% orthoclase, 5% quartz, 5-10% oxides, and traces of apatite, hornblende, biotite, chlorite, iddingsite, and prehnite.

Plagioclase ($An_{60}Ab_{37}Or_3$ to $An_{70}Ab_{28}Or_2$) (Fig. 6) occurs as euhedral to subhedral laths that range from 0.5 mm to 1 cm long with an average length of about 6 mm. The crystals are normally-zoned and have sharp albite twins. Some of the plagioclase shows local sericitization; samples taken closest to the ferrodiorite have the most extensive sericitization of plagioclase. Alkali feldspar occurs as thin rims on plagioclase crystals, and in interstitial areas the alkali feldspar occurs with quartz in

granophyric intergrowths; a larger percentage of interstitial granophyric material is present in samples taken closest to the ferrodiorite.

Clinopyroxene ($Ca_{35}Mg_{25}Fe_{40}$) (Fig. 7) occurs as large interstitial to subophitic patches that average 5 mm across. In plane light it is light yellow-brown and clouded by very fine exsolved oxide grains. Where pyroxene grains abut areas of mesostasis, the pyroxene is rimmed by hornblende. Most of the hornblende shows greenish to brown pleochroism; where it grew into large spaces it is strongly zoned, from light green to intense green at the edges. In these grains, the hornblende developed crystal faces.

Olivine has not survived as a recognizable phase in the syenogabbro, but patches of iddingsite plus chlorite and iron oxide indicate that it may have been present originally as subhedral to anhedral grains up to 2 mm across making up no more than 1% of the rock.

Both magnetite and ilmenite occur as large interstitial grains up to 4 mm across. Ilmenite also occurs in symplectic intergrowths with various minerals, mainly feldspar and secondary chlorite and iddingsite. Compositions of Fe-Ti oxides as determined by microprobe analyses are shown graphically in Figure 8.

Apatite and chalcopyrite are present in trace amounts. Prehnite is a conspicuous, but local, secondary mineral. Other secondary minerals include biotite, chlorite, and sericite.

Because of the coarse grain size and decussate texture of this unit, it appears to have crystallized slowly, but with no crystal settling. After initial crystallization of olivine and plagioclase, pyroxene and Fe-Ti oxides crystallized in interstitial areas. Rims of alkali feldspar and hornblende crystallized from the final liquid. Secondary alteration includes the breakdown of olivine to iddingsite and magnetite, sericitization of plagioclase, growth of symplectic ilmenite, and the development of prehnite, biotite, and chlorite. At least some of the interstitial granophyre is probably a result of later contamination by a more silica-rich liquid.

Ferrodiorite: South of the syenogabbro is a unit of medium-grained, locally laminated, cumulate-textured ferrodiorite (samples EM36, EM38, EM63, EM81, EM82). No exposures of the contact between the ferrodiorite and the syenogabbro were located. The distinguishing characteristics of the ferrodiorite include medium grain size, local igneous lamination, abundant needles of apatite (visible in hand sample), and interstitial quartz (visible in thin section).

In outcrop the ferrodiorite is dark rusty-brown, fine- to medium-grained, laminated, and magnetic. It is composed of approximately 60-70% light-colored but rust-stained plagioclase crystals averaging 2 mm long, up to 10% orthoclase, 10-15% clinopyroxene, 5% quartz, 5-10% olivine, 5-8% Fe-Ti oxides, 1-2% needles of apatite up to 2 mm long, and a trace of hornblende and biotite.

Cumulus plagioclase crystals are subhedral and tabular, averaging about 2 mm and reaching a maximum of 8 mm in length. Most grains are normally-zoned and

have sharp albite twins. Many also show simple Carlsbad twins. Probe analyses indicate the cores have compositions ranging from $An_{43}Ab_{52}Or_5$ to $An_{48}Ab_{48}Or_4$ (Fig. 6). Many grains are rimmed by alkali feldspar with an average composition of $An_4Ab_{31}Or_{65}$. The plagioclase grains show a distinct preferred orientation, giving rise to a fairly strong igneous lamination (Fig. 10). The feldspars show some alteration along fractures; K-rich rims are very cloudy.

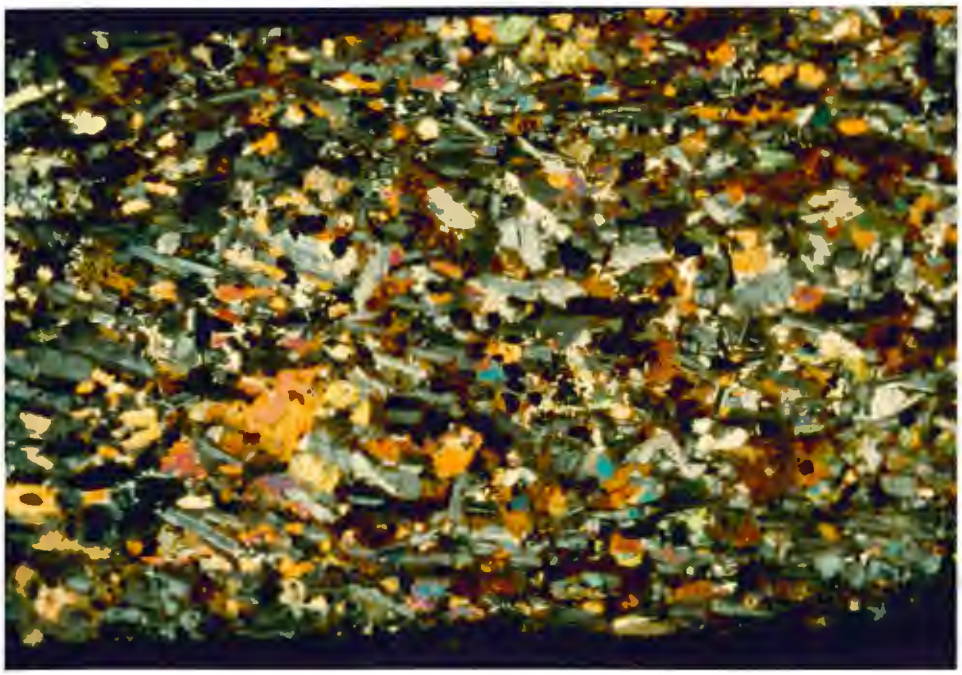

Figure 10: Photo of thin section of ferrodiorite (EM81) showing igneous lamination. Field of view is approximately 4 cm across; photographed under crossed polars.

Clinopyroxene ($Ca_{38}Mg_{12}Fe_{50}$) (Fig. 7) occurs as cumulus, subhedral to anhedral grains that average about 1 mm across and appear light brown in plane light. Some grains are elongate and reach 4 mm in length; most are aligned parallel to the plagioclase grains. Many of these prismatic grains show simple and very fine lamellar twins

that form a strong herringbone pattern. The pyroxene is relatively fresh with only a small amount of oxidation along fractures.

A small percentage of hornblende is present, rimming pyroxene grains. The hornblende shows strong light brown to dark brown pleochroism. As in the syeno-gabbro, the hornblende occurs primarily (but not exclusively) where grains are bounded by interstitial quartz. The hornblende exhibits crystal faces against the interstitial material.

Olivine (Fo_5Fa_{95}) (Fig. 7) occurs mainly as rounded cumulus grains 1-2 mm across; some grains are elongate, up to 2 mm in length. The olivine is light greenish-brown in plane light and heavily fractured. It is altered to iddingsite along fractures and grain boundaries.

Fe-Ti oxides include both magnetite and ilmenite. Blocky, equant, cumulus magnetite occurs as subhedral to anhedral grains with coexisting patches and fine lamellae of ilmenite. Average grain size is approximately 1 mm across. Cumulus platy ilmenite grains average 1 mm in length and 0.1 mm in width. Ilmenite also occurs as symplectic intergrowths with various silicates. Some ilmenite grains are rimmed by low-temperature Ti-free magnetite that probably resulted from the oxidation of olivine. Compositions of Fe-Ti oxides as determined by microprobe analyses are shown graphically in Figure 8. Minor amounts of chalcopyrite are also present.

Apatite is a significant accessory mineral occurring as cumulus, euhedral prisms up to 2 mm long and 0.1 mm across. Some apatite crystals are bent around larger olivine or feldspar crystals.

Interstitial areas are filled with quartz; only rarely is it intergrown with alkali feldspar. Near the contact with the Eagle Mountain granophyre, the ferrodiorite is poorly laminated and olivine is more completely altered to magnetite and iddingsite.

The lamination in this unit indicates that some sort of mechanism, such as crystal settling or current flow, controlled the orientation of crystals. Cumulate minerals include apatite, olivine, plagioclase, clinopyroxene, ilmenite, and magnetite. Euhedral apatite occurs as inclusions in all other phases, indicating that it was one of the earliest phases to crystallize. Intercumulate minerals include Fe-Ti oxides, K-feldspar, and quartz. Secondary alteration, probably deuteric, includes development of symplectic ilmenite and alteration of olivine to iddingsite and magnetite.

Eagle Mountain Granophyre: To the south, the ferrodiorite grades into the Eagle Mountain granophyre over a surface distance of approximately 150 m. In the area of the gradational contact, the rocks appear to be a mixture of diorite and granite of variable grain size. Coarser-grained samples have large clots of mafic minerals surrounded by large areas of coarse, salmon-pink alkali feldspar. In the finer-grained samples, the mafic minerals form smaller clots but are more dominant within a smaller percentage of feldspathic matrix.

The Eagle Mountain granophyre underlies most of Section 34 east of the Cascade River. It crops out on the southern side of the ridge in the north half of Section 34, and caps Eagle Mountain, the low hill south of Eagle Mountain in the southeast quarter of Section 34, and the hill east of Eagle Mountain in the northwest quarter of Section 35. The granophyre is distinguished by its fine grain size, brownish-red color, massive outcrops, and, in thin section, by variable textures that include spherulites and very fine granophyric intergrowths.

In outcrop, the granophyre is red-brown, fine-grained, massive, and varies from equigranular to somewhat porphyritic. It contains 60-75% feldspars, 20-25% quartz, and 5-15% ferromagnesian silicates/oxides; textures are variable (Fig. 11). In porphyritic facies, phenocrysts make up from 10% to 40% of the rock; some samples are slightly glomeroporphyritic. Feldspar phenocrysts are blocky and equant (averaging 2 mm across) or elongate laths (up to 6 mm long). On fresh surfaces they are creamy or salmon-colored; on weathered surfaces they are white and chalky and stand out in contrast against the red-brown groundmass. Quartz is not apparent in hand samples. Black, fine-grained Fe-Ti oxides and ferromagnesian silicates occur disseminated throughout the rock and as small aggregates (up to 4 mm across). Small mafic inclusions (up to 1 cm) and red, very fine-grained, hematite-rich veins 1-4 mm wide occur in some samples. Granophyric texture is not visible in hand sample.

All feldspars are clouded (to varying degrees) with very fine-grained hematite and kaolinite, making optical identification very difficult. Microprobe analysis of ten

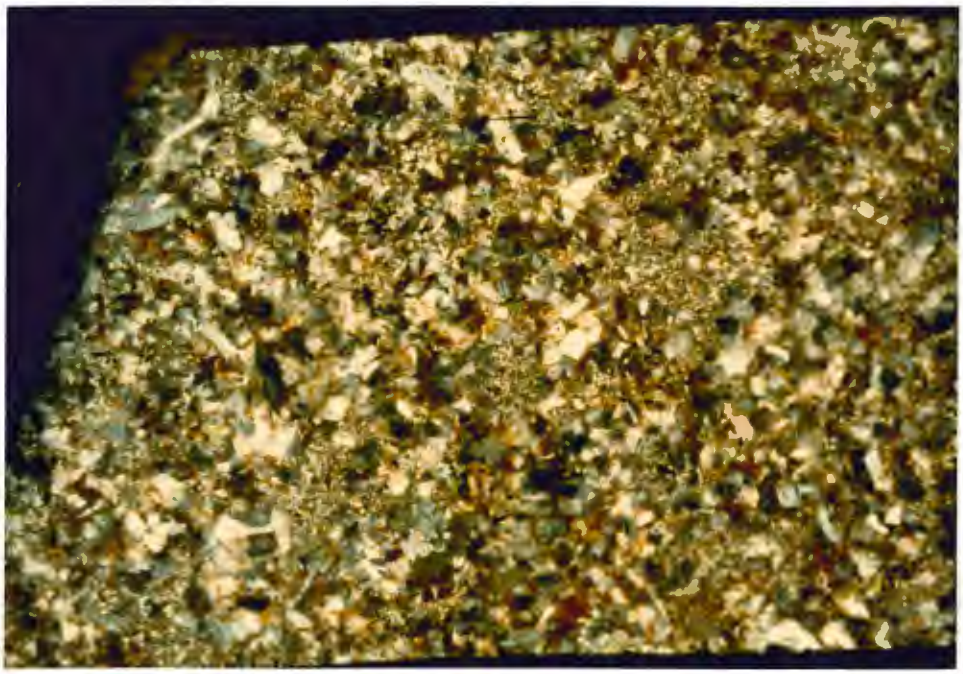

Figure 11: Photo of entire thin section of Eagle Mountain granophyre (EM11). Field of view is approximately 4 cm across; photographed under crossed polars.

grains from two thin sections (EM34 and EM21) indicate that feldspar phenocrysts are andesine with compositions ranging from $An_{30}Ab_{68}Or_2$ to $An_{51}Ab_{44}Or_5$ (Fig. 6). Most show slight normal zoning, and much of the hematite-clouded material surrounding the phenocrysts is K-rich. The clouded nature of the feldspars may reflect some alteration; Taylor (1978) found that clouded feldspars are common in granites that have undergone low temperature hydrothermal alteration.

The plagioclase grains occur in several different habits. Equant, blocky phenocrysts 1-2 mm across and elongate laths 1 mm wide and up to 5 mm long are most common. Most have sharp, very narrow albite twins along with some pericline twins in the equant crystals and Carlsbad twins in the elongate crystals. Some have inclu-

sions of pyroxene and/or magnetite; some clearly show overgrowths of untwinned feldspar. In some samples (e.g. EM34, EM49) the plagioclase laths appear skeletal, occurring as very narrow, elongate grains (0.2 mm wide and up to 3 mm long). The cores of these grains are either heavily clouded with hematite or hollow and filled with groundmass material.

Feldspar also occurs as 1-6 mm phenocrysts with resorbed grain boundaries and cores that are filled with inclusions of quartz or a very fine intergrowth of quartz and feldspar in intricate, wormy patterns, suggesting resorption (Fig. 12). Less common rhombic sections are about 1 mm across, show simple or no twinning, and very little resorption. Some feldspar phenocrysts are partly sericitized; most are clouded by exsolved and oxidized fine-grained Fe-oxides.

Ferromagnesian minerals include Fe-rich clinopyroxene, lesser hornblende, and minor biotite. Pyroxene (average $Ca_{43}Mg_{16}Fe_{41}$) (Fig. 7) is anhedral to subhedral, grassy green in plane light, and weakly pleochroic. It occurs mainly in granular aggregates up to 1 mm across with individual grains <0.5 mm. Most grains are full of small, anhedral inclusions of magnetite with no preferred orientation. Some pyroxenes are clearly rimmed by hornblende, but most show no distinctive relationship to the hornblende. Hornblende occurs as ragged, anhedral patches up to 0.5 mm across; it is pleochroic from light greenish-brown to a darker brown. Most grains have inclusions of quartz and magnetite.

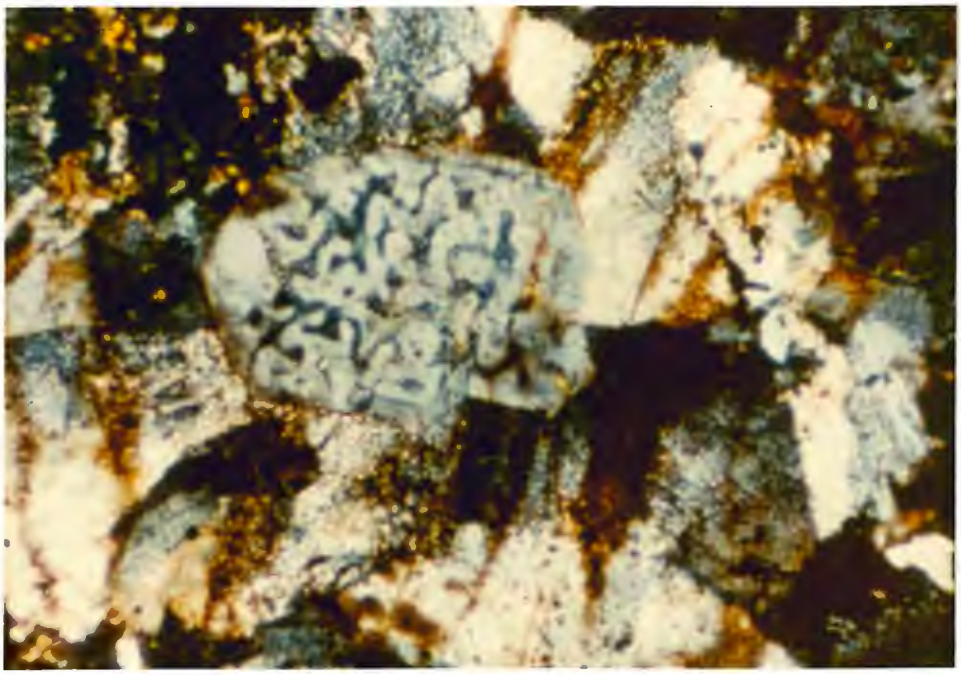

Figure 12: Photomicrograph of resorbed andesine phenocryst in Eagle Mountain granophyre (EM11). Field of view is approximately 3.5 x 2.0 mm; photographed under crossed polars.

Magnetite occurs in two distinct habits, possibly representing two generations. Larger, equant, sub- to anhedral grains, up to 0.5 mm, occur in clots with pyroxene and hornblende. Smaller sub- to anhedral grains, <0.1 mm, are scattered throughout the rock and in many cases form linear, sometimes radial, "chains" of grains outlining boundaries of granophyric intergrowths. Examination of polished sections in reflected light indicates the oxides are almost entirely magnetite with some alteration to hematite along grain edges and fractures.

Very fine-grained biotite is present in only a few samples where it occurs as a microscopic rim (<0.05 mm wide) surrounding magnetite grains. Apatite occurs in

trace amounts, mainly as inclusions in feldspar phenocrysts. Local mafic inclusions up to 1 cm across are oval and composed of very fine-grained granular pyroxene, oxide, and feldspar.

The groundmass of the granophyre is made up of very fine-grained intergrowths of quartz and feldspar with variable textures. Some occurs as fine, equigranular masses with or without micropoikilitic quartz, some as spherulites, and some as granophyric intergrowths.

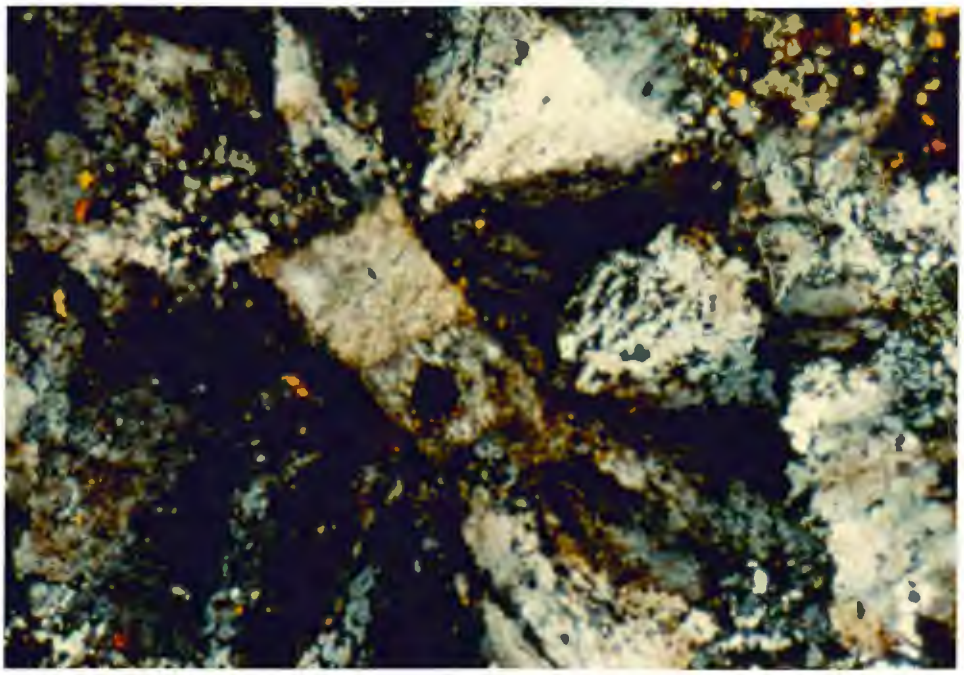

Figure 13: Photomicrograph of spherulite in Eagle Mountain granophyre (EM5). Spherulite is nucleated on a plagioclase phenocryst. Field of view is approximately 3.5 x 2.0 mm; photographed under crossed polars.

Many samples from close to the ferrodiorite contact (e.g. EM34, EM35, EM44, EM49) have about 95% groundmass in which quartz and hematite-clouded feldspar are

intergrown in irregular to crudely micrographic patterns. The groundmass intergrowths do not show particularly radial or geometrically regular patterns; some of the quartz is micropoikilitic. Some coarser-grained quartz aggregates have a distinct spherical form with little feldspar in the interior of the aggregate.

Farther from the ferrodiorite contact, especially on Eagle Mountain, spherulites and some granophyric intergrowths appear in the groundmass (e.g. EM5, EM11, EM12, EM20, EM22). The remainder of the groundmass in these samples is very fine-grained and equigranular. The spherulites, averaging 2-3 mm across, are distinctly circular structures made up of quartz and feldspar intergrown in a radial pattern (Fig. 13). Extinction moves around the sphere in a wave, but the sphere is divided into a number of optically continuous wedges. In some spherulites a distinct nucleus is visible (typically a euhedral feldspar phenocryst). The spherulites do not coarsen significantly away from the nucleus, and there is a fairly distinct boundary between the spherulite and the more granular groundmass. Spherulites are composed mostly of feldspar with intergrown, irregular blebs of quartz. Small oxides are common as inclusions that occur mainly along boundaries between the optically continuous wedges and along outer boundaries, accentuating the radial pattern of the intergrowth.

Samples EM28 and EM32, from the top of the knobs south and east of Eagle Mountain, have essentially no microgranular groundmass. These samples are composed entirely of phenocrysts of feldspar and ferromagnesian silicates surrounded by 2-3 mm patches of fairly well-developed but very fine-grained granophyre (Fig. 14).

Some of these granophyric patches are roughly circular and exhibit wedges with optical continuity, similar to the spherulites. The granophyre radiates outward from a feldspar nucleus. Each individual granophyre patch abuts against a neighboring patch with quartz grains and mafic phenocrysts "trapped" along the boundaries.

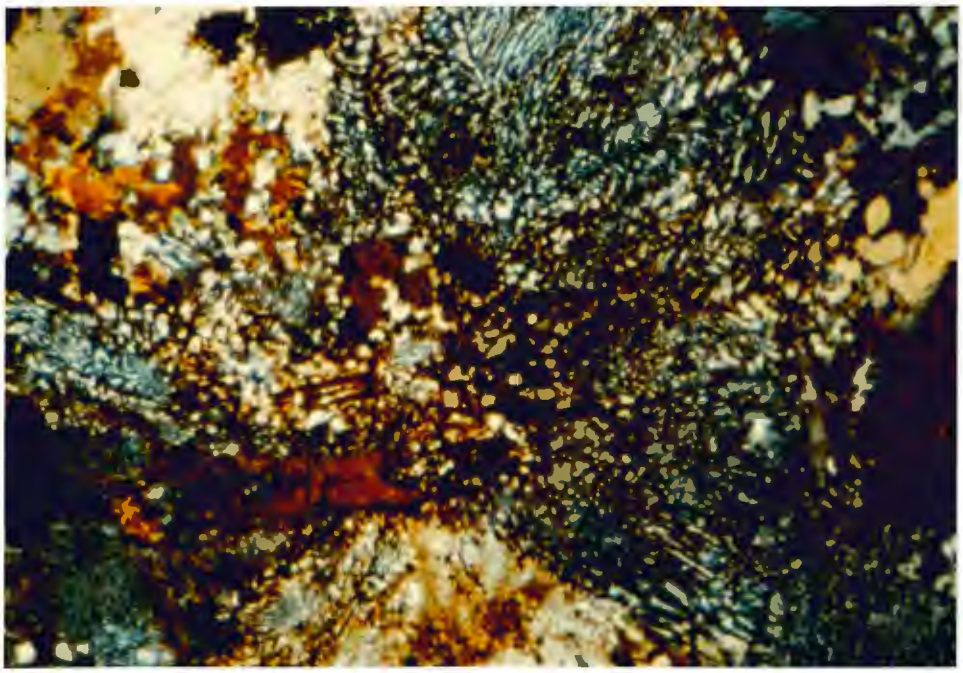

Figure 14: Photomicrograph of granophyric texture in Eagle Mountain granophyre (EM28). Field of view is approximately 3.5 x 2.0 mm; photographed under crossed polars.

The porphyritic nature of the granophyre indicates that physical conditions changed during crystallization of the magma. The feldspar, clinopyroxene, and magnetite phenocrysts may have crystallized at depth, before the magma rose toward the surface and reached the cooler, lower-pressure roof zone. The magma was undercooled enough to cause the formation of spherulites and some granophyric

intergrowths in the remaining liquid (Lofgren, 1971, 1974). The wide spatial variation in textures of this unit indicate local variations in physical conditions during crystallization. Deuteric alteration resulted in the oxidation and kaolinization of feldspars.

Metagabbro: South of the Eagle Mountain granophyre is a unit of medium-grained gabbro that shows the effects of high-temperature metamorphism and slight tectonic stress, possibly as a result of the intrusion of the magma that formed the granophyre. The distinguishing characteristics of this unit include medium grain size and black color, strong magnetism, and, in thin section, the presence of ubiquitous fine oxide grains and extensively altered interstitial material.

The metagabbro is exposed near the base of Eagle Mountain in the W ½ of the SW ¼ of Section 35 and near the base of the hills east and south of Eagle Mountain. The contact between the Eagle Mountain granophyre and this metagabbro is extremely sharp. There is no obvious chilled margin in either unit, but granophyre occurs as small veins (approximately 1 cm wide) within the metagabbro, indicating that the granophyre was emplaced after the gabbro. Based on the lack of chilled margins and the metamorphism of the gabbro, it seems likely that it was emplaced prior to the intrusion of the granophyre magma.

In hand sample the metagabbro is black, medium-grained, locally rust-stained, and very magnetic. Ophitic pyroxenes up to 1 cm across stand out in relief on the rough pitted surface where smaller grains of plagioclase and olivine have weathered away. It is composed of 60-70% plagioclase, 10-15% clinopyroxene, 5-10% olivine, 10-

15% opaque oxides, and about 10% secondary minerals including biotite, ortho-pyroxene, and epidote. In thin section it can be seen that the metagabbro contains abundant fine-grained granoblastic magnetite, biotite, and orthopyroxene in interstitial areas. The primary texture is ophitic with oikocrysts of clinopyroxene up to 1 cm across. Large Fe-Ti oxide grains are surrounded by a narrow reaction rim of very fine-grained biotite.

Plagioclase (average $An_{72}Ab_{26}Or_2$) (Fig. 6) occurs as sub- to euhedral, randomly-oriented laths that range from 0.5 mm to 4 mm in length, with an average length of 2 mm. The plagioclase appears slightly gray and cloudy in plane light due to minute inclusions, apparently of oxides. Many grains are slightly strained and exhibit undulatory extinction.

Clinopyroxene ($Ca_{45}Mg_{33}Fe_{22}$) (Fig. 7) occurs as large ophitic grains up to 1 cm across. The pyroxene is cloudy gray in plane light; under high power it can be seen that it is filled with minute grains of oxidized, exsolved minerals.

Olivine grains (Fo_{56}) (Fig. 7) are anhedral and average 1-2 mm in diameter. The center of most olivine grains is relatively fresh, but fractures and edges are almost all recrystallized to a very fine-grained, granular mixture of magnetite, orthopyroxene, and minor biotite.

Fe-Ti oxides are interstitial and have partially replaced silicate minerals along grain boundaries. They range from 1 mm to 7 mm across and are primarily magnetite with some fine lamellae and irregular inclusions of ilmenite. Most grains are surround-

ed by a rim (<0.1 mm wide) of very fine, red-brown biotite. Compositions of Fe-Ti oxides as determined by microprobe analyses are shown graphically in Figure 8.

Interstitial areas are filled with a mixture of fine-grained granular magnetite, clinopyroxene, orthopyroxene(?), and biotite. In sample EM52B, taken adjacent to the granophyre contact, some interstitial granophyre is present; this material may have been introduced into the gabbro by the intrusion of granophyre magma.

Olivine and plagioclase crystallized as discrete grains; pyroxene crystallized as oikocrysts enclosing plagioclase and olivine. Fe-Ti oxide grains crystallized interstitially, partially replacing silicate minerals along grain boundaries. Later high-temperature metamorphism caused feldspar and pyroxene grains to become clouded with exsolved, oxidized inclusions. Recrystallization of interstitial material produced fine-grained, granular pyroxene, biotite, and magnetite.

Metabasalt: Associated with the metagabbro is a zone of basalt and/or diabase that has also undergone high-temperature metamorphism. Basaltic hornfels might also be an appropriate name for this unit. In hand sample it is difficult to distinguish from the ophitic diabase; the distinction is based mainly on thin section examination. The metabasalt samples all contain ubiquitous fine-grained secondary oxides; the ophitic diabase samples do not contain these secondary oxide grains. Pyroxene grains in the metabasalt are all cloudy and gray with exsolved inclusions; in contrast, the pyroxene in the ophitic diabase looks very "clean" and free of inclusions. No recognizable olivine is present in the metabasalt, but olivine makes up 10-15% of the ophitic

diabase. The metabasalt samples have varying textures: grain size varies slightly, several samples are ophitic, and some samples are amygdaloidal.

Some of this metabasalt is found at the base of Eagle Mountain; it is most abundant in the hill south of Eagle Mountain, especially in the southwest corner of Section 35. The contact relationship between the metabasalt and metagabbro is ambiguous. The wide variation in geochemistry of analyzed metabasalt samples (see Appendix I) indicates that the unit may be made up of many individual blocks of either xenoliths or roof pendants within the metagabbro. A few local inclusions of metabasalt (too small to map) were also found within the granophyre in the valley north of Eagle Mountain, NE ¼ Section 34 (sample EM50); on the hill east of Eagle Mountain, NW ¼ Section 35 (sample EM33); and in the topographically lower areas in the center of Section 35 (sample EM73).

In outcrop the metabasalt is very dark gray, fine-grained, massive, and variably ophitic. Weathered surfaces are reddish-brown to light gray and featureless. It contains approximately 60-70% plagioclase, 10-20% clinopyroxene, up to 5% opaque oxides, and variable amounts of orthopyroxene and other secondary/metamorphic minerals.

Plagioclase laths (average $An_{77}Ab_{22}Or_1$) (Fig. 6) are sub- to euhedral and average 1 mm in length. The grains show polysynthetic twinning and slight normal zoning. Most feldspars are relatively unaltered.

Clinopyroxene ($Ca_{46}Mg_{39}Fe_{15}$) (Fig. 7) varies from subophitic to ophitic; the largest oikocrysts are about 7 mm across. In plane light the pyroxene is cloudy brownish-gray with exsolved oxidized inclusions.

Primary opaque oxide grains are rare, making up no more than 2% of the rock. Most are subhedral or interstitial and average 0.5 mm, with a maximum size of 1 mm across. Ilmenite is slightly more abundant than magnetite; ilmenite and magnetite occur as discrete grains or as grains with irregular patches of both minerals. Compositions of Fe-Ti oxides as determined by microprobe analyses are shown graphically in Figure 8.

Interstitial areas are filled with a fine-grained, granular material that appears to be a mixture of magnetite, biotite, chlorite, clinopyroxene, and, in at least one sample (EM8), orthopyroxene. In sample EM8 this material tends to be concentrated around oikocrysts. Two metabasalt samples (EM16, EM41) contain structures that may be amygdules. These areas are roughly circular and are now filled with very fine-grained reddish-brown material that could not be identified optically.

Miarolitic Granophyre: The miarolitic granophyre occurs in Section 35 on the north, northeast, east, and southeast shores of Whale Lake. It forms the small point that protrudes into the lake from the north shore as well as the entire point between Hand Creek and Whale Creek. The miarolitic granophyre and the Eagle Mountain granophyre are found only locally in direct contact; they are generally separated by the metagabbro unit. Where exposed, the contact between the two granophyres is

gradational, with small patches of what appears to be brick-red miarolitic granophyre occurring within red-brown Eagle Mountain granophyre. The distinguishing characteristics of the miarolitic granophyre include its brick-red color, the presence of miarolitic cavities, and, in thin section, the well-developed granophyric intergrowths.

In outcrop, the miarolitic granophyre is brick-red and medium-grained, with a rough, irregular weathered surface. It contains approximately 5% miarolitic cavities up to 5 mm across; the cavities are lined with euhedral feldspar and quartz crystals and indicate crystallization in the presence of a vapor phase (Lofgren, 1971). Granophyric texture is not obvious in hand sample. The rock also contains up to 5% quartz phenocrysts, approximately 1 mm across, and 5% greenish-yellow, altered mafic material.

In thin section it can be seen that the rock is composed primarily of well-developed granophyric intergrowths of feldspar and quartz (Fig. 15). Feldspar makes up 60-70% of the rock, quartz makes up about 30%, and opaque oxides make up less than 3% of the rock. The granophyric intergrowths radiate out from nuclei of euhedral alkali feldspar; the intergrowths are generally quite fine near the core and coarsen outward. The granophyric intergrowths form distinct grains, and where they grow into miarolitic cavities they have a blocky, equant feldspar habit. The feldspar within the granophyric intergrowths is generally in optical continuity with the feldspar nucleus, and, in at least one case, the feldspar of the granophyric intergrowth displays a simple twin that is continuous with the simple twin of the nucleus. The feldspar phenocrysts that act as nuclei to granophyric intergrowths average 1 mm across. Most

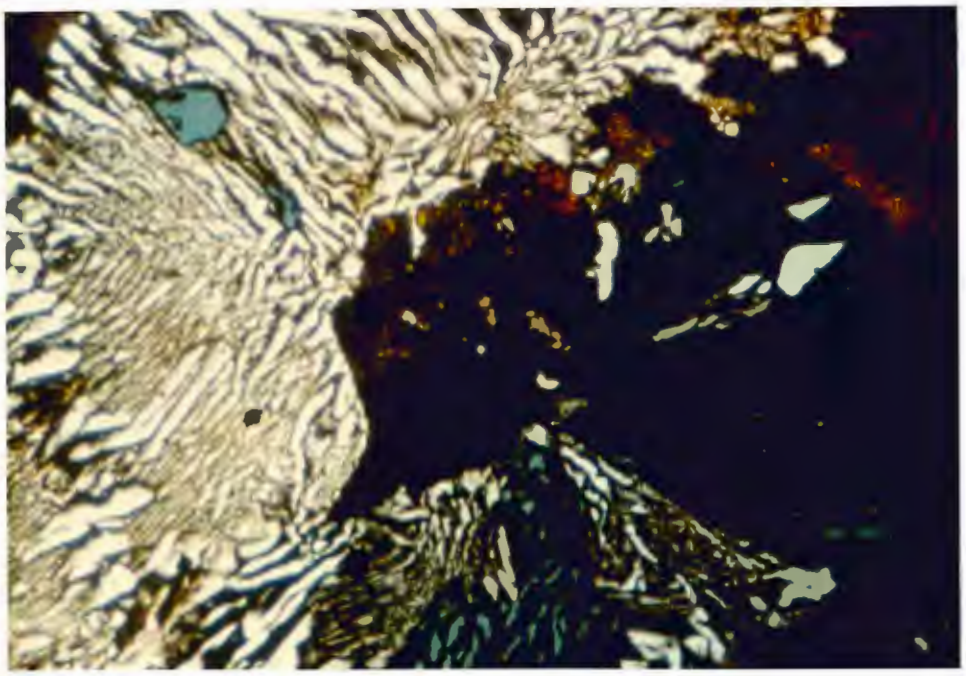

Figure 15: Granophyric texture in the miarolitic granophyre (EM57). At extinction is an alkali feldspar phenocryst that acted as the nucleus for the granophyric intergrowth. Field of view 3.5 x 2.0 mm; photographed under crossed polars.

show rectangular or rhombic sections. Many have very narrow albite twin lamellae, and some show simple twins. All feldspars are dark reddish-brown because of inclusions of very fine hematite dust. According to Taylor (1978) this is common in granitic rocks that have undergone low temperature hydrothermal alteration. Probe analyses indicate the composition of feldspar cores to be either albite ($Ab_{95\text{-}100}Or_{5\text{-}0}$) or orthoclase ($Ab_{5\text{-}0}Or_{95\text{-}100}$) (Fig. 6). If the granophyre crystallized at a temperature greater than approximately 660° C, one solid-solution alkali feldspar should have crystallized rather than two distinct feldspars (Tuttle and Bowen, 1958; Deer, Howie, and Zussman, 1966). This may also indicate that the granophyre has undergone low-

temperature hydrothermal alteration. Most of the feldspar phenocrysts contain no Ca whatsoever; the highest analyzed CaO content is 0.9 weight percent. Feldspar in the granophyric intergrowths varies from $Ab_{90}Or_{10}$ to Ab_1Or_{99}, with an average composition of $Ab_{42}Or_{68}$.

Independent quartz grains are concentrated along the boundaries between the granophyre intergrowths. Some quartz grains are in optical continuity with the quartz of the adjacent granophyre; other quartz grains, up to 2 mm across, are optically independent of the granophyre.

Magnetite grains are subhedral to anhedral, less than 0.5 mm across, scattered randomly throughout the rock, and partially oxidized to hematite. Euhedral zircon crystals are a minor accessory mineral. They occur primarily as inclusions within feldspar phenocrysts. Interstitial material and ferromagnesian siliates are completely altered to a yellowish-brown mixture of secondary limonite and chlorite.

Based on the CIPW norm for the average composition, the miarolitic granophyre is made up of approximately 38% quartz, 38% orthoclase, and 24% albite, indicating that it may have crystallized from a liquid of nearly eutectic composition. One or more feldspars, along with minor Fe-Ti oxides and ferromagnesian silicates, started to crystallize. Subsequently, quartz and feldspar crystallized simultaneously in granophyric intergrowths that nucleated on the feldspars. Extreme oxidation of Fe in the feldspars and opaque oxides, along with alteration of interstitial material to

limonite and chlorite, and production of end-member compositions in feldspar phenocrysts, indicates significant deuteric and/or hydrothermal alteration.

Rhyolite: Porphyritic rhyolite crops out on the south side of Whale Lake. In the SE ¼ of the SW ¼ of Section 35, the rhyolite is in contact with miarolitic granophyre. The contact is inconspicuous in outcrop and is gradational over a distance of about 2 m. At the contact the rhyolite is brecciated with small (1 cm) fragments in a matrix of granular quartz and feldspar (sample EM65). The rhyolite is distinguished by its massive nature, red-brown color, and aphyric groundmass with phenocrysts of feldspar and quartz.

In outcrop the rhyolite is reddish- or grayish-brown, massive, and porphyritic. Phenocrysts make up 5-15% of the rock; 5-10% are salmon-red alkali feldspar phenocrysts 1-8 mm across, and 1-5% are equant, euhedral quartz phenocrysts 1-3 mm in diameter. Quartz phenocrysts are more abundant near the contacts. The groundmass is aphyric to very fine-grained and varies from red-brown near the margins of the unit to gray-brown in the interior portions of the unit.

In thin section (Fig. 16), the rhyolite is porphyritic with phenocrysts of feldspar and quartz in a fine-grained groundmass with local micropoikilitic texture. Feldspar phenocrysts vary from anhedral to euhedral and range in size from 1 to 5 mm. Most have either embayments or ragged edges, indicating some resorption, and most are heavily clouded with minute hematite flakes, making optical identification nearly impossible. Simple twins are visible in a few grains. Probe analyses indicate the

feldspar phenocrysts have variable compositions; cores range from $Ab_{95}Or_5$ to Or_{100} (Fig 6). Zoning is inconsistent, but most phenocrysts probed have sodic rims. In grains with sodic cores there is a slight outward increase in K followed by an increase in Na near the rim. In grains with potassic cores, K decreases steadily from core to rim.

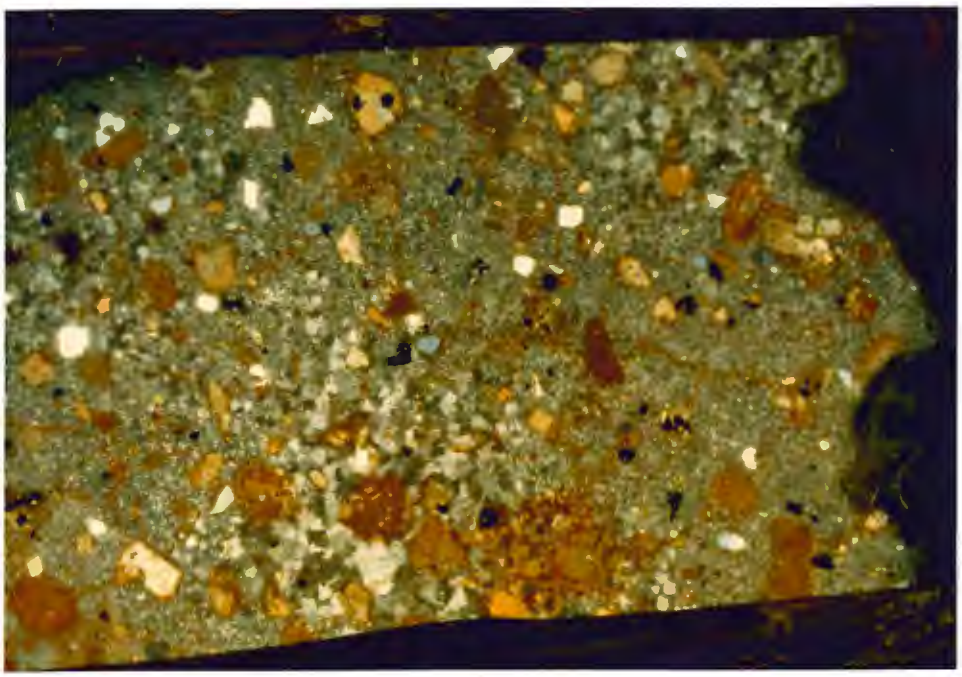

Figure 16: Photo of entire thin section of rhyolite (EM55). Note hematite-stained feldspar phenocrysts. Field of view is approximately 4 cm across; photographed under crossed polars.

Quartz phenocrysts range from 0.5 mm to 4 mm across; most are about 1 mm across and are inclusion-free. At least some are euhedral bipyramids of inverted beta-quartz. Some of the larger phenocrysts are embayed, and some of the smaller ones are angular, broken fragments.

Ferromagnesian silicates appear to have been a minor phase (1-2%) and are now almost totally replaced by magnetite and a mixture of secondary phyllosilicates. A few relict scraps of clinopyroxene remain; the best preserved ones are inclusions within feldspar phenocrysts. Magnetite occurs in three habits: as 1 mm subhedral phenocrysts making up 1-2% of the rhyolite, as tiny (<0.05 mm) anhedral grains scattered throughout the groundmass, and as scrappy grains resulting from the alteration of ferromagnesian silicates. Euhedral zircon occurs as accessory micro-phenocrysts.

Groundmass in the rhyolite is made up of very fine-grained quartz, feldspar, and hematite. The quartz is micropoikilitic, with variable grain size. It seems to be coarsest closest to contacts. In all samples the groundmass is full of very fine-grained hematite dust. The hematite is not uniformly distributed; it is concentrated most heavily around phenocrysts and along fine fractures. No textures are preserved that might indicate the mode of eruption of this rhyolite.

Rare mafic xenoliths range from 4 mm to 1 cm in size. The inclusions are now mainly fine-grained, granular magnetite plus feldspar and pyroxene. Borders of the xenoliths are fuzzy and indicate partial reaction with the rhyolite magma. Xenoliths are slightly more abundant near the contact with the miarolitic granophyre.

Ophitic Diabase: Ophitic diabase, which appears to be the youngest intrusive unit, is exposed discontinuously along a line that trends approximately N30°W through the northeastern part of the area, intruding the ferrodiorite, Eagle Mountain

granophyre, and miarolitic granophyre units. The characteristics that distinguish the diabase are the presence of olivine grains, the "clean", inclusion-free nature of the pyroxene and plagioclase, and the absence of fine-grained, secondary oxide grains.

In hand sample the diabase is dark gray, fine-grained, and massive. Weathered surfaces are red-brown and rough. Ophitic texture is apparent in most samples. The diabase is made up of 60-70% plagioclase, 10-20% ophitic clinopyroxene, 10-15% olivine, and 2-5% Fe-Ti oxides.

Plagioclase ($An_{75}Ab_{25}Or_1$) (Fig. 6) occurs in sub- to euhedral laths averaging 1 mm in length; slight normal zoning is common. Most grains show sharp albite twins and are relatively fresh.

Augite ($Ca_{42}Mg_{35}Fe_{23}$) (Fig. 7) occurs as large oikocrysts up to 6 mm across; they are light brown in plane light and have very little exsolved material.

Olivine (Fo_{35}) (Fig. 7) occurs in small (approximately 0.5 mm) rounded grains. In most cases, several grains occur together in interstitial areas. Most of the olivine is partially altered to iddingsite + serpentine + chlorite + magnetite.

Fe-Ti oxide grains are sub- to euhedral. Examination in reflected light reveals many platy grains of ilmenite averaging 0.5 mm in length, along with blocky, equant magnetite grains, up to 1 mm across, containing lamellae or irregular patches of ilmenite. Compositions of Fe-Ti oxides as determined by microprobe analyses are shown graphically in Figure 8.

The small percentage of mesostasis is mostly altered to a yellow-green mixture of what appears to be chlorite and serpentine.

Plagioclase, olivine, and Fe-Ti oxides crystallized from the magma early; pyroxene crystallized as oikocrysts enclosing plagioclase and olivine. The fine grain size of all minerals indicates the magma crystallized fairly rapidly. Minor alteration of mesostasis and olivine grains occurred following crystallization; the hydrous nature of most secondary minerals indicates low-temperature conditions of alteration.

GEOCHEMISTRY

INTRODUCTION

Thirty-six samples, chosen on the basis of freshness and geologic and geographic distribution, were analyzed for eleven major oxides, seventeen trace elements, H_2O^+, and CO_2. Major and trace element analyses were done by the author using a Siemens SRS 300 XRF. To prepare samples, an aliquot was taken from each sample, using a water-lubricated saw. Saw marks were removed using a lap wheel; samples were ground in steel jaw crushers, then reduced to powder using a tungsten carbide shatterbox. For major elements, glass discs were prepared by the following method: 0.4000 g of sample and 3.6000 g $Li_2B_4O_7$ were weighed into glass vials; the vials were placed in a mixer for 2 minutes, and the contents were then transferred to a Pt crucible; 2 drops of LiI was added to the powder; the crucible was heated for 10 minutes; the liquid was poured into a Pt pan and quenched. For trace elements, pellets were prepared by the following method: 1.0000 g sample, 0.5000 g microcrystalline cellulose, and an acetate ball were placed in a vial; the vial was placed in a mixer for 10 minutes; the acetate ball was removed, and the mixed powder was placed in a die with a small amount of cellulose acetate and pressed at 20 tons for 5 minutes. Several analyses have low totals, but standards that were run with each batch indicate the analyses are reproducible (See Appendix I). Two analyses, both in the syenogabbro unit, were rejected because totals were <97%.

One sample from each rock unit except the ferrodiorite was selected for rare earth element (REE) analysis. REE, H_2O^+, and CO_2 analyses were done by Nuclear Activation Services, Inc. A list of analyzed samples, arranged by lithologic unit, is given in Table 1. (See Figure 5 for a map of sample locations.) The average major and trace element composition of each unit is given in Table 2; calculated CIPW norms for these averages are given in Table 3. Complete major, trace, and rare earth element data for all analyzed samples can be found in Appendix I; CIPW norms for all analyzed samples are listed in Appendix II.

TABLE 1
Samples Analyzed for Major and Trace Elements
* = REE analysis + = from Green, 1986

Metabasalt (MB): EM16, EM19*, EM45
Metagabbro (MGA): EM9, EM30*, EM52B, EM78
Ophitic Diabase (OD): EM64*, EM75
Syenogabbro (SG): EM39, EM60*, EM61, EM62, EM80
Ferrodiorite (FD): EM38, EM63, EM81, EM82
Eagle Mt. Granophyre (EMG): EM1+, EM4, EM10A*, EM21, EM28, EM32, EM34, EM49, EM52A
Rhyolite (RY): EM17, EM53, EM54*, EM56, EM67
Miarolitic Granophyre (MG): EM57, EM68*, EM43

TABLE 2
AVERAGE COMPOSITIONS OF UNITS

	MB	MGA	OD	SG	FD	EMG	RY	MG
	N=3	N=4	N=2	N=3	N=4	N=10	N=5	N=3
SiO2	46.7	45.6	48.3	52	50.1	70.1	72.4	73.5
TiO2	1.5	2.6	1.8	2	2.1	0.6	0.4	0.3
Al2O3	15.8	13.8	15.6	16.2	12.1	12.7	12	12
FeO*	11.3	15.9	12.2	10.3	18.6	4.7	4.2	2.9
MnO	0.2	0.2	0.2	0.2	0.3	0.1	0.1	0.04
MgO	7.4	6.6	6.9	1.9	1.7	0.4	0.6	0.3
CaO	11.3	9.6	10	8.3	6.7	1.6	0.8	0.3
Na2O	2.3	2.3	2.5	3.8	3.4	3.7	3	2.6
K2O	0.3	0.6	0.6	1.4	1.3	4.2	4.8	5.8
H2O+	1	0.6	0.95	0.92	0.8	0.34	0.43	0.67
P2O5	0.1	0.1	0.2	0.4	0.8	0.1	0.02	---
CO2	<0.01	<0.01	<0.01	<0.01	<0.01	<0.01	<0.01	<0.01
TOTAL	97.9	97.9	99.25	97.42	97.9	98.54	98.73	98.37
Sc	34	31	24	23	24	6	5	1
V	260	433	209	41	6	13	12	5
Cr	196	80	150	37	24	19	15	12
Co	58	72	57	33	30	46	46	56
Ni	143	105	137	4	3	6	4	5
Cu	64	318	148	95	62	22	18	8
Zn	84	131	103	113	203	98	94	95
Ga	19	23	23	28	29	23	21	26
Rb	10	19	17	43	43	152	126	155
Sr	247	264	310	365	324	146	126	40
Y	19	25	29	46	80	60	72.2	95
Zr	78	126	143	195	331	524	689	736
Nb	5	7	9	14	24	32	34	57
Ba	84	132	170	358	485	978	1537	1010
La	9	11	15	26	36	67	72	63
Pb	4	5	2	6	4	23	17	63
Th	---	2	0.2	4	3	14	13	17

Major elements in weight %, trace elements in ppm
FeO* = total iron as Fe2+

MB = Metabasalt
MGA = Metagabbro
OD = Ophitic Diabase
SG = Syenogabbro
FD = Ferrodiorite
EMG = Eagle Mt. Granophyre
RY = Rhyolite
MG = Miarolitic Granophyre

TABLE 3
CIPW NORMS FOR AVERAGE COMPOSITIONS

	MB	MGA	OD	SG	FD	EMG	RY	MG
Apatite	0.19	0.26	0.44	0.91	1.75	0.14	0.05	0.16
Ilmenite	2.91	4.98	3.41	3.89	4.08	1.09	0.74	0.51
Magnetite	2.22	3.11	2.41	2.02	3.65	0.93	0.83	0.57
Orthoclase	1.83	3.31	3.37	7.98	7.87	25.06	28.31	34.44
Albite	19.06	19.66	21.11	32.01	28.41	31.32	25.22	21.83
Anorthite	32.19	25.69	29.67	23.26	14.14	5.39	3.89	0.78
Diopside	19.04	17.69	15.45	13.31	12.51	1.93	---	---
Hypersthene	8.72	10.28	15.79	9.92	21.83	6.09	6.97	4.53
Olivine	10.63	12.48	6.64	---	---	---	---	---
Quartz	---	---	---	2.82	2.87	26.25	31.72	33.74
Corundum	---	---	---	---	---	---	0.42	1.15
TOTAL	96.79	97.46	98.29	96.11	97.11	98.19	98.15	97.71
MG#	54	43	50	25	13	13	19	13
Plag An	77	72	75	65	45	40		

Calculated assuming Fe2+/Total Fe = 0.85

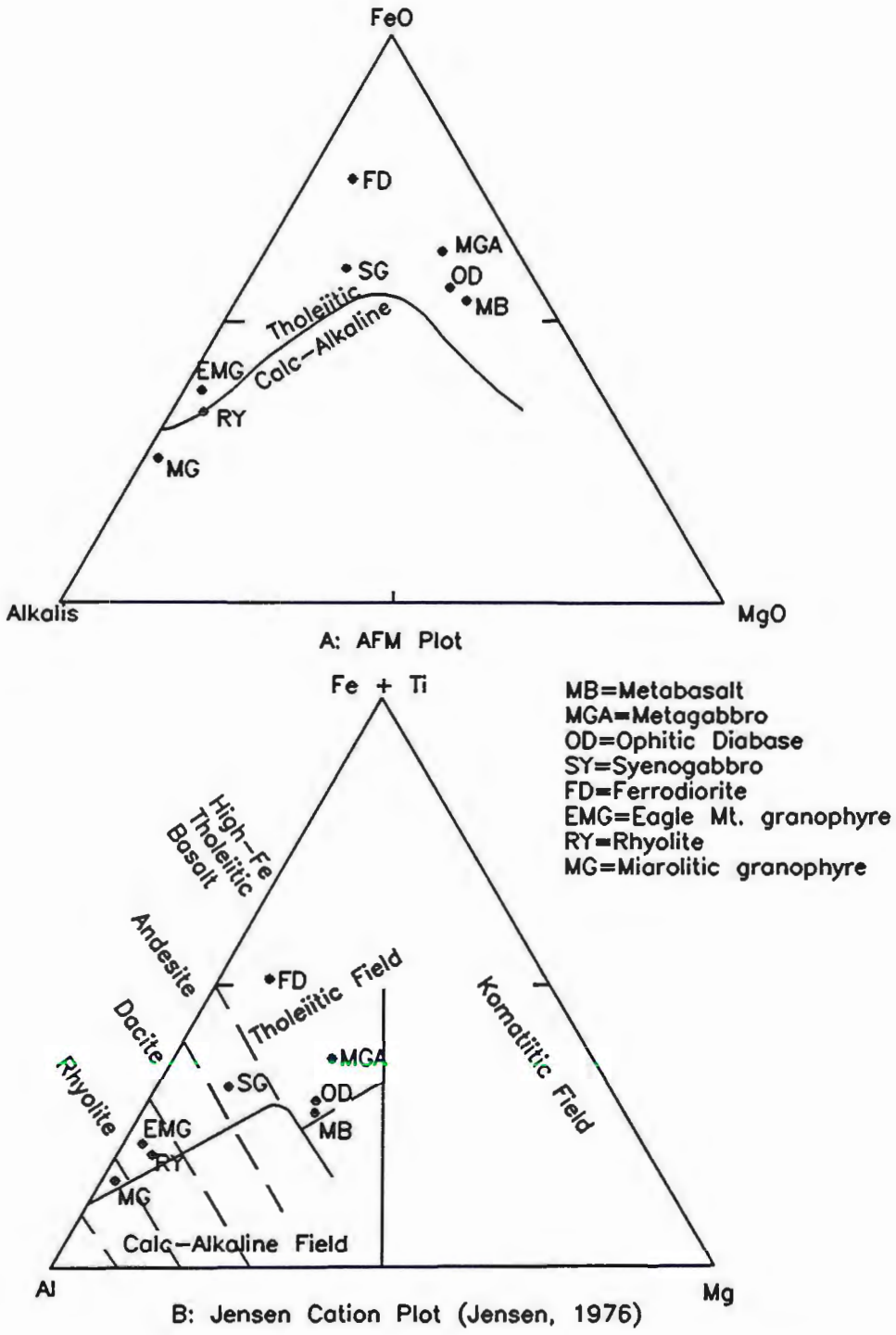

Figure 17: Average composition of units plotted on AFM and Jensen cation diagrams.

DESCRIPTION OF UNITS

Metabasalt and Metagabbro: The metabasalt and metagabbro units are chemically the most primitive units in the area, but neither is as primitive as many basalts in the North Shore Volcanic Group (Green, 1982a; Brannon, 1984). Both show some evidence of high temperature metamorphism. The average metabasalt composition has the highest Mg# (54) [the molar proportion of MgO/(MgO + FeO)], highest MgO, CaO, Cr, and Ni concentrations, and low SiO_2, P_2O_5, TiO_2, and incompatible trace elements (see Table 2). The average metagabbro has an Mg# of 43 and contains less MgO, CaO, Cr, and Ni but more TiO_2, FeO* (total Fe reported as Fe^{2+}), and incompatible trace elements (see Table 2). Analyses of individual samples show overlap in values for nearly all elements. All samples plot in the tholeiitic field on AFM and Jensen diagrams (Fig. 17A-B) and are basalts in the Irvine-Baragar classification (1971). Both units are olivine-normative. A REE plot for the most primitive metabasalt (EM19) shows a slight enrichment in light rare earth elements (LREE) and a positive Eu anomaly (Fig. 18), a pattern similar to that of other more primitive olivine tholeiites of the North Shore Volcanic Group (NSVG) (Basaltic Volcanism Study Project, 1981; Brannon, 1984; Green, 1986). A REE

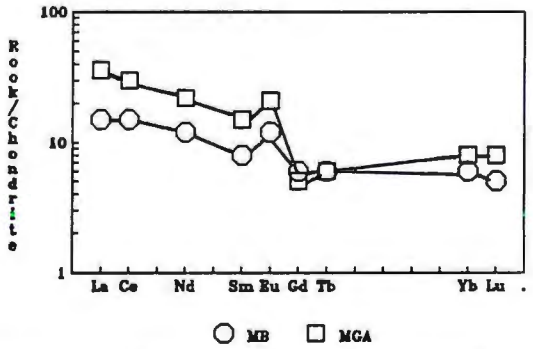

Figure 18: Rare earth element plot for metabasalt and metagabbro.

plot for the metagabbro (EM30) also shows enrichment of LREEs and a positive Eu anomaly (Fig. 18).

Ophitic Diabase: Chemically, the ophitic diabase is somewhat more evolved than the metabasalt and metagabbro. For the average composition the Mg# is 50, and it contains somewhat more SiO_2, FeO*, TiO_2, and incompatible trace elements than the metabasalt or metagabbro. The average composition for the ophitic diabase plots within the tholeiitic field on AFM and Jensen diagrams (Fig. 17A-B) and is a basalt in the Irvine-Baragar classification. The diabase is olivine-normative and contains modal olivine. A REE plot of sample EM64 shows a relatively straight line with a slight enrichment in LREEs and no Eu anomaly (Fig. 19).

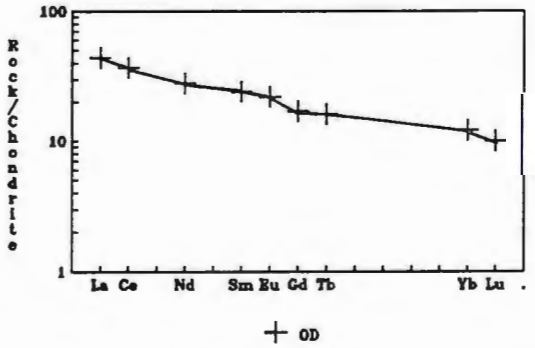

Figure 19: Rare earth element plot for ophitic diabase.

Syenogabbro and Ferrodiorite: These two units are strongly evolved mafic rocks. The syenogabbro has an Mg# of 25, and the ferrodiorite has an Mg# of 13. Both contain an average of approximately 50% SiO_2 and more than 2% TiO_2, but the average syenogabbro contains more Al_2O_3, MgO, and CaO and much less FeO* and P_2O_5 than the average ferrodiorite. Analyses of individual samples show some overlap in values between the two units. Both units are quartz normative.

Trace element compositions show the ferrodiorite to be somewhat more evolved than the syenogabbro: V and Cu are higher in most syenogabbro samples, but Zn, Y, Zr, and Nb are higher in the ferrodiorite; again there is overlap between units. The average composition for both units plots within the tholeiitic field on AFM and Jensen diagrams; on a Jensen diagram the ferrodiorite plots within the high-iron tholeiitic basalt field and the syenogabbro plots in the andesite field (Fig. 17B). A REE plot for the syenogabbro (EM60) shows a slight enrichment in LREEs (approximately 100X chondrites), a positive Eu anomaly, and heavy rare earth elements (HREE) approximately 25X chondrites (Fig. 20). No REE analysis was done for the ferrodiorite because it is not thought to represent a liquid composition.

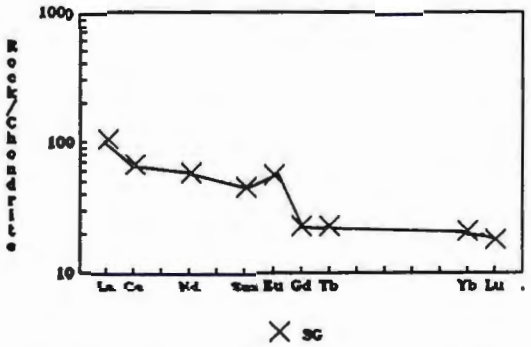

Figure 20: Rare earth element plot for syenogabbro.

Rhyolite, Eagle Mountain Granophyre, and Miarolitic Granophyre: Five rhyolite samples were analyzed; compositions are variable. SiO_2 ranges from 69% to 76%, Al_2O_3 from 11% to 12%, Na_2O from 2.2% to 3.3%, K_2O from 4.3% to 5.6%, and CaO from 0.5% to 1%. The two samples closest to the margins of the rhyolite (EM54 and EM67) have highest SiO_2. The rhyolites contain the highest average Ba and La of all the rock units analyzed. The average composition plots as a rhyolite on a Jensen plot (Fig. 17B) and in the IUGS classification (Streckeisen, 1979). The rhyolite

contains nearly equal amounts of normative albite and orthoclase. It also contains a small percentage of corundum in the norm, which is consistent with the visible alteration of the feldspars. The REE plot of sample EM54 shows a strong enrichment of LREEs (approximately 250X chondrites), a negative Eu anomaly, and HREEs approximately 30X chondrites (Fig. 21).

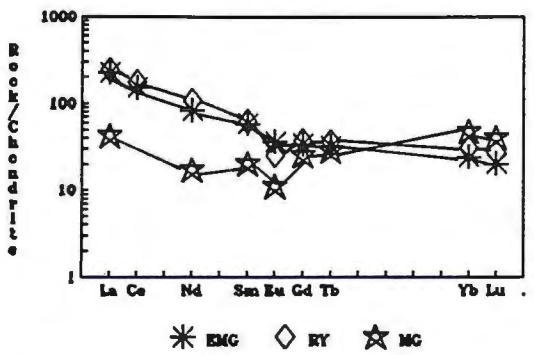

Figure 21: Rare earth element plots for rhyolite, Eagle Mountain granophyre, and miarolitic granophyre.

Ten samples of Eagle Mountain granophyre were analyzed, and the analyses are remarkably consistent. SiO_2 varies from 69% to 71%, Al_2O_3 from 12.5% to 12.8%, FeO* from 4% to 5%, Na_2O from 3% to 4%, K_2O from 3.8% to 5%, and CaO from 1.4% to 1.8%. Using the average composition, the ratio of K_2O/Na_2O is 1.1. Trace elements are also relatively consistent. The average composition for this granophyre unit plots within the tholeiitic field on AFM and Jensen diagrams (Fig. 17A-B); it is a dacite in the Irvine-Baragar classification, a rhyolite in the Jensen classification, and a rhyodacite in the IUGS classification. Normatively this granophyre contains slightly more albite than orthoclase and approximately equal amounts of quartz and orthoclase. A REE plot of Eagle Mountain granophyre sample EM10A is very similar to the rhyolite with a strong enrichment in LREEs (approximately 250X chondrites), a slight negative Eu anomaly, and HREEs approximately 30X chondrites (Fig. 21).

Three samples of miarolitic granophyre were analyzed, and these show only slight variations. SiO_2 ranges from 73% to 74%, Al_2O_3 from 11.8% to 12%, Na_2O from 2% to 3%, and K_2O from 5% to 6%. The miarolitic granophyre contains almost no calcium, with an average of only 0.25%. Using the average composition, the ratio of K_2O/Na_2O is 2.3. It has relatively high concentrations of the high field-strength trace elements Y, Zr, and Nb. The average composition for this granophyre plots in the calc-alkaline field of an AFM diagram, but in the tholeiitic field of the Jensen diagram (Fig. 17A-B). It is a rhyolite in all classification systems. Normatively, it contains more orthoclase than albite and approximately equal amounts of quartz and orthoclase; all samples contain minor corundum in the norm and are visibly somewhat altered. A REE plot for sample EM68 is quite distinctive and anomalous (Fig. 21), with LREEs (approximately 40X chondrites) depleted relative to HREEs (approximately 50X chondrites) and a large negative Eu anomaly. Several authors (Hanson, 1978; Nabelek & Russ-Nabelek, 1988; Simmons et al., 1988) have found a relationship between high HREE concentrations and F-rich volatiles; high F concentration is also fairly typical in A-type granites. However, no F analyses are available for the miarolitic granophyre, and no fluorite was identified in thin section.

To illustrate the distinctive geochemical character of the two granophyre units, the average composition for the Eagle Mountain granophyre is plotted against the average composition for the miarolitic granophyre in Figure 22. Points do not represent actual concentrations of elements, only a ratio between the two units. A line

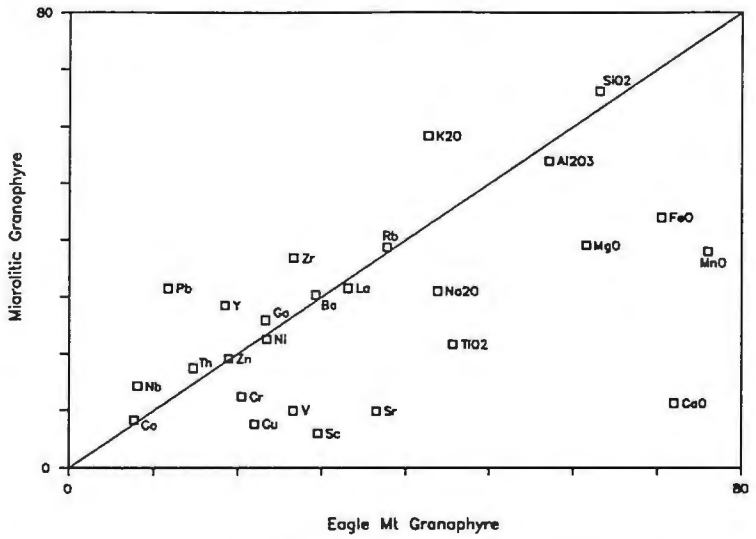

Figure 22: Comparison of chemistry of average composition of granophyre units. Points represent ratios of concentrations in the two units.

of slope=1 has been drawn to represent a line of equal concentrations in both units. Elements that fall on or within 10% of the line include SiO_2, Al_2O_3, Rb, La, Ba, Ga, Ni, Zn, and Co. Relative to the miarolitic granophyre, the Eagle Mountain granophyre is enriched in Na_2O, MgO, FeO, MnO, CaO, P_2O_5, TiO_2, Sr, Sc, Cu, V, and Cr. The miarolitic granophyre is enriched only in K_2O, Zr, Pb, Nb, and Y.

A-TYPE GRANITES

I-type (igneous-source partial melt) granites and S-type (sedimentary-source) granites were first described by Chappell and White (1974). This genetic type of discrimination was later extended to indicate tectonic setting when I-type granites were divided into two subgroups: A-type (anorogenic, alkaline, anhydrous) granites derived from recycled, dehydrated continental crust and M-type granites derived directly from melting of subducted oceanic crust or overlying mantle (Whalen et al., 1987). A-type

granites have been recognized in many parts of the world, and, although they are not confined to any one time period, they seem to be especially characteristic of the mid- to late-Proterozoic (1.77 to 1.03 b.y.). They typically form part of highly contrasting bimodal mafic/felsic associations; many of the granites are rapakivi, and they are commonly found with anorthosites and a mangeritic series of intermediate rocks (Anderson, 1983). A-type suites seem to represent the final plutonic event both in orogenic belts and in rift-related terranes of shield areas (Whalen et al., 1987). According to Anderson (1983), the most likely tectonic regime for the formation of A-type granites is one involving some form of mantle diapirism.

Textural and experimental evidence (Clemens et al., 1986; Whalen et al., 1987) indicate that A-type granites formed from relatively high temperature, water-under-saturated, completely molten magmas that were emplaced at high levels. Anderson (1983) has suggested that crystallization occurred over a temperature range of 640-790°C and over a wide range of oxygen fugacity. Several studies (Loiselle and Wones, 1979; Collins et al., 1982; Anderson, 1983) have shown that A-type granites, in comparison to I-, M-, and S-type granites, are characterized by higher K_2O, K_2O/-Na_2O, Fe/Mg, and F, and by lower CaO, MgO, and Al_2O_3. They are also enriched in some large-ion lithophile elements including Rb, Ba, Ga, Y, Zr, Th, Nb, U, and REE (except Eu). Mineralogically, alkali feldspars predominate over plagioclase feldspars; mafic silicates are extremely iron-rich and usually include annite-rich biotite, alkali amphiboles, and/or sodic pyroxene; fluorite is a common accessory mineral (Anderson,

1983). Micrographic intergrowths of quartz and alkali feldspars are very common. A-type suites often include a range of compositions from subalkaline to peralkaline (Whalen et al., 1987).

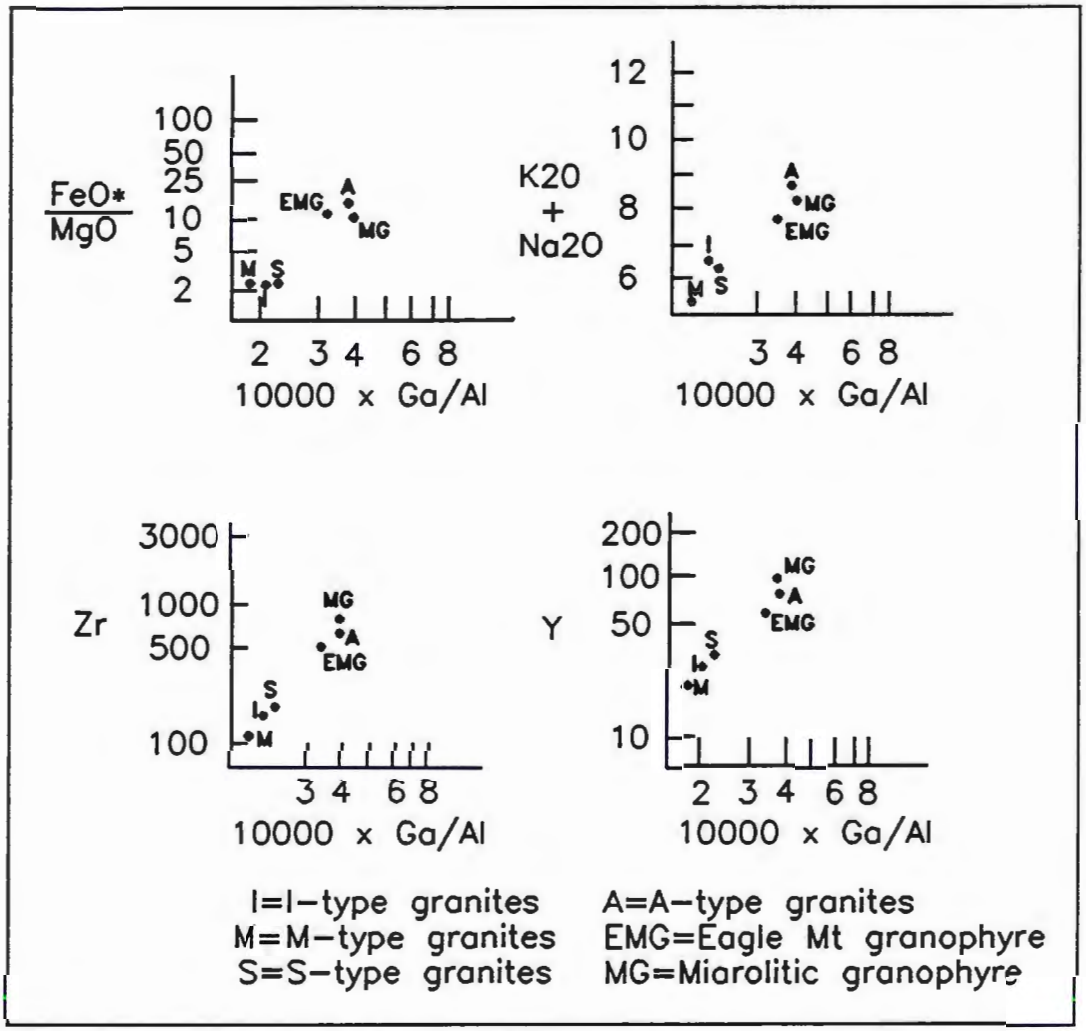

Figure 23: Ga/Al ratios for granites. All represent average compositions. Adapted from Whalen et al., 1987.

One of the most diagnostic features of the A-type granites is a high Ga/Al ratio (Collins et al., 1982; Whalen et al., 1987). In Figure 23 values for various major and

trace elements are plotted against Ga/Al for the Eagle Mountain granophyre, the miarolitic granophyre, and the average A-type, I-type, S-type, and M-type granites from Whalen et al. (1987). Both granophyre units from the study area plot near Whalen's average A-type granite and far from the I, M, and S granites.

Another approach to granite classification is based entirely on tectonic setting. Pearce et al. (1984) use trace element discrimination diagrams to subdivide granites into four tectonic settings: ocean ridge granites (ORG), volcanic arc granites (VAG), within-plate granites (WPG), and collision granites (COLG). Based on tectonic setting, most A-type granites are within-plate granites; these are further subdivided into three groups based on the type of crust they intruded: 1) crust of normal thickness, 2) strongly attenuated crust, and 3) oceanic crust. Pearce et al. (1984) interpret WPG as being derived from enriched mantle sources. Significant trace element differences were recognized between these groups: ORG and WPG have high Y concentrations and high HREE concentrations; WPG also have high Nb and Ta concentrations. The miarolitic granophyre of Eagle Mountain fits well into this category with nearly 100ppm Y, 57ppm Nb, and HREE concentrations approximately 50X chondrites. In Figure 24, values for Nb vs. Y and Rb vs. (Y + Nb) from the Eagle Mountain granophyre and miarolitic granophyre are plotted on two discrimination diagrams. The values for both units plot well inside the within-plate granite field.

Although the granophyres of the Eagle Mountain area do not constitute a typical A-type granite suite, since they lack biotite, fluorite, and a peralkaline phase,

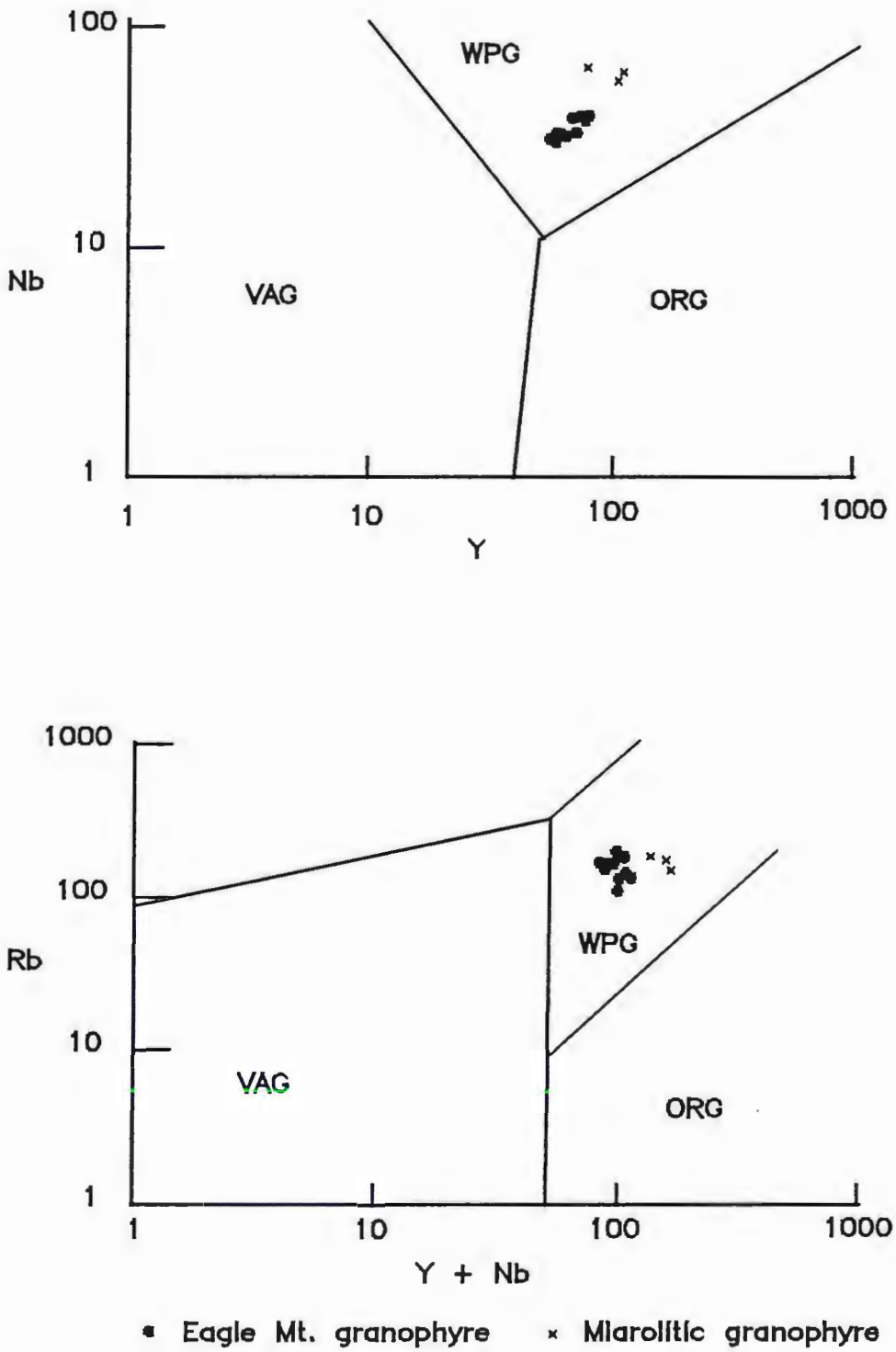

Figure 24: Granite discrimination diagrams. Adapted from Pearce et al., 1984.

their tectonic setting (within-plate, rift-related) and many of their chemical characteristics (high K_2O, high K_2O/Na_2O, and low CaO, MgO, and Al_2O_3) are consistent with the A-type granite classification.

PETROGENESIS

INTRODUCTION

One of the most fundamental ideas in igneous petrology is that of fractionation (or differentiation)--the formation of more than one rock type from a single parental magma. The various mechanisms of fractionation all involve the movement of atoms of one element relative to atoms of other elements, thus producing variations in the chemical composition of a magma. The inferred extent of fractionation, especially in tholeiitic suites, is based on the SiO_2 content and the Mg#, which is the molar proportion of MgO/(MgO+FeO). Rocks with low SiO_2, TiO_2, and incompatible trace elements, but high Mg# and compatible trace elements, are considered to be less fractionated (primitive), and those with high SiO_2, TiO_2, and incompatible trace elements and low Mg# and compatible trace elements are considered to be highly fractionated (evolved).

Based strictly on chemical variation, the rock units in this field area could be interpreted as a possible fractionation series ranging from relatively primitive mafic rocks with SiO_2<50% and Mg#>50 to highly evolved felsic rocks with SiO_2>70% and Mg#<20. If there is a genetic relationship among these rocks of varying composition, several fractionation mechanisms could explain the relationship:

1) Fractional crystallization: Assuming a relatively primitive gabbroic parent magma, if crystallizing phases are separated from the liquid by settling, floating, or some other process, the crystals could be isolated from reacting with the remaining

liquid. As the early-formed mafic minerals are removed, the liquid continues to evolve to more and more felsic compositions. After solidification of the magma, the resulting rocks show successively mafic, intermediate, and felsic compositions. If crustal material is assimilated by the crystallizing magma, it may not significantly change the major-element composition of the resulting rocks, but it may alter the proportion of differentiated low-temperature end products, depending on the composition and volume of the assimilated material. Trace element and radioisotope ratios may be changed more significantly by assimilation.

2) Partial melting of mantle or crustal rocks: During partial melting of mantle or crustal rocks, liquid composition varies as melting proceeds. Liquid extracted at an early stage of melting is richer in incompatible components; liquid extracted at a later stage of melting contains a larger proportion of the more compatible components. Liquid composition also varies depending on the frequency with which the liquid is removed. During batch partial melting, the liquid remains at the site of melting and is in equilibrium with the residual solid until it is removed as a single batch. Batch partial melting should produce a single magma composition that is controlled by the extent of the melting. During fractional partial melting, the liquid is removed continuously from the magma chamber, preventing equilibration of liquid and solid. This produces step-like, discontinuous changes in magma composition with no intermediate compositions.

3) Silicate liquid immiscibility: As a tholeiitic magma crystallizes at low pressure, it can reach a certain composition at which it is no longer stable; two coexisting but immiscible liquids become the stable configuration of the system. An Fe-rich liquid separates from a Si-rich liquid; if spatially segregated, these liquids can crystallize to form rocks of contrasting mafic and felsic composition (Roedder, 1951; Philpotts, 1976, 1982).

For this study, these three mechanisms were examined in relation to the Eagle Mountain units in an attempt to determine the nature of the relationships among the rock units.

FRACTIONAL CRYSTALLIZATION VS. PARTIAL MELTING

Variation Diagrams: If a series of rocks representing magma compositions are the result of fractional crystallization of a single parent magma, plots of major elements vs. SiO_2 should reveal systematic variations in the concentration of major elements. Comparison of geochemical analyses of the Eagle Mountain rocks with analyses of representative NSVG rocks indicates that, with the exception of the syenogabbro and ferrodiorite units which show anomalous concentrations of TiO_2, MgO, K_2O, and P_2O_5, the rock units at Eagle Mountain may be fairly representative of magma compositions. As a first test of formation by fractional crystallization, variation diagrams showing plots of major elements vs. SiO_2 for the units at Eagle Mountain are presented in Figure 25. Examination of these plots shows that in a very broad sense the rock units do exhibit the trends that would be expected from fractional

crystallization of a tholeiitic magma, although there is considerable scatter in the low-SiO_2 units and a wide compositional gap between the mafic and felsic rocks. The scatter can be at least partially explained by the high-temperature metamorphism of the metabasalt and metagabbro units and the cumulate nature of the ferrodiorite. In general, MgO and CaO decrease with increasing SiO_2; Na_2O varies from only 2% to 4.5%, but it increases steeply until SiO_2 reaches about 56%, then it decreases sharply; K_2O increases with increasing SiO_2; FeO values show much scatter, but generally decrease with increasing SiO_2. The ferrodiorite, which is fairly evolved, shows higher FeO and lower CaO values than the other mafic rocks of equivalent SiO_2 content.

However, the process of melting is in many ways the reverse of crystallization, and a magma formed by partial melting can also undergo fractionation while crystallizing. Thus, magmas generated by partial melting of crustal material can show major element variations very similar to the variations produced by fractional crystallization, and the two processes cannot be discriminated on the basis of major element chemistry alone.

Trace elements also show characteristic patterns in rocks formed by fractional crystallization or by partial melting. Trace elements show an affinity for particular phases; the distribution coefficient (K_d) is the ratio of the concentration of a given element in a particular mineral phase to the concentration of the same element in the liquid. If the K_d is >1, the element will be preferentially concentrated in the solid. If the K_d is <1, the element will be preferentially concentrated in the liquid. Those trace

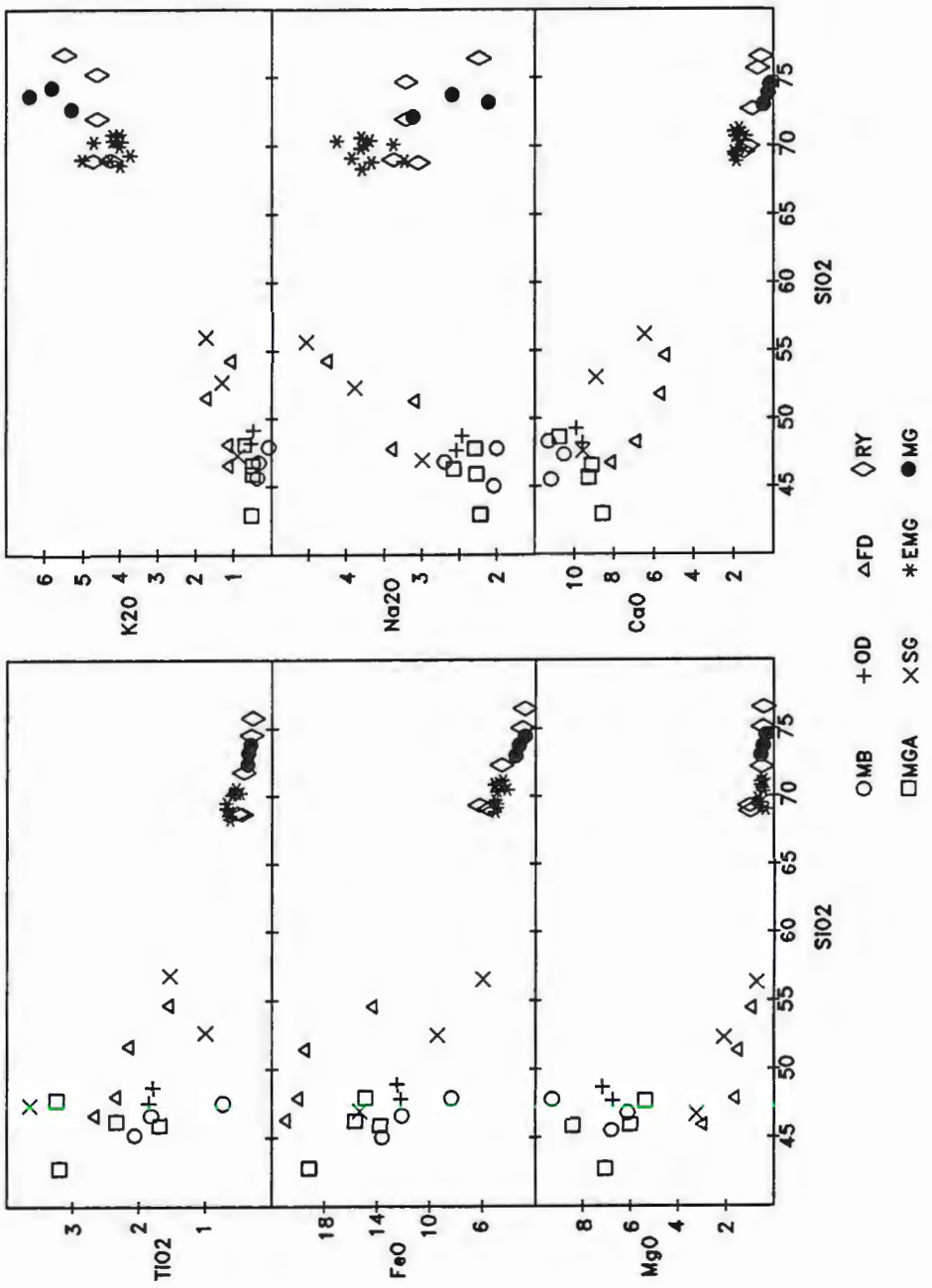

Figure 25: Major elements vs. SiO_2 for Eagle Mountain units.

elements that are concentrated in early-formed minerals during crystallization are considered to be compatible elements. Those trace elements that are strongly concentrated into the liquid and enter only late-formed minerals are considered to be incompatible elements. During fractional crystallization, then, early-formed minerals are rich in compatible trace elements and low in incompatible elements. In late-forming minerals, the abundance of the compatible trace elements is low and the abundance of the incompatible elements is high. In a suite of comagmatic rocks related by fractional crystallization, highly compatible elements with $K_d>>1$ should show a large variation in concentration (Hanson, 1978). During batch partial melting, compatible elements with $K_d>>1$ remain in the residual solid until late in the melting process. Because the liquid remains with the solid and equilibrates as melting proceeds, concentration of the compatible elements should be relatively constant in a suite of rocks related by batch partial melting (Hanson, 1978).

Two common compatible trace elements are Ni ($K_{d[olivine]} = 10$; $K_{d[cpx]} = 2$) and Cr ($K_{d[cpx]} = 10$). Incompatible elements include Zr ($K_{d[olivine]} = 0.03$, $K_{d[biotite]} = 4.12$) and Ba ($K_{d[olivine]} = 0.001$, $K_{d[K\text{-}feldspar]} = 6$) (Cox, Bell, and Pankhurst, 1984). The distribution of Cr, Ni, Zr, and Ba vs. SiO_2 in the Eagle Mountain units, as shown in Figure 26, appears to be more consistent with fractional crystallization than with batch partial melting. The concentrations of the compatible elements, Ni and Cr, are high in the more primitive rocks and low in the more evolved rocks; concentrations of the incompatible elements, Ba and Zr, are low in the primitive rocks and very high in the

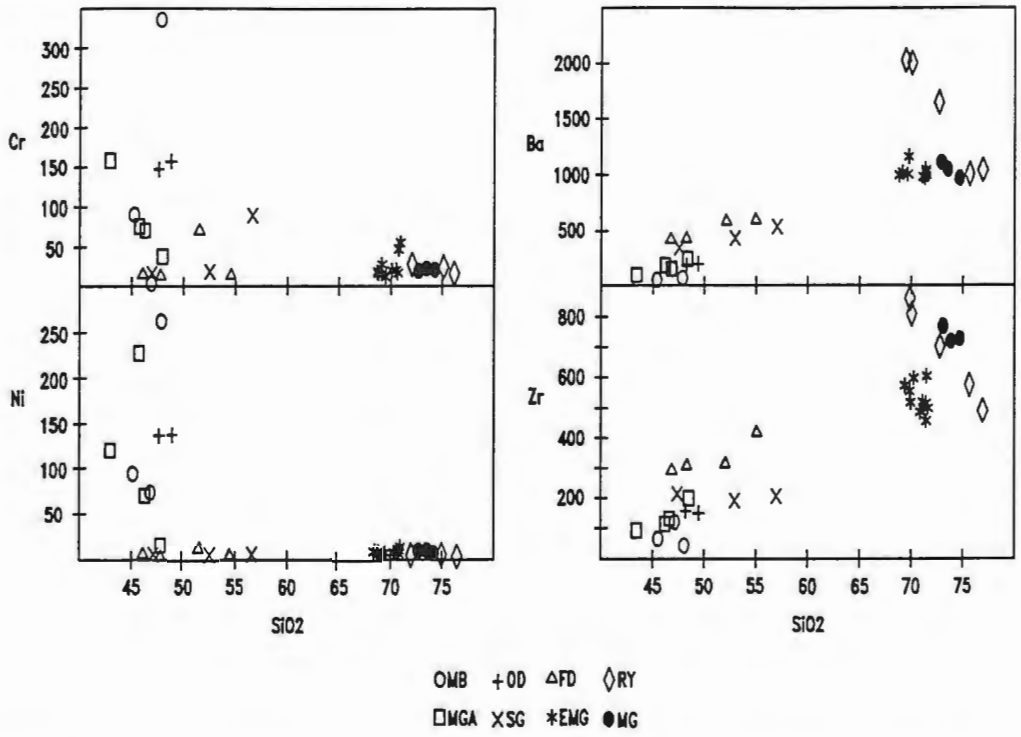

Figure 26: Compatible (Ni, Cr) and incompatible (Zr, Ba) elements vs. SiO_2 for Eagle Mountain units.

more evolved rocks.

Another pattern characteristic of trace elements during fractional crystallization is extreme depletion of compatible elements in late residual liquids with little change in the ratios of incompatible elements (Cox, Bell, and Pankhurst, 1984). This occurs because the compatible elements are taken into the first minerals to crystallize and are essentially used up early in the crystallization process, while the incompatible elements remain in the liquid until late in the crystallization process. Even though the concentrations of the incompatible elements increase as the amount of liquid decreases, the

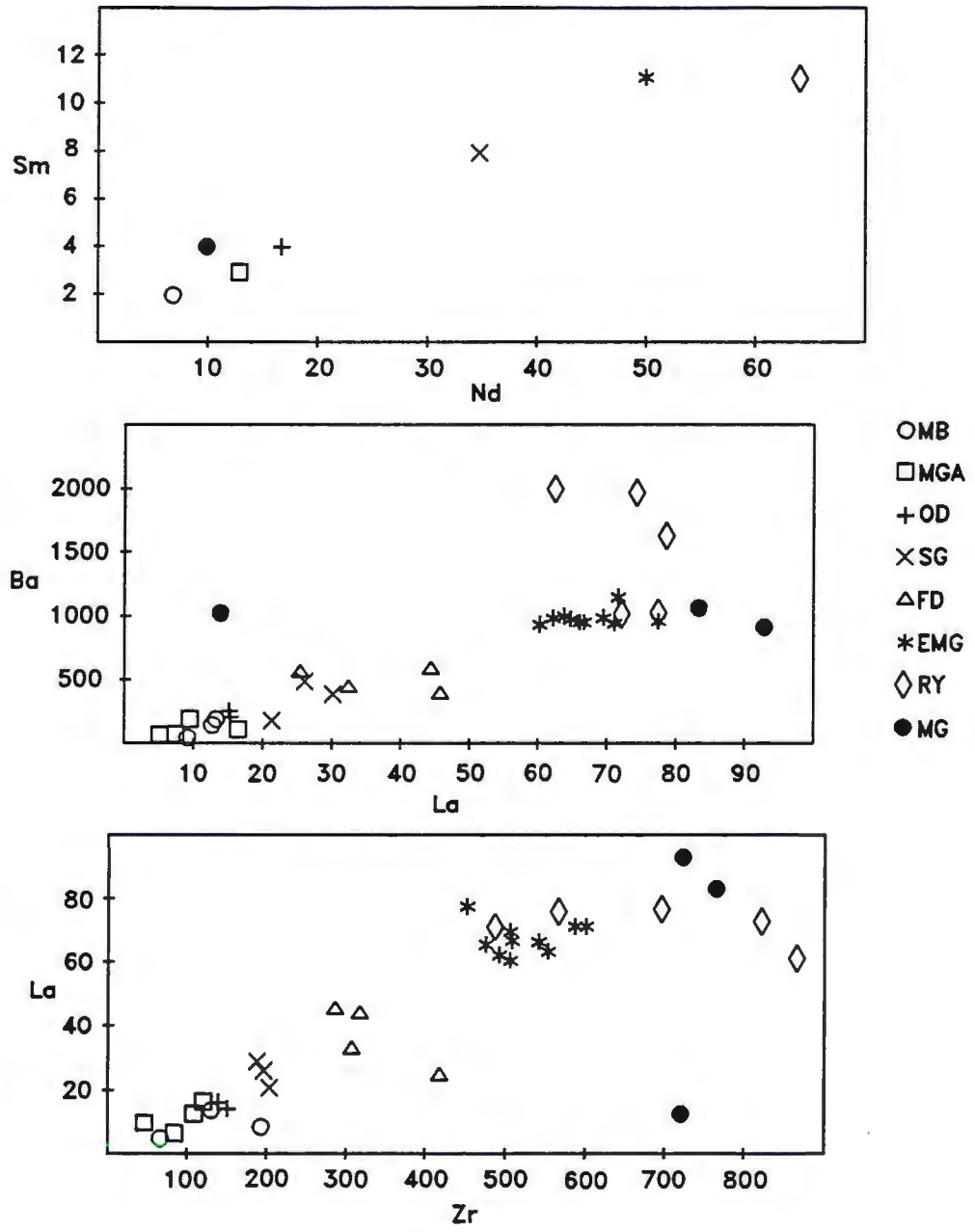

Figure 27: Ratios of some incompatible elements in Eagle Mountain units.

ratios of the elements remain fairly constant. During partial melting, however, even a small difference in bulk distribution coefficient can result in significant changes in the

ratio of the incompatible elements in the liquid. With a small degree of partial melting, only the incompatible elements with smallest K_d will be released to the liquid. If melting continues, elements with larger K_d will be added to the liquid, changing the ratios of the incompatible elements present. The ratios of several incompatible elements (Sm vs. Nd, Ba vs. La, La vs. Zr) are shown in Figure 27. As predicted for a fractional crystallization series, the ratios of the elements are relatively constant, with the exception of the miarolitic granophyre and some rhyolite samples.

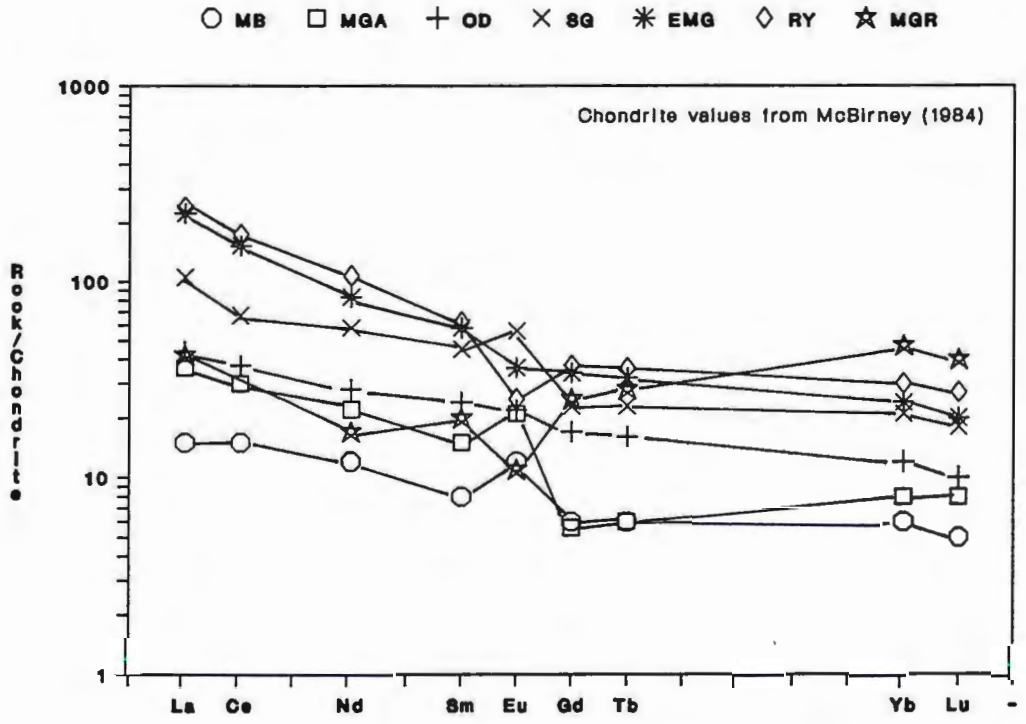

Figure 28: Rare earth element plot for all Eagle Mountain units.

Rare earth element (REE) patterns for the units (Fig. 28) are also relatively consistent with a fractional crystallization model, except for the miarolitic granophyre. During fractional crystallization, the REEs, which are all incompatible, are excluded

from the crystallizing phases and become steadily enriched in the liquid. Thus, REE concentrations are low in the primitive rocks and high in the more evolved rocks. With the exception of the miarolitic granophyre, REE concentrations for the Eagle Mountain units increase with increasing fractionation and all have roughly the same slope with light rare earth elements (LREEs) moderately enriched over heavy rare earth elements (HREEs). The REE pattern of the miarolitic granophyre, however, sharply crosscuts the general trend of the other units. It is strongly depleted in LREEs with concentrations comparable to the most primitive mafic units.

Mass Balance Calculations: Based on simple major and trace element patterns, fractional crystallization of one parental magma seems to be a more likely mode of formation for the units at Eagle Mountain than partial melting. To further test fractional crystallization vs. partial melting, mass balance calculations were carried out using the GPP program of Geist et al. (1985). The program is based on a matrix inversion procedure that works by determining the proportions of a specified set of components which, when subtracted from or added to a parental liquid, yield the best least-squares fit to a given daughter composition. The output gives the weight percentages of the minerals in the fractionated assemblage and includes an R^2 value, which is a measure of the fit of the solution. R^2 values less than 1 are considered a reasonable fit, values less than 0.3 are considered a good fit, and values less than 0.1 are considered an excellent fit. (See Appendix IV for specific solutions.)

Many calculations were attempted using the diabase, the metagabbro, and the metabasalt as representative parental liquids/rocks in an attempt to model the various units as the products of progressive fractional crystallization of one magma or partial melting of one rock type. None of these calculations was very successful, with R^2 values between 1 and 10 and unrealistic compositions for the resulting cumulate assemblages. This indicates that the units in the field area are not a simple series related by either partial melting or crystallization from one parent magma in a closed system. The relationships between the units are much more complex.

Modeling using just the Eagle Mountain granophyre and the ferrodiorite was more successful. The gradational contact between the granophyre and the ferrodiorite and the similar composition of plagioclase and ferroaugite in the two units is strong evidence for a genetic relationship between them. Because the ferrodiorite is a cumulate rock, it is unlikely that it represents a liquid composition. For this reason modeling was done to try to establish a hypothetical parent liquid composition from which the minerals of the ferrodiorite could be subtracted to form a cumulate rock similar to the ferrodiorite, leaving a daughter composition similar to the Eagle Mountain granophyre (see complete data in Appendix IV). The following minerals were subtracted from the hypothetical parent composition: olivine (Fo_6Fa_{94}), cpx ($Ca_{38}Mg_{12}Fe_{50}$), plagioclase ($An_{47}Ab_{49}Or_4$), magnetite ($Ti_{10}Fe^{2+}_{40}Fe^{3+}_{50}$), ilmenite ($Ti_{51}Fe^{2+}_{44}Fe^{3+}_{5}$), and apatite. Mineral compositions, except for apatite, were determined by microprobe analysis of ferrodiorite sample EM63. Because no probe compositions

were available for apatite, a published analysis from a quartz diorite was used (Deer, Howie, and Zussman, 1966). For these calculations the weight factor of K_2O was changed to 0.5 because very little K_2O was used by the minerals in the calculations; all other weight factors were 1. Subtracting the six minerals, the closest fit was achieved with the following parent liquid composition:

SiO_2	=	58.92	MgO	=	0.88
TiO_2	=	1.67	CaO	=	4.91
Al_2O_3	=	12.77	Na_2O	=	3.68
FeO	=	14.73	K_2O	=	3.04
MnO	=	0.25	P_2O_5	=	0.68

This produced a cumulate composed of approximately 3.5% olivine, 23% cpx, 46% plagioclase, 22% magnetite, 1% ilmenite, and 3.5% apatite. This is high in cpx and magnetite when compared to the ferrodiorite, but this is the closest match that could be produced. The daughter composition is fairly close to the composition of the Eagle Mountain granophyre, and R^2 has a value of 0.331. The hypothetical parent liquid composition is similar to some NSVG andesites analyzed by Green (1986), for example Green's samples C-14, T-96, C-23, ML-34, and LM-9, but FeO* and K_2O are higher and MgO and TiO_2 are lower in the hypothetical parent liquid (see Table 4).

TABLE 4
Compositions of some NSVG Andesites and a Hypothetical Liquid

ELEMENT	HYPOTH PARENT	C-14	T-96	C-23	ML-34	LM-9
SiO_2	58.92	57.80	59.20	56.40	56.60	53.60
TiO_2	1.67	1.94	1.96	1.95	2.34	2.46
Al_2O_3	12.77	12.20	12.60	12.80	13.1	16.4
FeO	14.73	12.70	11.90	12.90	12.5	10.9
MnO	0.25	0.16	0.18	0.18	0.15	0.09
MgO	0.88	1.74	1.89	2.74	2.59	2.46
CaO	4.91	4.71	5.02	6.0	4.53	6.21
Na_2O	3.68	3.03	3.37	3.1	3.8	4.0
K_2O	3.04	2.82	2.01	1.93	2.8	1.81
P_2O_5	0.68	0.45	0.72	0.34	0.38	0.4

Mass balance calculations indicate that the Eagle Mountain granophyre and the ferrodiorite could have been derived from a single andesitic parent by crystal fractionation; chemical analyses of lavas show that similar andesitic magma compositions did occur in this portion of the Midcontinent Rift.

The miarolitic granophyre unit is more difficult to model. On the basis of major elements and most trace elements, it could be the result of further fractionation of a magma similar to the one which produced the Eagle Mountain granophyre. However, the REE pattern of the miarolitic granophyre is unique and does not fit well with a fractional crystallization model, because it has LREE values comparable to the

most primitive units in the area and HREE values comparable to those of the more evolved units. The compositions of the feldspar phenocrysts in this unit are also suspect; microprobe analysis indicates that the phenocrysts are either pure albite or pure orthoclase. At the high temperature and low pressure at which these granophyres probably crystallized (see discussion beginning on page 90), feldspars should have formed as one solid solution phase rather than two distinct phases; therefore, they probably do not represent original compositions. This, along with the complete alteration of interstitial material is strong evidence that the miarolitic granophyre has undergone metasomatic alteration. It is likely that this alteration also disturbed the original trace element concentrations.

Nevertheless, mass balance calculations using the Eagle Mountain granophyre as the parent and the miarolitic granophyre as the daughter were attempted. The calculations were not successful; unrealistic cumulate assemblages were produced and R^2 had a value of approximately 3.

If the miarolitic granophyre is the product of partial melting rather than fractional crystallization, its REE pattern (if original) indicates that the source rock must be composed of minerals with high K_d for the LREEs and low K_d for the HREEs. With a small degree of partial melting, this source rock would retain the LREEs and lose the HREEs early in the melting process. According to Hanson (1978), LREEs are retained only by apatite. HREEs are retained somewhat by cpx; the high HREE and low LREE concentrations in the miarolitic granophyre would

indicate that the parent rock was poor in cpx and rich in apatite. Hanson also states that in the daughter rock, Rb/Sr ratios are increased and Sr/Ba ratios are decreased if plagioclase is a major component in the residual rock. Plagioclase in the residual rock also contributes to a negative Eu anomaly in the daughter. The miarolitic granophyre does have a Rb/Sr ratio nearly 4 times that of any other unit and a Sr/Ba ratio slightly lower than that in the other felsic units. It also shows a distinct negative Eu anomaly in the REE pattern, indicating that plagioclase probably was a major component of the parent rock.

If the parent rock was similar to one of the units in the field area, the only unit that fits these stipulations for a parent (high in apatite and plagioclase, relatively low in cpx) is the ferrodiorite. Mass balance calculations were carried out to see if the miarolitic granophyre could be modeled as a partial melt of the ferrodiorite. Quartz, K-feldspar (Ab_1Or_{99}), and albite ($Ab_{98}Or_2$) were subtracted from the parent composition of ferrodiorite EM63. Weight factors were 1 except for P_2O_5, which was set at zero because it was not used by any of the minerals being subtracted. This produced a daughter liquid very similar to the miarolitic granophyre, with an R^2 value of 0.901. However, no evidence of partial melting of the ferrodiorite was recognized in the field area, in hand sample, or in thin section. The same calculations were done using the rhyolite, Eagle Mountain granophyre, and metagabbro as the parent rock; none of these produced a match as good as the ferrodiorite. (See complete calculations in Appendix IV). If the miarolitic granophyre did form by partial melting, it is likely that

the true parent rock is not exposed in the field area, but is located at some depth in the crust.

Trace Element Modeling: Another approach to determining the origin of comagmatic rocks is trace element modeling using equations that attempt to quantify changes in trace element concentrations. According to Henry's Law, very dilute components in a liquid have nearly constant activity coefficients and the chemical potential of the component in a particular phase varies directly with its concentration. Therefore, the ratio of the concentration in the solid (C_s) to the concentration in the liquid (C_l) will be a constant. This constant is the distribution coefficient (K_d). K_d varies for each element in a given mineral, and the K_d for a given element varies with magma composition, temperature, pressure, and oxygen fugacity (Allegré & Minster, 1978). Distribution coefficients used in these calculations are given in Appendix V.

Under conditions of a closed system and ideal fractional crystallization, the distribution of a given trace element should be governed by equation #1 (Arth, 1976):

$$\frac{C_l}{C_o} = F^{(D-1)} \qquad \text{Equation 1}$$

C_l is the concentration of the element in the remaining liquid, C_o is the concentration of the element in the original liquid, F is the fraction of melt remaining, and D is the bulk distribution coefficient. The bulk distribution coefficient for a given element is the sum of individual mineral-liquid partition coefficients for that element in the

crystallizing minerals multiplied by the weight proportion of those minerals in the crystallized assemblage. For any trace element, if C_l, C_o, and D are known, a value for F can be calculated by rearranging equation #1:

$$F = e^{\left[\frac{\ln\left(\frac{C_l}{C_o}\right)}{(D-1)}\right]} \qquad \text{Equation 2}$$

If closed-system fractionation was the only process relating the suite of rocks, F values calculated for a variety of trace elements should all show the same degree of fractionation.

For modeling the Eagle Mountain granophyre, the hypothetical liquid that was developed in the mass balance calculations was used for the parent liquid. Trace element concentrations for this hypothetical parent liquid are from Green's (1986) analyses of NSVG andesites (C-14, T-96, C-23, ML-34, and LM-9). Table 5 shows bulk distribution coefficients, trace element concentrations, and calculated F values for models using the Eagle Mountain granophyre and the hypothetical parent liquid.

TABLE 5
Results of Trace Element Modeling of Fractional Crystallization
as a Mode of Formation of Eagle Mountain Granophyre

Element	D	Parent rock concentration (ppm)	EMG concentration (ppm)	Calculated F
Rb	0.039	100	152	.65
Sr	4.10	310	146	.78
Zr	0.264	360	524	.60
Ba	0.290	800	978	.75
La	0.190	61.4	73.9	.79
Sm	0.078	8.2	10.5	.76
Eu	0.404	2	2.5	.68
Yb	0.050	3.8	4.9	.77

The calculated F values range from 0.60 to 0.79--a reasonable match that indicates the Eagle Mountain granophyre could have formed as a result of approximately 20-40% crystallization of an andesitic liquid with these trace element concentrations.

For modeling the miarolitic granophyre as the result of fractional crystallization, the Eagle Mountain granophyre was used as a parental liquid. F values were calculated for seven trace elements (Rb, Sr, Ba, Nd, Sm, Yb, Eu). Table 6 shows bulk distribution coefficients, trace element concentrations, and calculated F values for this model.

TABLE 6
Results of Trace Element Modeling of Fractional Crystallization
as a Mode of Formation of Miarolitic Granophyre

Element	D	Parent rock concentration (ppm)	MG concentration (ppm)	Calculated F
Rb	0.216	152	155	0.975
Sr	3.96	146	39.5	0.643
Ba	3.73	978	1010	1.01
Nd	0.161	50	10	6.80
Sm	0.154	10.5	3.6	3.55
Eu	1.58	2.5	0.78	0.133
Yb	8.126	4.89	9.45	1.09

Calculated F values range from 0.13 to 6.8, indicating that it is unlikely that the miarolitic granophyre could be simply the result of fractional crystallization of a magma similar to the Eagle Mountain granophyre.

Because the fractional crystallization modeling did not give good results for the miarolitic granophyre, further modeling was done using equations for partial melting. Equations have been developed for three partial melt mechanisms: 1) continuous removal of melt from the residual solid, 2) continuous removal of melt from the residual solid followed by collection of this melt in a single, completely mixed chamber, and 3) continuous equilibration of the melt with the residual solid until the liquid is removed (batch partial melting). Batch partial melting is perhaps the most geologi-

cally realistic mechanism (Arth, 1976). Equation #3 (Arth, 1976) describes this process:

$$\frac{C_l}{C_o} = \frac{1}{D + F(1 - P)} \qquad \text{Equation 3}$$

where C_l is the concentration of a given trace element in the liquid, C_o is the initial concentration of the same element in the bulk solid, D is the bulk distribution coefficient for the mineral assemblage in the original solid, F is the fraction of partial melting, and P represents the sum of the fraction of liquid contributed by each phase multiplied by a distribution coefficient for that phase. To simplify the calculations, P is set equal to D, indicating that the minerals contribute to the melt in the same proportions as their abundances. Equation #3 can then be rearranged to solve for F:

$$F = \frac{C_o - C_l D}{C_l (1-D)} \qquad \text{Equation 4}$$

If batch partial melting is the only mechanism involved in the formation of a particular rock, F values calculated for a variety of trace elements should show approximately the same fraction of melting.

For the miarolitic granophyre, F values were calculated for various trace elements using the local rhyolite, metagabbro, and ferrodiorite as well as the granodioritic phase of the the Giant's Range granite as possible parent rocks. Selection of

trace elements used for different parent rocks was dependent on available analyses and on availability of appropriate K_d values for elements in the different rock types. Table 7 presents the bulk distribution coefficients, trace element concentrations, and calculated F values for each parent rock.

TABLE 7
Results of Trace Element Modeling of Batch Partial Melting as a Mode of Formation of Miarolitic Granophyre

RHYOLITE PARENT

Element	D	Parent rock concentration (ppm)	MG concentration (ppm)	Calculated F
Rb	0.259	126	155	0.75
Sr	4.068	126	40	0.30
Zr	0.044	689	736	0.93
Ba	3.771	1537	1010	0.81
La	0.375	80	14	8.5
Nd	0.022	64	10	6.5
Sm	0.260	11	3.6	3.8
Eu	1.574	1.75	0.78	-1.2
Yb	0.026	6.04	9.45	0.63

METAGABBRO PARENT

Element	D	Parent rock concentration (ppm)	MG concentration (ppm)	Calculated F
Rb	0.049	19	155	0.08
Sr	1.155	264	40	-9.9
Zr	0.178	126	736	-0.01
Ba	0.147	132	1010	-0.02
La	0.269	12	14	0.80
Sm	0.242	2.8	3.6	0.71
Eu	0.375	1.44	0.78	2.4
Yb	0.141	1.67	9.45	0.04

FERRODIORITE PARENT

Element	D	Parent rock concentration (ppm)	MG concentration (ppm)	Calculated F
Rb	0.030	43	155	0.26
Sr	1.53	324	40	-12.4
Zr	0.261	331	736	0.26
Ba	0.196	485	1010	0.35
La	0.121	37	14	2.9
Zn	0.610	203	95.5	3.9

GIANTS RANGE GRANODIORITE
PARENT
(Data from Sims and Viswanathan, 1972; J. Reichhoff, pers. com.)

Element	D	Parent rock concentration (ppm)	MG concentration (ppm)	Calculated F
Rb	0.149	123	155	0.76
Sr	3.829	1138	40	-8.7
Zr	0.139	290	736	0.30
Ba	1.938	1293	1010	0.70
Sm	0.608	3.7	3.6	1.07
Eu	2.020	1.11	0.78	0.59
Yb	0.60	0.80	9.45	-1.26

None of these parent rock compositions gave satisfactory results; in all cases, the calculated F values varied widely. This could indicate that 1) the chosen K_ds and/or starting assemblages were inappropriate, 2) the correct parent rock composition was not tried, 3) the original trace element concentrations have been altered, or 4) the miarolitic granophyre did not form by simple batch partial melting.

SILICATE LIQUID IMMISCIBILITY

As early as 1918, Grout suggested that separation of an immiscible granitic fraction from the mafic magma was responsible for the granophyres of the Duluth Complex. This idea of silicate liquid immiscibility, or unmixing, then lost favor until the early 1970s when indisputable evidence of immiscibility was identified in lunar basalts (Roedder & Weiblen, 1970, 1971). This evidence was the existence of two

chemically distinct glasses preserved as globules of one within the other. Since that time, similar evidence of immiscibility has been found in some terrestrial basalts, including one sample from the North Shore Volcanic Group (Roedder & Weiblen, 1971). This has established silicate liquid immiscibility as a recognized mechanism of magmatic differentiation. It is, however, nearly impossible to find petrographic evidence of immiscibility in plutonic rocks because the two liquids will tend to segregate and crystallize separately; unless the crystallization is interrupted and the two liquids are in some way preserved, the final products of crystallization will show no physical evidence of the system having passed through a two-liquid field (McBirney, 1984). For this reason, it is necessary to rely on more indirect evidence to test the hypothesis that related rock units may be the crystallized products of two immiscible liquids.

Experiments with liquids of tholeiitic basalt compositions (Naslund, 1975; Philpotts, 1979) as well as detailed studies of natural tholeiitic basalts (Philpotts, 1976, 1982) have shown that unmixing of a tholeiitic magma results in an Fe-rich liquid and a Si-rich liquid. The Fe-rich liquid commonly contains approximately 43% Si and the Si-rich liquid contains approximately 73% Si; Mg and P are partitioned strongly into the Fe-rich liquid, and Al, K, and Na are partitioned into the Si-rich liquid (Philpotts, 1982). Immiscibility is not restricted to a K-rich residual liquid, but occurs in liquids with all possible Na/K ratios. The width of the immiscibility field varies with magma composition and oxygen fugacity; it expands with increased Ti and P and decreases

with increased Na (Philpotts, 1982). With increased fO_2, the width of the field expands and unmixing occurs at higher temperatures and earlier stages of crystallization (Naslund, 1975; Philpotts, 1979). In natural systems, immiscible liquids form just above 1000°C (Philpotts, 1982).

Trace elements are not partitioned equally into the two immiscible liquids. One of the most strongly partitioned elements is phosphorus. During normal fractional crystallization, P is enriched in the felsic liquid until apatite crystallizes; P is also strongly enriched in the first liquid produced by partial melting. But during unmixing of immiscible liquids, P is strongly partitioned into the Fe-rich (Si-poor) liquid and depleted from the coexisting Si-rich liquid.

For immiscibility to be an important mechanism of differentiation, unmixing must occur early enough in the fractionation process to produce a significant amount of the two liquids. To determine the stage at which unmixing occurs, Philpotts (1982) considered the compositions of the minerals coexisting with immiscible globules. In tholeiitic basalts he found plagioclase of composition An_{50} and augite of composition $Ca_{34}Mg_{19}Fe_{47}$.

When considered in relation to these characteristics of immiscible liquids, the Eagle Mountain granophyre and the ferrodiorite show some interesting traits. There is a distinct gap in SiO_2 content for the two units, from 50.1 wt% in the ferrodiorite to 70.1 wt% in the Eagle Mountain granophyre; there is also a wide gap in FeO* content, from 18.6 wt% in the ferrodiorite to 4.7 wt% in the Eagle Mountain granophyre. The

Mg# for the two units is identical (13.5 for the ferrodiorite and 13.4 for the Eagle Mountain granophyre). The composition of the plagioclase is very similar in the two units; in the Eagle Mountain granophyre it ranges from An_{31} to An_{52} and in the ferrodiorite from An_{45} to An_{50}. The average augite composition in the Eagle Mountain granophyre is $Ca_{43}Mg_{16}Fe_{41}$ and in the ferrodiorite, $Ca_{38}Mg_{12}Fe_{50}$--similar to the compositions Philpotts (1982) found in minerals coexisting with immiscible globules. The trace element P appears to be strongly partitioned into the ferrodiorite; the ferrodiorite contains 0.75 wt% P_2O_5, and the Eagle Mountain granophyre contains only 0.06 wt%.

In Figure 29 whole rock analyses of the Eagle Mountain granophyre, the ferrodiorite, and the hypothetical liquid are plotted on a triangle with apices of (Na_2O + K_2O + Al_2O_3)--(TiO_2 + FeO + MnO + MgO + CaO + P_2O_5)--SiO_2. Values from experimentally determined liquids for several of the units from the Skaergaard Intrusion, which were interpreted by McBirney and Nakamura (1974) to have been governed by liquid immiscibility, are plotted for comparison. The hatched area represents the two-liquid field determined by Roedder (1951). The Upper Zone Skaergaard units plot progressively closer to the Fe-rich end of the field; the ferro-diorite from Eagle Mountain is more intermediate, plotting slightly further from the Fe-rich end of the two-liquid field. Both the Skaergaard granophyre and the Eagle Mountain granophyre plot near the Si-rich end of the field. The hypothetical liquid composition determined by mass balance calculations to be a possible parent for both

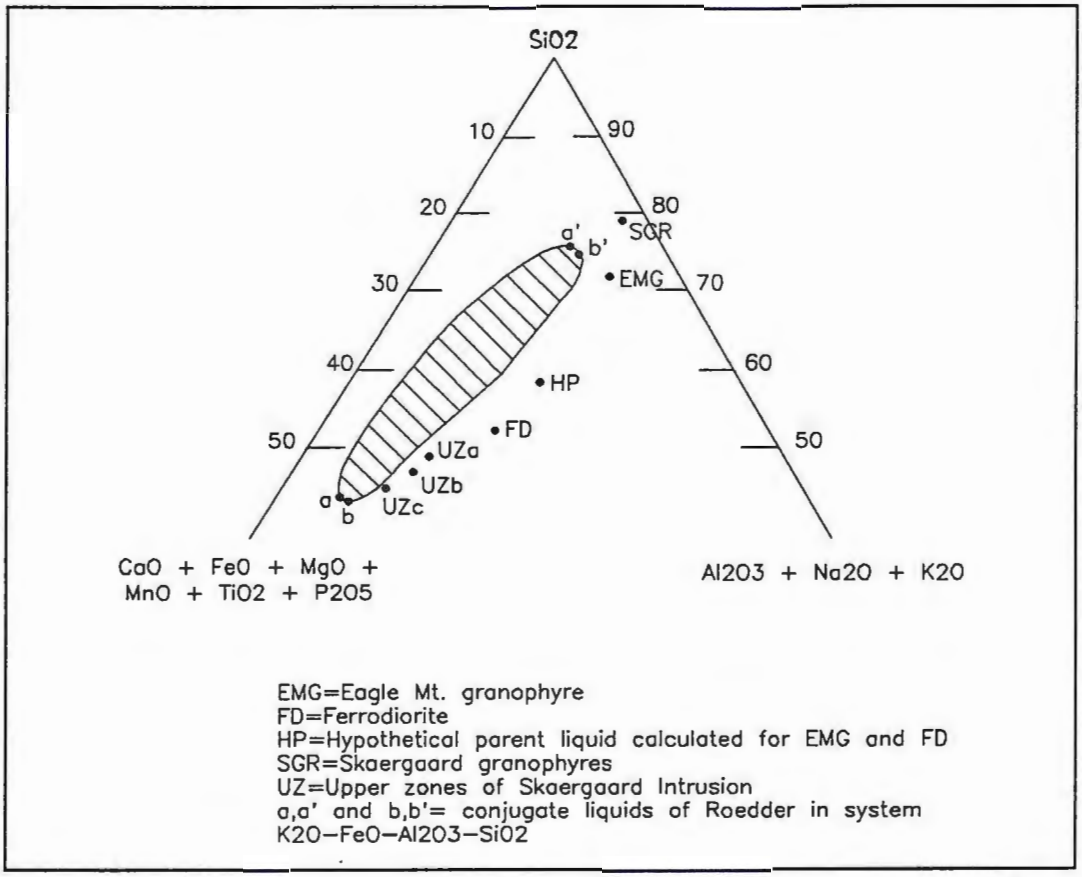

Figure 29: Whole rock compositions of Eagle Mountain units and experimentally determined liquid compositions of Skaergaard units plotted in relation to the two-liquid field of Roedder (1951). Skaergaard data from McBirney & Nakamura (1974).

the ferrodiorite and Eagle Mountain granophyre falls on a line between the two units.

The similarity in composition of the plagioclase and pyroxene between the two units, the strong concentration of P in the ferrodiorite with corresponding depletion in the Eagle Mountain granophyre, and the gap in SiO_2 and FeO content all suggest that these two rocks could be the result of the separation of two immiscible silicate liquids, one Fe-rich and the other Si-rich.

PHYSICAL CONDITIONS OF CRYSTALLIZATION

Pressure: The granophyre units at Eagle Mountain underlie a rhyolite flow, indicating that they were intruded at the base of or into the volcanic pile. An estimate of the total thickness of the Keweenawan lavas in the Eagle Mountain area is 3.6-5.6 km (Green, 1972, 1982b). If pressure increases at the rate of approximately 1 kb per 3.33 km, the maximum pressure at which the granophyres crystallized would be 2 kb. The actual pressure of crystallization could have been less, depending on the thickness of the overlying volcanic pile at the time and the level at which the granophyre magma was intruded into the volcanic pile.

Granite Phase Diagram: The granophyres of Eagle Mountain appear to have crystallized from relatively dry (H_2O-undersaturated) magmas. This is indicated by the presence of Fe-rich pyroxene and olivine, a lack of hydrous phases, and by the extreme Fe-enrichment of the Duluth Complex as a whole. In the analyses of nine samples of the Eagle Mountain granophyre, H_2O^+ ranges from 0.2 to 0.6 wt%. Miarolitic cavities in the miarolitic granophyre indicate that this magma completed crystallization in the presence of some vapor phase (Lofgren, 1971). H_2O^+ in the miarolitic granophyre ranges from 0.6% to 0.8%; the only hydrous phases now present are secondary chlorites and clays.

Experimental data for the dry granite system at low pressures are not abundant. Schairer's phase diagram (1957) for "petrogeny's residua system" shows a thermal minimum near 990° C. Tuttle and Bowen (1958), in their pioneering work on

the granite system, worked with water-saturated melts, starting with P_{H2O} of 500 bars. Huang and Wyllie (1975) present only estimated field boundaries for dry melts in the system $NaAlSi_3O_8$-$KAlSi_3O_8$-SiO_2; shapes of field boundaries and compositions at the temperature minima were not determined. Whitney (1975) studied the system $CaAl_2Si_2O_8$-$NaAlSi_3O_8$-$KAlSi_3O_8$-SiO_2 at various pressure, temperature, and X_{H2O}; the lowest pressure studied was 2 kb. For a synthetic granite composition at 2 kb, he found the dry solidus to be approximately 990° C, but the exact temperature was not fixed. The dry liquidus occurs at 1180° C. Whitney also found that the liquidus temperature rises with decreasing H_2O content and is strongly affected by the An content of the liquid.

When CIPW norms calculated from average compositions are plotted on the phase diagram for the system nepheline-kalsilite-silica at 1 atmosphere pressure (Schairer, 1957), the Eagle Mountain granophyre plots in the feldspar field near the thermal minimum of 990° C and the miarolitic granophyre plots in the silica field at a temperature slightly above the thermal minimum (Fig. 30). Because the compositions of the feldspars in the miarolitic granophyre are likely to have been altered, this may not be a true representation of its original composition.

Although exact temperature and pressure of crystallization cannot be calculated, all evidence supports the formation of both granophyre units at Eagle Mountain as shallow intrusions that crystallized at less than 2 kb pressure and temperatures near 990° C, the thermal minimum for the dry granite system. This close correspondence

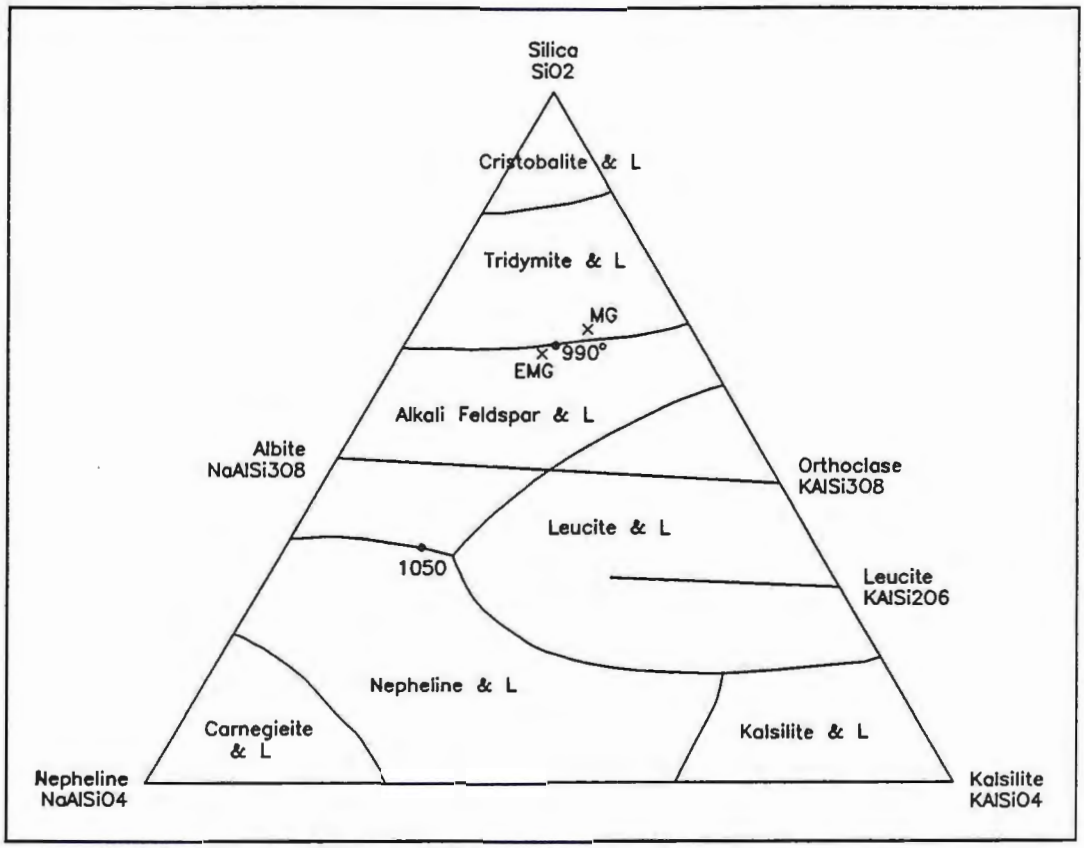

Figure 30: CIPW norms for Eagle Mountain granophyre and miarolitic granophyre plotted on Schairer's (1957) phase diagram at 1 atm pressure. (Adapted from Ehlers and Blatt, 1982).

with the minimum temperature region on the phase diagram indicates that the rocks could be either the last products of differentiation of a more primitive magma or the first products of melting of a feldspar/quartz-rich rock such as Archean crust or older felsic Keweenawan rocks.

Spherulites: Undercooling (ΔT), the difference between the theoretical temperature of crystallization and the actual temperature at which crystals form, strongly influences the shape and habit of crystals in a cooling magma (Lofgren, 1974). Using

water-saturated plagioclase gels of varying An content (An ≤60) at 5 kb P_{H2O}, the general sequence of crystal morphology identified by Lofgren is:

$\Delta T \leq 100°C$, tabular crystals

$\Delta T = 100\text{-}200°C$, acicular or skeletal crystals

$\Delta T = 150\text{-}250°C$, dendritic crystals

$\Delta T > 250°C$, spherulites

A change in ΔT during crystallization produces a variety of crystal morphologies within one rock.

Several of the samples of Eagle Mountain granophyre (EM5, EM11, EM12, EM22) contain 1-2 mm spherulites surrounded by very fine-grained granular ground-mass of quartz and feldspar. Local tabular feldspar phenocrysts approximately 1 mm across and rare acicular feldspar phenocrysts also occur in the same rocks. The presence of spherulites in the Eagle Mountain granophyre indicates a large degree of undercooling, and the occurrence of tabular crystals within the same rocks indicates that ΔT changed during the course of crystallization. This is consistent with a shallow intrusion mode of formation. The tabular crystals, which form at lower ΔT than the spherulites, must have crystallized at higher temperature and greater depth before the liquid was chilled against the cooler roof rocks where a larger ΔT resulted in the formation of spherulites.

SUMMARY AND CONCLUSIONS

The main goal of this study was to examine a major granophyre body in the roof zone of the Duluth Complex in an attempt to understand its crystallization history, relationship to other rock units, and ultimate origin. The rock units identified in the Eagle Mountain area include metabasalt, metagabbro, ophitic diabase, syeno-gabbro, ferrodiorite, rhyolite, and two granophyre units. The following interpretations have been made on the basis of field relations, petrography, and geochemistry.

The rhyolite appears to be the oldest unit in the field area and formed the roof zone beneath which the intrusive units were emplaced. The metabasalt unit may be as old as or older than the rhyolite and is probably composed of a number of xenoliths that were carried in and slightly altered by a gabbroic magma that was impounded beneath the rhyolite. This gabbro was later slightly metamorphosed by the intrusion of the magma that formed the adjacent Eagle Mountain granophyre. The Eagle Mountain granophyre shares a gradational contact and similar mineral compositions with the ferrodiorite, and, thus, these two units appear to be genetically related. The syenogabbro shows no clear genetic relationship to the ferrodiorite with which it is in contact and is probably a separate intrusion. Based on contact relations, the miarolitic granophyre is younger than the rhyolite, but its age relations to the other units are ambiguous. The ophitic diabase crosscuts all but the rhyolite unit in this area; it probably represents the youngest unit.

The two granophyre units identified within the field area are distinctive physically and chemically. The two units, informally named the Eagle Mountain granophyre and the miarolitic granophyre, are distinguishable in hand sample, in thin section, and in chemical characteristics.

The Eagle Mountain granophyre is red-brown, fine-grained, variably porphyritic, and fairly massive. The texture, as seen in thin section, is variable. Some samples are equigranular, some contain spherulites, and some contain very fine granophyric intergrowths. All samples contain 2-6 mm plagioclase phenocrysts of composition An_{31}-An_{52} and about 10% mafic minerals, primarily iron-rich augite. Chemically, the Eagle Mountain granophyre is the less evolved of the two units; its composition is very close to the minimum temperature melt in the dry Ab-Or-Qz system. It contains more MgO, FeO, Na_2O, and nearly 7 times more CaO than the miarolitic granophyre. The average ratio of K_2O/Na_2O is 1.1. The Eagle Mountain granophyre is enriched in LREEs over HREEs, with LREEs approximately 250X chondritic values and HREEs approximately 30X chondritic values.

The miarolitic granophyre is brick-red, medium-grained, and contains 5% miarolitic cavities up to 5 mm across. In thin section, it is made up almost entirely of well-developed granophyric intergrowths that coarsen outward from a core of euhedral albite (Or_{0-5}) or orthoclase (Or_{95-100}). Interstitial material is altered to a fibrous mixture of secondary minerals, probably chlorite and limonite. The miarolitic granophyre contains more SiO_2 and K_2O than the Eagle Mountain granophyre and has a K_2O/-

Na_2O ratio of 2.3, but the unit may have been altered deuterically or metasomatically. Perhaps the most distinctive chemical difference between the units is in the REE patterns. The miarolitic granophyre shows an anomalous REE distribution, with a strong depletion in LREEs, approximately 40X chondritic values, and HREEs approximately 50X chondritic values.

The Eagle Mountain granophyre appears to be the product of differentiation of the same magma that formed the ferrodiorite; mass balance calculations and trace element modeling lend support to a model of differentiation due to fractional crystallization. Alternatively, similarities in mineralogy, partitioning of P, and the gap in SiO_2 and FeO content lend some support to differentiation due to silicate liquid immiscibility in a hypothetical andesitic parent magma. The Eagle Mountain granophyre is found underlying an extrusive unit; using the estimated thickness of the entire volcanic pile, the maximum pressure of crystallization was 2.0 kb, equivalent to a depth of approximately 6 km. If the granophyre magma was intruded before the volcanic sequence reached its final thickness, or if it was intruded into a high level of the sequence, the pressure could have been significantly lower. When the average norm composition is plotted on Schairer's (1957) granite phase diagram at 1 atm pressure, the Eagle Mountain granophyre appears to have crystallized near the thermal minimum of 990°C. The presence of spherulites indicates a high degree of undercooling.

The miarolitic granophyre is more enigmatic. It contains no recognizable spherulites, and the granophyric intergrowths are better developed and coarsen outward from individual nuclei, perhaps indicating a smaller degree of undercooling. When the average norm composition is plotted on Schairer's granite phase diagram at 1 atm pressure, a crystallization temperature between 1050°C and 1000°C is indicated; however, postmagmatic alteration may have involved some metasomatism so that its composition is no longer primary. Mass balance calculations and trace element models do not support either simple closed-system fractional crystallization or simple batch melting as a mode of formation for the miarolitic granophyre.

Based on field relations, petrography, REE patterns, mass balance calculations, and trace element models it seems likely that the miarolitic granophyre originated from a different source than the Eagle Mountain granophyre. Whether fractional crystallization or partial melting was the more significant mechanism involved in the formation of the magma is not clear. Isotopic studies could help to determine the amount of crustal contribution to both magmas.

The results of this study indicate that the granophyric bodies of the Duluth Complex could have formed in several ways. The various models that have been proposed over the years may all be correct--each for a specific granophyre unit. Each granophyre body must be examined on an individual basis, and a combination of all analytical techniques available must be used to determine the mode of formation.

In the Eagle Mountain area, detailed mapping of a much larger area would help to define the extent and volume of the units and might also establish a clearer relationship between the two granophyres. Isotopic studies would be especially important to help determine the origin of the units and the extent of alteration in the miarolitic granophyre.

REFERENCES

Allegré, C. J., and Minster, J. F., 1978, Quantitative models of trace element behavior in magmatic processes: Earth and Planetary Science Letters, V.38, p. 1-25.

Anderson, J. L., 1983, Proterozoic anorogenic granite plutonism of North America, *in* Medaris, L. G., Jr., Byers, C. W., Mickelson, D. M., and Shanks, W. C., eds., Proterozoic Geology: Selected Papers from an International Proterozoic Symposium: Geological Society of America, Memoir 161, p. 133-154.

Arth, J. G., 1976, Behavior of trace elements during magmatic processes--a summary of theoretical models and their applications: U. S. Geological Survey Journal of Research, V.4, p. 41-47.

Arth, J. G., and Barker, F., 1976, Rare-earth partitioning between hornblende and dacitic liquid and implications for the genesis of trondhjemitic-tonalitic magmas: Geology, V.4, p. 534-536.

Basaltic Volcanism Study Project, 1981, Basaltic Volcanism on the Terrestrial Planets: New York, Pergamon Press, 1286p.

Bastin, E. S., 1938, Hydrothermal alteration in the rocks of Pigeon Point, Minnesota: Journal of Geology, V.46, p. 1058-1072.

Bayley, W. S., 1893, The eruptive and sedimentary rocks on Pigeon Point, Minnesota, and their contact phenomena: USGS Bulletin 109, 121p.

Brannon, J. C., 1984, Geochemistry of successive lava flows of the Keweenawan North Shore Volcanic Group: Unpubl. Ph.D. Thesis, Washington University, St. Louis, MO, 100p.

Cannon, W. F., Green, A. G., Hutchinson, D. R., Lee, M., Milkereit, B., Behrendt, J. C., Halls, H. C., Green, J. C., Dickas, A. B., Morey, G. B., Sutcliffe, R., and Spencer, C., 1989, The North American midcontinent rift beneath Lake Superior from GLIMPCE seismic reflection profiling: Tectonics, V.8, p. 305-332.

Chappell, B. W., and White, A. J. R., 1974, Two contrasting granite types: Pacific Geology, V.8, p. 173-174.

Clemens, J. D., Holloway, J. R., and White, A. J. R., 1986, Origin of an A-type granite: experimental constraints: American Mineralogist, V.71, p. 317-324.

Collins, W. J., Beams, S. D., White, A. J. R., and Chappell, B. W., 1982, Nature and origin of A-type granites with particular reference to southeastern Australia: Contributions to Mineralogy and Petrology, V.80, p. 189-200.

Cox, K. G., Bell, J. D., and Pankhurst, R. J., 1984, The Interpretation of Igneous Rocks: London, George Allen & Unwin (Publishers) Ltd., 450p.

Daly, R. A., 1917, The geology of Pigeon Point, Minnesota: American Journal of Science, 4th Ser., V.43, p. 423-448.

Davidson, D. M., Jr., 1972, Eastern part of the Duluth Complex, *in* Sims, P. K., and Morey, G. B., eds., Geology of Minnesota, A Centennial Volume: Minnesota Geological Survey, p. 354-360.

_____, 1977, Eagle Mountain Quadrangle, Cook County, Minnesota (1:24000): Minnesota Geological Survey, Miscellaneous Map Series, Map M-28.

_____, 1982, Geological evidence relating to interpretation of the Lake Superior Basin structure, *in* Wold, R. J., and Hinze, W. J., eds., Geology and tectonics of the Lake Superior Basin: Geological Society of America Memoir 156, p. 5-14.

Deer, W. A., Howie, R. A., and Zussman, J., 1966, An Introduction to the Rock-forming Minerals: Longman Group Limited, 528p.

Ehlers, E. G., and Blatt, H., 1982, Petrology: Igneous, Sedimentary, and Metamorphic: San Francisco, W. H. Freeman and Company, 732p.

Ernst, W. G., 1960, Diabase-granophyre relations in the Endion Sill, Duluth, Minnesota: Journal of Petrology, V.1, p. 286-303.

Faure, G., Chaudhuri, S., and Fenton, M. D., 1969, Ages of the Duluth Gabbro Complex and of the Endion Sill, Duluth, Minnesota: Journal of Geophysical Research, V.74, p. 720-725.

Gehman, H. M., Jr., 1957, The petrology of the Beaver Bay Complex, Lake County, Minnesota: Unpubl. Ph.D. Thesis, University of Minnesota, Minneapolis, MN, 92p.

Geist, D. J., Baker, B. H., and McBirney, A. R., 1985, GPP: A program package for creating and using geochemical data files: University of Oregon, Center for Volcanology.

Green, J. C., 1972, North Shore Volcanic Group, *in* Sims, P. K., and Morey, G. B., eds., Geology of Minnesota, A Centennial Volume: Minnesota Geological Survey, p. 294-332.

_____, 1977, Keweenawan plateau volcanism in the Lake Superior region, *in* Baragar, W. R. A., Coleman, L. C., and Hall, J. M., eds., Volcanic regimes in Canada: Geological Association of Canada Special Paper Number 16, p. 407-422.

_____, 1982a, Geology of Keweenawan extrusive rocks, *in* Wold, R. J., and Hinze, W. J., eds., Geology and tectonics of the Lake Superior Basin: Geological Society of America Memoir 156, p. 47-55.

_____, 1982b, Two Harbors Sheet, bedrock geology (1:250,000): Minnesota Geological Survey, Geologic Map of Minnesota.

_____, 1983, Geologic and geochemical evidence for the nature and development of the Middle Proterozoic (Keweenawan) Midcontinent Rift of North America: Tectonophysics, V.94, p. 413-437.

_____, 1986, Lithogeochemistry of Keweenawan igneous rocks: Report 241-4, Minnesota Department of Natural Resources, 94+p.

_____, 1987, Petrology of the igneous rocks of the Midcontinent Rift System, *in* Midcontinent Rift System Scientific Drilling Workshop: Duluth, Minnesota, September 24-25, p. 4-8.

_____, 1989, Physical volcanology of mid-Proterozoic plateau lavas: the Keweenawan North Shore Volcanic Group, Minnesota: Geological Society of America Bulletin, V.101, p. 486-500.

Green, J. C., Bornhorst, T. J., Chandler, V. W., Mudrey, M. G., Jr., Myers, P. E., Pesonen, L. J., and Wilband, J. T., 1987, Keweenawan dykes of the Lake Superior Region: evidence for evolution of the Middle Proterozoic midcontinent rift of North America, *in* Halls, H. C., and Fahrig, W. F., eds., Mafic Dyke Swarms: Geological Association of Canada Special Paper 34, p. 289-302.

Grout, F. F., 1918, A type of igneous differentiation: Journal of Geology, V.26, p. 626-658.

_____, 1928, Anorthosite and granite as differentiates of a diabase sill on Pigeon Point, Minnesota: Geological Society of America Bulletin, V.39, p. 555-578.

Grout, F. F., and Schwartz, G. M., 1933, The geology of the Rove Formation and associated intrusives in northeastern Minnesota: Minnesota Geological Survey Bulletin 24, 99p.

Grout, F. F., Sharp, R. P., and Schwartz, G. M., 1959, The geology of Cook County, Minnesota: Minnesota Geological Survey Bulletin 39, 160p.

Hanson, G. N., 1978, The application of trace elements to the petrogenesis of igneous rocks of granitic composition: Earth and Planetary Science Letters, V.38, p. 26-43.

Huang, W., and Wyllie, P. J., 1975, Melting reactions in the system $NaAlSi_3O_8$-$KAlSi_3O_8$-SiO_2 to 35 kb, dry and with excess water: Journal of Geology, V.83, p. 737-748.

Irvine, T. N., and Baragar, W. R. A., 1971, A guide to chemical classification of the common volcanic rocks: Canadian Journal of Earth Sciences, V.8, p. 523-548.

Jensen, L. S., 1976, A new cation plot for classifying subalkalic volcanic rocks: Ontario Geological Survey Misc. Paper 66, 22p.

Klewin, K. W., 1987, The petrology and geochemistry of the Keweenawan Potato River Intrusion, northern Wisconsin: Unpubl. Ph.D. Thesis, Northern Illinois University, DeKalb, IL, 357p.

Leighton, M. W., 1954, Petrogenesis of a gabbro-granophyre complex in northern Wisconsin: Geological Society of America Bulletin, V.65, p. 401-442.

Lofgren, G., 1971, Experimentally produced devitrification textures in natural rhyolitic glass: Geological Society of America Bulletin, V.82, p. 111-124.

_____, 1974, An experimental study of plagioclase crystal morphology: isothermal crystallization: American Journal of Science, V.274, p. 243-273.

Loiselle, M. C., and Wones, D. R., 1979, Characteristics and origin of anorogenic granites: Geological Society of America Abstracts with Programs, V.11, p. 468.

McBirney, A. R., 1984, Igneous Petrology: San Francisco, Freeman, Cooper & Company, 504p.

McBirney, A. R., and Nakamura, Y., 1974, Immiscibility in late-stage magmas of the Skaergaard intrusion: Carnegie Institution of Washington Yearbook, V.73, p. 348-352.

Morey, G. B., and Green, J. C., 1982, Status of the Keweenawan as a stratigraphic unit in the Lake Superior region, *in* Wold, R. J., and Hinze, W. J., eds., Geology and tectonics of the Lake Superior Basin: Geological Society of America Memoir 156, p. 15-25.

Mudrey, M. G., Jr., 1973, Structure and petrology of the sill on Pigeon Point, Cook County, Minnesota: Unpubl. Ph.D. Thesis, University of Minnesota, Minneapolis, MN, 310p.

Nabelek, P. I., and Russ-Nabelek, C., 1988, The role of fluorine in the crystallization of granites in St. Francois mountains, Missouri: Geological Society of America, Abstracts with Programs, V.20, No. 7, p. A250.

Nagasawa, H., and Schnetzler, C. C., 1971, Partitioning of rare earth, alkali and alkaline earth elements between phenocrysts and acidic igneous magma: Geochimica et Cosmochimica Acta, V.35, p. 953-968.

Naslund, H. R., 1975, Liquid immiscibility in the system $KAlSi_3O_8$-$NaAlSi_3O_8$-FeO-Fe_2O_3-SiO_2 and its application to natural magmas: Carnegie Institution of Washington, Yearbook 75, 1975-76, p. 592-597.

Nicholson, S. W., and Shirey, S. B., 1990, Midcontinent Rift volcanism in the Lake Superior region; Sr, Nd, and Pb isotopic evidence for a mantle plume origin: Journal of Geophysical Research, V. 95B, p. 10851-10868.

Paster, T. P., Schauwecker, D. S., and Haskin, L. A., 1974, The behaviour of some trace elements during solidification of the Skaergaard layered series: Geochimica et Cosmochimica Acta, V.38, p. 1549-1577.

Pearce, J. A., Harris, N. B. W., and Tindle, A. G., 1984, Trace element discrimination diagrams for the tectonic interpretation of granitic rocks: Journal of Petrology, V. 25, p. 956-983.

Philpotts, A. R., 1976, Silicate liquid immiscibility: its probable extent and petrogenetic significance: American Journal of Science, V.276, p. 1147-1177.

_____, 1979, Silicate liquid immiscibility in tholeiitic basalts: Journal of Petrology, V.20, p. 99-118.

_____, 1982, Compositions of immiscible liquids in volcanic rocks: Contributions to Mineralogy and Petrology, V.80, p. 201-218.

Phinney, W. C., 1972, Duluth Complex, history and nomenclature, *in* Sims, P. K., and Morey, G. B., eds., Geology of Minnesota, A Centennial Volume: Minnesota Geological Survey, p. 333-345.

Roedder, E., 1951, Low temperature liquid immiscibility in the system K_2O-FeO-Al_2O_3-SiO_2: American Mineralogist, V.36, p. 282-286.

Roedder, E., and Weiblen, P. W., 1970, Lunar petrology of silicate melt inclusions, Apollo 11 rocks: Proceedings of the Apollo 11 Lunar Science Conference, V.1, p. 801-837.

_____, 1971, Petrology of silicate melt inclusions, Apollo 11 and Apollo 12 and terrestrial equivalents: Proceedings of the Second Lunar Science Conference, V.1, p. 507-528.

Schairer, J. F., 1957, Melting relations of the common rock-forming oxides: Journal of the American Ceramic Society, V.40, p. 215-235.

Schnetzler, C. C., and Philpotts, J. A., 1970, Partition coefficients of rare-earth elements between igneous matrix material and rock-forming mineral phenocrysts--II: Geochimica et Cosmochimica Acta, Vol. 34, p. 331-340.

Schwartz, G. M., and Sandberg, A. E., 1940, Rock series in diabase sills at Duluth, Minnesota: Geological Society of America Bulletin, V.51, p. 1135-1172.

Silver, L. T., and Green, J. C., 1963, Zircon age for Middle Keweenawan rocks of Lake Superior region [abs.]: Eos, V.44, p. 107.

Simmons, W. B., Hanson, S. L., and Rog, A. M., 1988, Fluorine abundance and HREE/LREE separation in low phosphate pegmatitic melts in the Pikes Peak Batholith, Colorado: Geological Society of America, Abstracts with Programs, V.20, No. 7, p. A251.

Sims, P. K, and Viswanathan, S., 1972, Giants Range Batholith, *in* Sims, P. K., and Morey, G. B., eds., Geology of Minnesota, A Centennial Volume: Minnesota Geological Survey, p. 120-139.

Stevenson, R. J., 1974, A mafic layered intrusion of Keweenawan age near Finland, Lake County, Minnesota: Unpubl. M.S. Thesis, University of Minnesota, Minneapolis, MN, 160p.

Streckeisen, A., 1979, Classification and nomenclature of volcanic rocks, lamprophyres, carbonatites, and melitic rocks: recommendations and suggestions of the IUGS Subcommission on the Systematics of Igneous Rocks: Geology, V.7, p. 331-335.

Taylor, H. P., Jr., 1978, Oxygen and hydrogen isotope studies of plutonic granitic rocks: Earth and Planetary Science Letters, V.38, p. 177-210.

Taylor, R. B., 1964, Geology of the Duluth Gabbro Complex near Duluth, Minnesota: Minnesota Geological Survey Bulletin 44, 63p.

Tuttle, O. F., and Bowen, N. L., 1958, Origin of granite in the light of experimental studies in the system $NaAlSi_3O_8$-$KAlSi_3O_8$-SiO_2-H_2O: Geological Society of America Memoir 74, 153p.

Van Schmus, W. R., Green, J. C., and Halls, H. C., 1982, Geochronology of Keweenawan rocks of the Lake Superior region: a summary: *in* Wold, R. J., and Hinze, W. J., eds., Geology and tectonics of the Lake Superior Basin: Geological Society of America Memoir 156, p. 165-171.

Van Schmus, W. R., and Hinze, W. J., 1985, The Midcontinent Rift System: Annual Review of Earth and Planetary Sciences, V.13, p. 345-383.

Wager, L. R., and Brown, G. M., 1967, Layered igneous rocks: San Francisco, W. H. Freeman and Company, 588p.

Walraven, F., 1985, Genetic aspects of the granophyric rocks of the Bushveld Complex: Economic Geology, V.80, p. 1166-1180.

Weiblen, P. W., 1982, Keweenawan intrusive igneous rocks, *in* Wold, R. J., and Hinze, W. J., eds., Geology and tectonics of the Lake Superior Basin: Geological Society of America Memoir 156, p. 57-82.

Weiblen, P. W., and Morey, G. B., 1980, A summary of the stratigraphy, petrology, and structure of the Duluth Complex: American Journal of Science, V.280-A, p. 88-133.

Whalen, J. B., Currie, K. L., and Chappell, B. W., 1987, A-type granites: geochemical characteristics, discrimination and petrogenesis: Contributions to Mineralogy and Petrology, V.95, p. 407-419.

Whitney, J. A., 1975, The effects of pressure, temperature, and X_{H2O} on phase assemblage in four synthetic rock compositions: Journal of Geology, V.83, p. 1-31.

Williams, H., Turner, F. J., and Gilbert, C. M., 1982, Petrography: An Introduction to the Study of Rocks in Thin Section, 2nd Ed.: New York, W. H. Freeman and Company, 626p.

APPENDIX I

Whole Rock Analyses

Whole rock analyses were done by the author using a Siemens SRS 300 XRF at Northern Illinois University, DeKalb, Illinois. Volatiles (H_2O^+ and CO_2) and rare earth elements were analyzed by Nuclear Activation Service, Inc., Ann Arbor, Michigan. Rare earth element analysis for sample EM64 was done by Eric Jerde at UCLA. The following table contains published major element analyses for standards W-2 and G-2 and corresponding values established by XRF analyses.

Element	Published analysis Standard W-2	W-2 in batch # 1	W-2 in batch # 2	Published analysis Standard G-2	G-2 in batch # 3	G-2 in batch # 4
SiO_2	52.8	52.3	52.3	69.1	69.3	69.4
TiO_2	1.06	1.05	1.06	0.49	0.49	0.49
Al_2O_3	15.5	14.9	15.0	15.1	15.8	15.8
Fe_2O_3	1.53			1.07		
FeO	8.36	9.85	9.85	1.45	2.30	2.30
MnO	0.167	0.168	0.168	0.034	0.034	0.032
MgO	6.39	6.44	6.36	0.763	0.89	0.89
CaO	10.9	10.9	10.9	1.97	1.91	1.91
Na_2O	2.21	2.19	2.19	4.07	4.12	4.21
K_2O	0.63	0.63	0.63	4.49	4.48	4.48
P_2O_5	0.14	0.12	0.12	0.14	0.15	0.15
TOTAL	99.69	98.59	98.58	98.68	99.51	99.60

Detection limits for the analyses from NAS are as follows:

H_2O^+	0.1000 %
CO_2	0.0100 %
La	0.1000 ppm
Ce	1.0000 ppm
Nd	3.0000 ppm
Sm	0.1000 ppm
Eu	0.0500 ppm
Tb	0.1000 ppm
Yb	0.0500 ppm
Lu	0.0100 ppm

In the following table major elements are given in weight %, and trace elements are given in ppm. FeO* indicates that total iron is given as FeO and "nd" indicates not determined. Abbreviations used for rock units are: MB = metabasalt, MGA = metagabbro, OD = ophitic diabase, SG = syenogabbro, FD = ferrodiorite, EMG = Eagle Mt. granophyre, RY = rhyolite, and MGR = miarolitic granophyre.

APPENDIX I: WHOLE ROCK ANALYSES

UNIT	MB	MB	MB	MGA	MGA	MGA	MGA	OD	OD
SAMPLE	EM16	EM19	EM45	EM9	EM30	EM52B	EM78	EM64	EM75
SiO2	46.9	47.9	45.3	46.2	45.8	47.8	42.8	48.9	47.8
TiO2	1.81	0.73	2.03	2.32	1.68	3.26	3.18	1.74	1.83
Al2O3	15.3	17.2	15	14.7	15.5	11.2	13.9	15.9	15.3
FeO*	12	8.32	13.6	15.6	13.8	14.9	19.1	12.4	12.1
MnO	0.19	0.14	0.17	0.21	0.18	0.23	0.21	0.18	0.18
MgO	6.02	9.24	6.82	6.04	8.48	5.39	7.08	7.11	6.75
CaO	11	11.2	11.7	9.29	9.34	11.3	8.43	10.1	9.89
Na2O	2.68	2.01	2.07	2.56	2.25	2.27	2.2	2.45	2.52
K2O	0.39	0.13	0.41	0.54	0.51	0.67	0.53	0.51	0.63
P2O5	0.17	0.04	0.03	0.12	0.1	0.16	0.05	0.17	0.2
H2O+	1.3	1.3	0.4	0.5	0.6	0.7	0.6	1	0.9
CO2	<0.01	<0.01	<0.01	<0.01	<0.01	<0.01	<0.01	<0.01	<0.01
TOTAL	97.76	98.21	97.53	98.08	98.24	97.88	98.08	100.46	98.1
Mg#	47.2	66.5	47.4	41	52.3	39.2	39.8	50.6	49.9
Sc	36	29	36	27	20	52	27	25	24
V	293	173	314	366	229	346	792	201	216
Cr	2	333	90	68	69	31	154	156	144
Co	59	53	62	71	75	57	85	58	57
Ni	73	263	94	67	223	14	114	137	137
Cu	99	62	30	188	207	735	145	139	156
Zn	97	64	92	123	115	140	144	103	103
Ga	19	16	21	27	20	23	23	25	21
Rb	11	6	13	18	17	25	15	14	19
Sr	266	211	264	288	289	217	262	318	301
Y	31	13	14	24	19	40	17	28	29
Zr	127	47	61	124	109	186	86	137	148
Nb	9	4	3	8	7	10	4	9	10
Ba	156	27	71	123	142	185	79	164	176
La(XRF)	14	9	5	16	13	9	7	15	15
Pb	4	3	5	8	6	3	nd	nd	2
Th	nd	nd	nd	0.6	3	3	nd	nd	0.2
La(INAA)		5.8			12			14.5	
Ce		13			26			32.6	
Nd		7			13			16.7	
Sm		1.5			2.8			4.3	
Eu		0.81			1.44			1.49	
Tb		0.3			0.3			0.74	
Yb		1.19			1.67			2.3	
Lu		0.18			0.27			0.33	

APPENDIX I: WHOLE ROCK ANALYSES

UNIT	SG	SG	SG	FD	FD	FD	FD	EMG	EMG
SAMPLE	EM39	EM60	EM62	EM38	EM63	EM81	EM82	EM1	EM4
SiO2	47	52.4	56.5	47.9	51.6	46.3	54.6	70.8	70.8
TiO2	3.65	0.99	1.48	2.31	2.1	2.64	1.5	0.53	0.52
Al2O3	13.1	16.5	19.1	12.2	11	10.2	15	12.4	12.5
FeO*	15.3	9.37	6.09	20	19.4	20.8	14.2	4.97	4.33
MnO	0.23	0.16	0.09	0.37	0.37	0.34	0.26	0.08	0.07
MgO	3.15	2.01	0.66	1.57	1.44	2.95	0.84	0.38	0.35
CaO	9.48	9.01	6.53	7.06	5.97	7.96	5.88	1.67	1.61
Na2O	2.99	3.87	4.49	3.37	3.1	2.69	4.23	4.13	3.65
K2O	0.87	1.31	1.86	1.14	1.85	1.1	1.21	4.06	4.06
P2O5	0.56	0.46	0.15	0.74	0.69	1.44	0.13	0.08	0.04
H2O+	0.9	1.1	1.1	0.6	0.9	0.9	0.8	nd	0.3
CO2	<0.01	<0.01	<0.01	<0.01	<0.01	<0.01	<0.01	nd	<0.01
TOTAL	97.23	97.18	98.05	97.26	98.42	97.32	98.65	99.1	98.23
Mg#	26.9	27.7	16.22	12.3	11.7	20.2	9.6	14	12.6
Sc	36	22	11	25	24	29	18	7	8
V	87	19	18	2	2	15	nd	nd	15
Cr	12	16	82	10	66	45	11	10	42
Co	49	27	24	27	27	46	20	5	46
Ni	4	3	4	0.1	8	4	1	10	6
Cu	187	35	63	71	74	84	20	26	29
Zn	177	99	63	214	209	235	157	130	90
Ga	26	29	29	31	28	24	33	nd	25
Rb	27	38	65	35	64	35	38	160	161
Sr	311	407	377	347	269	257	424	140	128
Y	50	52	36	73	101	96	49	50	68
Zr	203	186	197	306	314	286	418	450	600
Nb	14	10	17	26	27	20	23	30	37
Ba	186	401	487	431	566	390	554	1000	944
La(XRF)	21	30	26	32	44	45	25	77	71
Pb	3	5	9	nd	7	2	5	24	23
Th	3	3	7	4	7	0.5	3	13	16
La(INAA)		34.6							
Ce		67							
Nd		35							
Sm		8.1							
Eu		3.86							
Tb		1.1							
Yb		4.12							
Lu		0.62							

APPENDIX I: WHOLE ROCK ANALYSES

UNIT	EMG	EMG	EMG	EMG	EMG	EMG	EMG	EMG	RY
SAMPLE	EM10A	EM21	EM28	EM29	EM32	EM34	EM49	EM52A	EM17
SiO2	70.7	70.6	70.4	69.3	70.9	68.9	69.6	69.3	69.1
TiO2	0.55	0.49	0.58	0.59	0.52	0.6	0.65	0.63	0.48
Al2O3	12.7	12.5	12.8	12.8	12.8	12.7	12.7	12.7	12.3
FeO*	4.71	4.11	4.76	4.93	4.37	5.03	5.08	5.02	5.35
MnO	0.08	0.07	0.08	0.09	0.07	0.09	0.11	0.09	0.06
MgO	0.41	0.35	0.35	0.48	0.35	0.31	0.58	0.5	0.83
CaO	1.72	1.37	1.61	1.67	1.49	1.74	1.47	1.76	1.14
Na2O	3.7	3.37	3.8	3.66	3.77	3.77	3.92	3.25	3.04
K2O	4.24	4.71	4.05	4.3	4.21	4.01	3.76	5	4.76
P2O5	0.05	0.04	0.07	0.06	0.05	0.07	0.08	0.07	0.02
H2O+	0.3	0.3	0.2	0.4	0.3	0.3	0.6	0.4	nd
CO2	<0.01	0.01	<0.01	0.01	<0.01	<0.01	<0.01	<0.01	nd
TOTAL	99.16	97.91	98.7	98.28	98.83	97.52	98.55	98.72	97.08
Mg#	13.5	13.2	11.6	14.8	12.5	9.9	16.9	15.1	21.7
Sc	6	6	6	6	3	4	8	6	8
V	7	12	13	11	13	11	19	16	8
Cr	15	14	15	21	48	11	8	10	11
Co	36	59	69	64	33	52	56	45	43
Ni	3	5	5	5	7	5	5	6	3
Cu	30	27	24	27	17	13	8	25	14
Zn	87	94	94	96	81	99	122	87	96
Ga	23	24	22	24	23	25	23	22	24
Rb	148	154	138	152	153	152	124	177	134
Sr	136	131	129	151	131	150	193	172	162
Y	59	56	58	64	55	61	68	65	73
Zr	510	512	476	508	493	558	589	544	869
Nb	31	29	30	33	30	32	37	32	38
Ba	945	934	956	978	978	971	1119	951	2012
La(XRF)	66	60	66	69	62	64	71	66	62
Pb	22	21	39	22	19	22	23	20	14
Th	14	15	13	16	15	16	15	13	10
La(INAA)	73.9								
Ce	134								
Nd	50								
Sm	10.5								
Eu	2.5								
Tb	1.5								
Yb	4.89								
Lu	0.69								

APPENDIX I: WHOLE ROCK ANALYSES

UNIT	RY	RY	RY	RY	MGR	MGR	MGR
SAMPLE	EM53	EM54	EM56	EM67	EM57	EM68	EM43
SiO2	69.2	76.4	72.2	75.1	74.2	73.6	72.7
TiO2	0.56	0.25	0.39	0.29	0.25	0.28	0.29
Al2O3	12.4	11	12	12	12.1	11.8	12.1
FeO*	5.97	2.69	4.26	2.79	2.61	2.94	3.25
MnO	0.08	0.04	0.07	0.03	0.04	0.03	0.05
MgO	0.9	0.34	0.38	0.37	0.19	0.25	0.35
CaO	1.08	0.47	0.87	0.5	0.16	0.16	0.43
Na2O	3.32	2.2	3.17	3.19	2.56	2.08	3.1
K2O	4.28	5.57	4.7	4.64	5.84	6.34	5.32
P2O5	0.04	0.01	0.01	nd	nd	nd	nd
H2O+	0.5	0.4	0.3	0.5	0.8	0.6	0.6
CO2	<0.01	<0.01	<0.01	<0.01	<0.01	<0.01	<0.01
TOTAL	98.33	99.37	98.35	99.41	98.75	98.08	98.19
Mg#	21.2	18.4	13.8	19.2	11.5	13.2	16.1
Sc	9	1	3	5	1	1	1
V	14	13	15	8	2	6	8
Cr	14	11	21	19	12	15	10
Co	47	51	35	53	67	53	47
Ni	5	4	5	3	4	5	6
Cu	35	16	13	9	9	5	9
Zn	128	67	121	56	121	47	119
Ga	22	19	21	19	26	26	26
Rb	122	149	127	100	140	168	156
Sr	171	72	129	98	33	29	57
Y	79	64	76	69	107	76	102
Zr	823	488	698	569	724	720	763
Nb	37	30	36	31	56	61	54
Ba	1989	1031	1633	1018	947	1017	1066
La(XRF)	74	72	78	77	93	13	83
Pb	20	14	23	15	13	17	21
Th	11	14	13	15	16	19	17
La(INAA)		79.8				14	
Ce		153				nd	
Nd		64				10	
Sm		11.2				3.6	
Eu		1.75				0.78	
Tb		1.7				1.3	
Yb		6.04				9.45	
Lu		0.91				1.36	

APPENDIX II

CIPW Norms

CIPW norms for all analyzed samples were calculated using GPP (Geist, Baker, & McBirney, 1985). All values are in percent. The ratio of Fe^{2+}/Total Fe was assumed to be 0.85. Abbreviations used in the table indicate the following minerals:

Ap = apatite
Il = ilmenite
Mt = magnetite
Or = orthoclase
Ab = albite
An = anorthite
Di = diopside
Hy = hypersthene
Ol = olivine
Q = quartz
C = corundum

APPENDIX II: CIPW NORMS FOR ALL ANALYZED SAMPLES

	MB EM16	MB EM19	MB EM45	MGA EM9	MGA EM30	MGA EM52B	MGA EM78	OD EM64	OD EM75
Ap	0.40	0.09	0.07	0.28	0.23	0.37	0.12	0.40	0.47
Il	3.45	1.39	3.87	4.42	3.20	6.22	6.07	3.32	3.49
Mt	2.36	1.63	2.66	3.06	2.71	2.93	3.76	2.43	2.37
Or	2.31	0.77	2.42	3.20	3.02	3.96	3.14	3.02	3.73
Ab	22.70	17.02	17.54	21.70	19.06	19.24	18.65	20.76	21.35
An	28.52	37.43	30.55	27.10	30.70	18.37	26.54	30.90	28.48
Di	20.51	14.33	22.46	15.27	12.39	30.71	12.57	14.95	15.97
Hy	6.35	16.05	3.31	10.63	8.58	14.82	4.56	17.60	14.08
Ol	9.85	8.11	14.18	11.85	17.69		22.10	6.03	7.17
Q						0.59			
C									
Total	96.45	96.82	97.06	97.51	97.60	97.21	97.50	99.41	97.10

	SG EM39	SG EM60	SG EM61	SG EM62	SG EM80	FD EM38	FD EM63	FD EM81	FD EM82
Ap	1.31	1.07	0.51	0.35	0.21	1.73	1.61	3.37	0.30
Il	6.96	1.89	5.20	2.82	3.98	4.41	4.01	5.04	2.86
Mt	3.00	1.84	1.97	1.20	2.22	3.93	3.81	4.09	2.78
Or	5.15	7.75	5.38	11.00	4.38	6.75	10.95	6.51	7.16
Ab	25.34	32.78	29.99	38.02	26.68	28.59	26.29	22.82	35.85
An	19.65	23.89	24.97	26.54	22.66	14.91	10.66	12.62	18.43
Di	20.21	15.23	17.45	4.23	25.70	13.41	12.69	15.12	8.73
Hy	14.17	9.51	7.92	6.02	1.55	22.83	22.35	26.09	16.10
Ol					6.02				
Q	0.45	2.14	1.78	6.84		0.07	5.11	0.78	5.63
C									
Total	96.25	96.10	95.18	97.01	93.41	96.63	97.48	96.45	97.85

APPENDIX II: CIPW NORMS FOR ALL ANALYZED SAMPLES

	EMG EM4	EMG EM10A	EMG EM21	EMG EM28	EMG EM29	EMG EM32	EMG EM34	EMG EM49	EMG EM52A
Ap	0.09	0.12	0.09	0.16	0.14	0.12	0.16	0.19	0.16
Il	0.99	1.05	0.93	1.10	1.12	0.99	1.14	1.24	1.20
Mt	0.85	0.92	0.81	0.93	0.97	0.86	0.99	1.00	0.99
Or	23.99	25.06	27.83	23.93	25.41	24.88	23.70	22.22	29.55
Ab	30.89	31.32	28.52	32.17	30.98	31.91	31.91	33.18	27.51
An	5.76	5.44	5.07	5.85	5.72	5.49	6.00	6.04	5.16
Di	1.72	2.41	1.28	1.47	1.90	1.38	1.91	0.64	2.71
Hy	5.53	5.84	5.49	6.20	6.56	5.77	6.25	7.62	6.25
Ol									
Q	28.11	26.68	27.62	26.64	25.05	27.11	25.25	25.87	24.74
C									
Total	97.94	98.84	97.65	98.47	97.85	98.50	97.31	97.99	98.27

	RY EM17	RY EM53	RY EM54	RY EM56	RY EM67	MGR EM57	MGR EM68	MGR EM43
Ap	0.05	0.09	0.02	0.02				
Il	0.91	1.07	0.48	0.74	0.55	0.48	0.53	0.55
Mt	1.05	1.17	0.53	0.84	0.55	0.51	0.58	0.64
Or	28.13	25.30	32.91	27.77	27.41	34.50	37.46	31.43
Ab	25.74	28.11	18.62	26.83	26.99	21.66	17.60	26.24
An	5.53	5.10	2.27	4.25	2.48	0.79	0.79	2.13
Di								
Hy	9.15	10.13	4.41	6.61	4.54	3.92	4.48	5.20
Ol								
Q	26.42	26.46	39.18	30.80	35.52	34.80	34.85	30.94
C	0.08	0.43	0.54	0.17	0.77	1.25	1.18	0.50
Total	97.06	97.86	98.95	98.04	98.82	97.92	97.47	97.63

APPENDIX III

Mineral Chemistry Determined by Microprobe Analysis

Microprobe analyses were done by the author using the semi-automated MAC microprobe at the Natural Resources Research Institute in Duluth, Minnesota. Total Fe was analyzed as FeO; final FeO and Fe_2O_3 values were recalculated based on stoichiometry using the Petro computer program. The following standards from the C. M. Taylor Corporation were used:

Ti	Rutile
Cr	Chromite #5
Mn	Spessartine Garnet #4b
Fe	Hematite #2
Si	Olivine #1 (for olivine)
Si	Diopside #5a (for all other silicates)
Si	Spessartine Garnet #4b (for Fe-Ti oxides)
K	Orthoclase MAD-10
Ca	Diopside #5a
Na	Albite #4
Mg	Olivine #1 (for olivine)
Mg	Diopside #5a (for all other silicates)
Mg	Chromite #5 (for Fe-Ti oxides)
Al	Albite #4 (for all silicates)
Al	Spinel (for Fe-Ti oxides)

APPENDIX III: MICROPROBE ANALYSES - FELDSPAR

UNIT	(MB)	(MB)	(MB)	(MB)	(MB)	(MB)	(MB)	(MB)	(MB)	(MB)	(MB)	(MGA)	(MGA)
SAMPLE	EM19	EM19	EM19	EM19	EM19	EM19	EM19	EM19	EM19	EM19	EM19	EM30	EM30
TiO2	0.13	0.16	0.08	0.04	0.12	0.13	0.07	0.11	0.05	0	0	0	0.08
FeO	0.46	0.3	0.5	0.44	0.59	0.47	0.29	0.3	0.32	0.23	0.32	0.68	0.82
SiO2	46.23	52.95	52.14	48.86	47.54	51.89	51.84	52.32	51.71	52.09	51.99	51.98	51.75
K2O	0.04	0.13	0.08	0.06	0.02	0.06	1.11	0.12	0.63	0.11	0.11	0.4	0.33
CaO	16.71	11.48	13.16	15.4	16.14	13.34	14.33	13.34	13.58	13.15	12.75	12.38	12.63
Na2O	1.88	5.11	4.19	3.06	2.49	4.33	3.94	4.55	4.54	4.28	4.43	4	4.13
MgO	0.05	0	0.33	0.09	0.16	0	0.06	0.1	0.06	0.06	0.11	0.02	0
Al2O3	32.55	28.61	29.07	31.16	31.63	29.11	27.53	30.32	29.8	30.27	29.49	28.83	29.58
Total	98.05	98.74	99.55	99.11	98.69	99.33	99.17	101.16	100.69	100.19	99.2	98.29	99.32
	Cations-based on 8 oxygen												
Si	2.168	2.429	2.384	2.261	2.215	2.379	2.4	2.356	2.351	2.363	2.382	2.403	2.374
Al	1.799	1.547	1.565	1.699	1.737	1.573	1.501	1.608	1.596	1.617	1.592	1.571	1.599
Total	3.967	3.976	3.949	3.96	3.952	3.952	3.901	3.964	3.947	3.98	3.974	3.974	3.973
Ti	0.004	0.005	0.002	0	0.004	0.004	0.001	0.002	0.001	0	0	0	0.002
Mg	0.002	0	0.021	0.005	0.009	0	0.004	0.006	0.004	0.004	0.006	0	0
Fe	0.018	0.011	0.019	0.016	0.021	0.017	0.011	0.01	0.012	0.008	0.012	0.025	0.031
Na	0.169	0.454	0.37	0.274	0.224	0.385	0.353	0.396	0.399	0.375	0.393	0.358	0.366
Ca	0.839	0.564	0.644	0.763	0.805	0.655	0.71	0.643	0.662	0.639	0.625	0.613	0.62
K	0.001	0.006	0.004	0.002	0	0.002	0.065	0.006	0.036	0.005	0.005	0.023	0.019
Total	1.033	1.04	1.06	1.06	1.063	1.063	1.144	1.063	1.114	1.031	1.041	1.019	1.038

APPENDIX III: MICROPROBE ANALYSES - FELDSPAR

UNIT	(MGA)	(MGA)	(MGA)	(MGA)	(MGA)	(MGA)	(MGA)	(MGA)	(MGA)	(OD)	(OD)	(OD)	(OD)
SAMPLE	EM30	EM30	EM30	EM30	EM30	EM30	EM30	EM30	EM30	EM64	EM64	EM64	EM64
TiO2	0.07	0.24	0.16	0.09	0.17	0.12	0.03	0.09	0.05	0.04	0.27	0.08	0.06
FeO	1.18	0.93	0.58	0.59	0.58	0.49	0.52	1.15	0.57	0.47	0.64	0.64	4.3
SiO2	54.02	51.01	53.63	53.47	54.91	53.19	53.38	53.32	56.78	48.74	52.52	49.05	51.13
K2O	0.39	0.24	0.39	0.37	0.4	0.38	0.34	0.41	0.57	0.15	0.29	0.22	0.28
CaO	11.93	14.22	11.89	11.83	11.03	11.96	11.71	11.63	10.51	14.8	12.97	14.08	10.44
Na2O	4.43	3.59	4.48	4.19	4.93	4.52	4.41	4.23	5.54	2.88	4.08	3.52	4.11
MgO	0.13	0.04	0	0	0	0	0.02	0.14	0.06	0.12	0.2	0.19	1.39
Al2O3	28.9	30.54	28.12	28.86	27.96	29.12	28.96	28.91	26.54	31.23	29.22	30.49	26.66
Total	101.05	100.81	99.25	99.4	99.98	99.78	99.37	99.88	100.62	98.43	100.19	98.27	98.37
	Cations-based on 8 oxygen												
Si	2.429	2.317	2.45	2.437	2.483	2.418	2.433	2.424	2.548	2.264	2.384	2.286	2.396
Al	1.532	1.634	1.514	1.55	1.49	1.56	1.555	1.549	1.402	1.709	1.563	1.674	1.472
Total	3.961	3.951	3.964	3.987	3.973	3.978	3.988	3.973	3.95	3.973	3.947	3.96	3.868
Ti	0.001	0.008	0.005	0.002	0.005	0.004	0	0.002	0.001	0	0.009	0.002	0.001
Mg	0.008	0.001	0	0	0	0	0	0.009	0.004	0.008	0.012	0.012	0.096
Fe	0.043	0.034	0.021	0.021	0.021	0.019	0.019	0.042	0.021	0.018	0.024	0.024	0.167
Na	0.385	0.316	0.397	0.369	0.433	0.397	0.389	0.372	0.482	0.257	0.358	0.317	0.373
Ca	0.574	0.691	0.582	0.578	0.533	0.582	0.571	0.565	0.504	0.736	0.63	0.703	0.524
K	0.022	0.013	0.021	0.021	0.022	0.021	0.019	0.022	0.031	0.008	0.016	0.012	0.016
Total	1.033	1.063	1.026	0.991	1.014	1.023	0.998	1.012	1.043	1.027	1.049	1.07	1.177

APPENDIX III: MICROPROBE ANALYSES - FELDSPAR

UNIT	(OD)	(OD)	(OD)	(OD)	(OD)	(OD)	(OD)	(OD)	(OD)	(OD)	(OD)	(OD)	(OD)
SAMPLE	EM64	EM64	EM64	EM64	EM64	EM64	EM64	EM64	EM64	EM64	EM64	EM64	EM64
TiO2	0.07	0.03	0.11	0.03	0.05	0	0.04	0.11	0.04	0	0.1	0.13	0.3
FeO	0.59	0.62	0.7	0.66	0.74	0.71	0.53	1.4	0.58	0.53	0.74	0.53	0.71
SiO2	52.73	52.12	52.96	50.54	58.17	49.39	50.39	50.81	51.75	50.38	53.44	50.55	55.2
K2O	0.22	0.24	0.2	0.12	0.57	0.16	0.14	0.27	0.22	0.17	0.33	0.17	0.43
CaO	11.96	12.63	13.13	13.49	7.59	14.26	14.16	12.37	12.39	13.73	11.43	13.33	8.92
Na2O	4.96	4.11	4.15	3.71	6.66	3.47	3.59	4.17	4.31	3.71	4.88	4	5.94
MgO	0.2	0.14	0.16	0.09	0.1	0.2	0.11	0.47	0.12	0.14	0.08	0.17	0.04
Al2O3	27.7	29.18	29.67	30.23	25.77	30.5	29.64	28.73	29.45	30.65	28.2	30.38	26.89
Total	98.43	99.07	101.08	98.87	99.65	98.69	98.6	98.33	98.86	99.31	99.2	99.26	98.43
	Cations-based on 8 oxygen												
Si	2.437	2.393	2.385	2.333	2.615	2.292	2.336	2.363	2.378	2.312	2.445	2.324	2.526
Al	1.508	1.579	1.574	1.645	1.366	1.668	1.619	1.576	1.596	1.658	1.52	1.646	1.45
Total	3.945	3.972	3.959	3.978	3.981	3.96	3.955	3.939	3.974	3.97	3.965	3.97	3.976
Ti	0.001	0	0.002	0	0.001	0	0	0.002	0.001	0	0.002	0.004	0.009
Mg	0.013	0.008	0.01	0.005	0.006	0.013	0.006	0.033	0.008	0.009	0.005	0.011	0.001
Fe	0.021	0.022	0.025	0.024	0.027	0.027	0.02	0.053	0.021	0.02	0.028	0.02	0.027
Na	0.443	0.365	0.362	0.331	0.581	0.312	0.321	0.375	0.383	0.33	0.432	0.356	0.526
Ca	0.591	0.621	0.633	0.667	0.365	0.708	0.702	0.616	0.61	0.674	0.56	0.656	0.437
K	0.012	0.013	0.01	0.006	0.031	0.008	0.008	0.015	0.012	0.009	0.019	0.009	0.024
Total	1.081	1.029	1.042	1.033	1.011	1.068	1.057	1.094	1.035	1.042	1.046	1.056	1.024

APPENDIX III: MICROPROBE ANALYSES - FELDSPAR

UNIT	(OD)	(SG)	(SG)	(SG)	(SG)	(SG)	(SG)	(SG)	(SG)	(SG)	(SG)	(SG)	(SG)
SAMPLE	EM64	EM80	EM80	EM80	EM80	EM80	EM80	EM80	EM80	EM80	EM80	EM80	EM80
TiO2	0.02	0.03	0.17	0.11	0.13	0.12	0.2	0.03	0	0	0.12	0.17	0.2
FeO	0.59	0.45	0.3	0.38	0.29	0.27	0.3	0.38	0.43	0.36	0.34	0.3	0.28
SiO2	50.35	53.64	54.13	53.59	55.28	52.57	51.68	55.12	54.33	56.95	54.76	53.86	54.86
K2O	0.15	0.33	0.37	0.41	0.49	0.32	0.32	0.31	0.31	0.51	0.32	0.31	0.4
CaO	13.95	11.51	11.17	10.76	9.34	11.87	11.73	11.85	11.95	9.49	11.38	11.32	10.08
Na2O	3.52	4.98	5.36	5.18	5.79	4.86	4.88	4.93	4.87	5.99	4.75	4.56	5.78
MgO	0	0	0	0	0	0.02	0.01	0.02	0.02	0.01	0	0	0.05
Al2O3	30.12	28.35	28.51	28.3	27.18	28.04	29.13	28.91	28.75	27	28.65	28.24	27.48
Total	98.7	99.29	100.01	98.73	98.5	98.07	98.25	101.55	100.66	100.31	100.32	98.76	99.13
	Cations-based on 8 oxygen												
Si	2.33	2.451	2.451	2.458	2.525	2.431	2.389	2.458	2.445	2.556	2.465	2.462	2.496
Al	1.643	1.525	1.521	1.529	1.462	1.528	1.587	1.52	1.525	1.427	1.519	1.521	1.475
Total	3.973	3.976	3.972	3.987	3.987	3.959	3.976	3.978	3.97	3.983	3.984	3.983	3.971
Ti	0	0	0.005	0.002	0.004	0.004	0.006	0	0	0	0.004	0.005	0.006
Mg	0	0	0	0	0	0.001	0	0	0	0	0	0	0.002
Fe	0.021	0.016	0.01	0.013	0.01	0.009	0.011	0.013	0.016	0.013	0.012	0.01	0.009
Na	0.315	0.441	0.469	0.46	0.512	0.436	0.437	0.427	0.424	0.52	0.413	0.404	0.509
Ca	0.691	0.563	0.541	0.529	0.457	0.587	0.581	0.565	0.576	0.456	0.548	0.554	0.491
K	0.008	0.019	0.02	0.024	0.028	0.018	0.019	0.017	0.017	0.029	0.018	0.017	0.022
Total	1.035	1.039	1.045	1.028	1.011	1.055	1.054	1.022	1.033	1.018	0.995	0.99	1.039

APPENDIX III: MICROPROBE ANALYSES - FELDSPAR

UNIT	(FD)	(FD)	(FD)	(FD)	(FD)	(FD)	(FD)	(FD)	(FD)	(FD)	(FD)	(EMG)	(EMG)
SAMPLE	EM63	EM63	EM63	EM63	EM63	EM63	EM63	EM63	EM63	EM63	EM63	EM21	EM21
TiO2	0.09	0.04	0.05	0.17	0.05	0.11	0.13	0.05	0	0	0.04	nd	nd
FeO	0.3	0.32	0.24	0.14	0.17	0.25	0.32	0.33	0.38	0.26	0.2	0.29	0.36
SiO2	60.09	59.51	59.71	63.57	64.34	60.17	57.99	57.31	57.79	59.48	60.56	58.88	59.09
K2O	0.74	0.63	0.75	9.79	9.58	0.63	0.71	0.59	0.51	0.7	0.67	0.74	0.86
CaO	6.74	7.08	6.61	0.35	0.57	6.8	6.67	7.13	6.97	7.28	7.16	7.46	6.9
Na2O	7.84	7.65	8.08	3.92	5.09	7.46	7.04	7.27	7.37	7.72	7.53	6.93	7.13
MgO	0	0.05	0.01	0	0	0	0	0	0.03	0.05	0	nd	nd
Al2O3	25.85	25.98	26.26	20.32	20.43	25.77	25.42	26.73	26.78	23.25	23.16	26.21	25.37
Total	101.65	101.26	101.71	98.26	100.23	101.19	98.28	99.41	99.83	98.74	99.32	100.51	99.71
	Cations-based on 8 oxygen												
Si	2.648	2.633	2.631	2.924	2.913	2.656	2.636	2.584	2.593	2.701	2.725	2.624	2.652
Al	1.342	1.354	1.362	1.102	1.089	1.341	1.362	1.419	1.416	1.243	1.228	1.376	1.342
Total	3.99	3.987	3.993	4.026	4.002	3.997	3.998	4.003	4.009	3.944	3.953	4	3.994
Ti	0.002	0	0.001	0.005	0.001	0.002	0.004	0.001	0	0	0.001	nd	nd
Mg	0	0.002	0	0	0	0	0	0	0.001	0.003	0	nd	nd
Fe	0.01	0.012	0.008	0.005	0.005	0.009	0.012	0.012	0.013	0.009	0.007	0.01	0.013
Na	0.668	0.656	0.69	0.349	0.446	0.637	0.619	0.635	0.641	0.679	0.656	0.598	0.62
Ca	0.318	0.335	0.312	0.016	0.027	0.321	0.324	0.344	0.334	0.353	0.345	0.356	0.332
K	0.041	0.035	0.041	0.574	0.553	0.035	0.041	0.033	0.029	0.04	0.038	0.042	0.049
Total	1.039	1.04	1.052	0.949	1.032	1.004	1	1.025	1.018	1.084	1.047	1.006	1.014

APPENDIX III: MICROPROBE ANALYSES - FELDSPAR

UNIT	(EMG)	(EMG)	(EMG)	(EMG)	(EMG)	(EMG)	(EMG)	(EMG)	(EMG)	(EMG)	(EMG)	(EMG)	(EMG)
SAMPLE	EM21	EM21	EM21	EM21	EM21	EM21	EM21	EM21	EM34	EM34	EM34	EM34	EM34
TiO2	nd	nd	0	0	0	0.05	0.05	0	0	0	0.05	0.05	0
FeO	0.42	0.33	0.36	0.43	0.36	0.32	0.34	0.39	0.34	0.18	0.39	0.45	0.39
SiO2	59.64	59.27	60.83	60.29	62.34	58.31	58.13	60.06	63.69	68.68	60.2	58.43	61
K2O	0.93	0.87	0.92	1.13	0.13	0.81	0.72	0.89	0.88	10.92	0.65	0.65	1.75
CaO	6.4	6.29	6.13	5.56	3.84	7.17	7.11	5.99	5.67	0.24	7.07	7.43	6.21
Na2O	7.05	7.27	7.92	8.1	8.61	6.95	6.74	7.11	8.18	1.49	7.75	7.03	7.84
MgO	nd	nd	0	0.05	0.14	0.04	0	0.04	0	0.02	0	0.05	0
Al2O3	24.31	24.18	24.36	23.6	22.73	25.14	25.32	24.59	21.33	17.26	23.32	24.29	24.26
Total	98.75	98.21	100.52	99.16	98.15	98.79	98.41	99.07	100.09	98.79	99.43	98.38	101.45
	Cations-based on 8 oxygen												
Si	2.697	2.695	2.705	2.72	2.802	2.64	2.639	2.7	2.831	3.107	2.709	2.659	2.701
Al	1.295	1.295	1.276	1.253	1.203	1.341	1.355	1.302	1.117	0.919	1.236	1.302	1.265
Total	3.992	3.99	3.981	3.973	4.005	3.981	3.994	4.002	3.948	4.026	3.945	3.961	3.966
Ti	nd	nd	0	0	0	0.001	0.001	0	0	0	0.001	0.001	0
Mg	nd	nd	0	0.002	0.009	0.001	0	0.001	0	0	0	0.003	0
Fe	0.014	0.012	0.013	0.016	0.013	0.012	0.012	0.014	0.017	0.007	0.014	0.016	0.014
Na	0.617	0.64	0.682	0.708	0.75	0.61	0.593	0.62	0.705	0.13	0.676	0.619	0.673
Ca	0.309	0.305	0.291	0.267	0.185	0.347	0.345	0.288	0.27	0.011	0.341	0.362	0.293
K	0.053	0.049	0.052	0.064	0.006	0.046	0.041	0.05	0.049	0.629	0.037	0.037	0.099
Total	0.993	1.006	1.038	1.057	0.963	1.017	0.992	0.973	1.041	0.777	1.069	1.038	1.079

APPENDIX III: MICROPROBE ANALYSES - FELDSPAR

UNIT	(EMG)	(EMG)	(EMG)	(EMG)	(EMG)	(EMG)	(EMG)	(RY)	(RY)	(RY)	(RY)	(RY)	(RY)
SAMPLE	EM34	EM34	EM34	EM34	EM34	EM34	EM34	EM66	EM66	EM66	EM66	EM66	EM66
TiO2	0.07	0.04	0.04	0	0.03	0.11	0	0.07	0	0.01	0	0	0.05
FeO	0.44	0.43	0.23	0.42	0.27	0.21	0.32	0.14	0.2	1.09	0.37	1.04	0.59
SiO2	59.46	60.68	61.11	60.51	61.83	62.51	58.93	63.68	64.84	64.93	64.21	64.57	68.31
K2O	1	1.02	0.45	0.23	0.2	0.06	0.84	17.06	12.48	6.21	2.84	0.43	0.29
CaO	8.09	6.34	5.09	5.13	5.18	4.27	7.8	0.17	0	0.46	0.53	0.36	0.4
Na2O	7.4	8.43	8.45	8.6	8.3	8.99	7.79	0.15	4.54	7.95	8.55	10.66	10.8
MgO	0	0	0.01	0	0.02	0	0.07	0	0	0	0.03	0.11	0
Al2O3	24.78	24.36	23.57	24.35	23.99	24.05	25.55	18.9	19.08	19.81	22.45	21.28	20.84
Total	101.24	101.3	98.95	99.24	99.82	100.2	101.3	100.17	101.14	100.46	98.98	98.45	101.28
	Cations-based on 8 oxygen												
Si	2.645	2.691	2.744	2.712	2.745	2.76	2.621	2.953	2.948	0.356	2.866	2.889	2.951
Al	1.299	1.272	1.247	1.286	1.255	1.252	1.339	1.033	1.022	5.075	1.18	1.121	1.061
Total	3.944	3.963	3.991	3.998	4	4.012	3.96	3.986	3.97	5.431	4.046	4.01	4.012
Ti	0.001	0	0	0	0	0.002	0	0.001	0	0	0	0	0.001
Mg	0	0	0	0	0	0	0.004	0	0	1.048	0.001	0.006	0
Fe	0.016	0.015	0.007	0.014	0.009	0.008	0.012	0.005	0.006	2.917	0.013	0.038	0.02
Na	0.638	0.725	0.736	0.747	0.714	0.768	0.672	0.012	0.399	0	0.74	0.924	0.904
Ca	0.385	0.3	0.245	0.246	0.246	0.201	0.371	0.008	0	0.692	0.024	0.017	0.018
K	0.056	0.057	0.025	0.013	0.01	0.002	0.047	1.008	0.723	0.021	0.161	0.023	0.015
Total	1.096	1.097	1.013	1.02	0.979	0.981	1.106	1.034	1.128	4.678	0.939	1.008	0.958

APPENDIX III: MICROPROBE ANALYSES - FELDSPAR

UNIT	(RY)	(RY)	(RY)	(RY)	(RY)	(RY)	(RY)	(RY)	(RY)	(MG)	(MG)	(MG)	(MG)
SAMPLE	EM66	EM66	EM66	EM66	EM66	EM66	EM66	EM66	EM66	EM68	EM68	EM68	EM68
TiO2	0	0.04	0.01	0	0.04	0	0	0	0	0.13	0.14	0.18	0.03
FeO	2.75	0.38	1.66	0.81	0.66	0.26	0.4	0.61	2.16	1.93	0.77	7.43	0.89
SiO2	62.75	66.94	65.24	65.99	66.13	66.19	66.44	63.02	65.91	66.31	64.5	60.9	65.64
K2O	10.7	1.05	1.65	6.84	0.38	1.35	0.56	15.84	3.16	3.02	0.46	7.66	6.37
CaO	0	0.39	0.39	0	0.66	0.02	0.47	0	0.84	0.26	0.93	0	0
Na2O	5.28	9.75	9.59	5.54	10.44	9.65	9.62	1.12	7.36	7.36	10.85	5.25	6.88
MgO	0.08	0.05	0.05	0.04	0.07	0	0.09	0	0	0.08	0.07	0	0.07
Al2O3	19.22	20.59	21.28	19.51	21.24	20.7	20.93	18.84	19.75	19.71	20.47	17.06	18.93
Total	100.78	99.19	99.87	98.73	99.62	98.17	98.51	99.43	99.18	98.8	98.19	98.48	98.81
	Cations-based on 8 oxygen												
Si	2.886	2.954	2.894	2.981	2.912	2.951	2.944	2.948	2.952	2.966	2.897	2.89	2.974
Al	1.042	1.069	1.111	1.038	1.102	1.087	1.092	1.037	1.042	1.038	1.083	0.954	1.01
Total	3.928	4.023	4.005	4.019	4.014	4.038	4.036	3.985	3.994	4.004	3.98	3.844	3.984
Ti	0	0.001	0	0	0.001	0	0	0	0	0.004	0.004	0.005	0
Mg	0.004	0.002	0.002	0.001	0.003	0	0.005	0	0	0.004	0.004	0	0.004
Fe	0.105	0.013	0.061	0.03	0.023	0.009	0.014	0.023	0.08	0.072	0.029	0.293	0.033
Na	0.471	0.833	0.824	0.484	0.891	0.833	0.826	0.1	0.639	0.638	0.945	0.481	0.604
Ca	0	0.018	0.018	0	0.031	0	0.022	0	0.039	0.012	0.043	0	0
K	0.627	0.058	0.092	0.394	0.021	0.076	0.031	0.944	0.18	0.172	0.026	0.462	0.367
Total	1.207	0.925	0.997	0.909	0.97	0.918	0.898	1.067	0.938	0.902	1.051	1.241	1.008

APPENDIX III: MICROPROBE ANALYSES - FELDSPAR

UNIT	(MG)	(MG)	(MG)	(MG)	(MG)	(MG)	(MG)	(MG)	(MG)	(MG)	(MG)	(MG)	(MG)
SAMPLE	EM68	EM68	EM68	EM68	EM68	EM68	EM68	EM68	EM68	EM68	EM68	EM68	EM68
TiO2	0	0.04	0	0	0.01	0.07	0.05	0	0	0	0	0	0
FeO	0.96	0.23	0.49	0.61	0.8	0.83	0.93	0.54	0.85	0.86	2.59	0.54	0.14
SiO2	66.01	69.14	67.04	67.61	67.43	61.81	63.55	64.41	66.72	67.09	66.28	71.36	63.56
K2O	4.11	0.22	0.28	0.16	11.06	15.89	15.85	8.71	1.18	0.11	0.29	7.32	16.22
CaO	0	0.07	0.06	0.26	0	0	0	0	0	0	0	0	0
Na2O	8.06	11.78	11.58	10.8	3.06	0	0.63	7.07	10.84	11.14	11.35	4.39	0.14
MgO	0.02	0	0.01	0.07	0	0	0	0.03	0	0	0	0.05	0.04
Al2O3	19.29	19.88	20.02	20.29	18.64	20.57	18.96	19.45	19.55	19.79	19.62	16.64	18.45
Total	98.45	101.36	99.48	99.8	101	99.17	99.97	100.21	99.14	98.99	100.13	100.3	98.55
	Cations-based on 8 oxygen												
Si	2.977	2.986	2.956	2.961	3.022	2.893	2.95	2.921	2.965	2.969	2.935	3.144	2.983
Al	1.024	1.011	1.04	1.047	0.983	1.134	1.036	1.04	1.023	1.032	1.023	0.863	1.02
Total	4.001	3.997	3.996	4.008	4.005	4.027	3.986	3.961	3.988	4.001	3.958	4.007	4.003
Ti	0	0	0	0	0	0.001	0.001	0	0	0	0	0	0
Mg	0	0	0	0.003	0	0	0	0.001	0	0	0	0.002	0.002
Fe	0.036	0.007	0.017	0.021	0.029	0.031	0.035	0.02	0.031	0.031	0.095	0.019	0.004
Na	0.704	0.986	0.99	0.917	0.266	0	0.056	0.62	0.934	0.956	0.973	0.375	0.012
Ca	0	0.002	0.002	0.011	0	0	0	0	0	0	0	0	0
K	0.235	0.011	0.015	0.007	0.632	0.948	0.938	0.503	0.066	0.005	0.015	0.411	0.971
Total	0.975	1.006	1.024	0.959	0.927	0.98	1.03	1.144	1.031	0.992	1.083	0.807	0.989

APPENDIX III: MICROPROBE ANALYSES - FELDSPAR

UNIT	(MG)	(MG)	(MG)	(MG)
SAMPLE	EM68	EM68	EM68	EM68
TiO2	0	0	0	0
FeO	0.12	0.38	0.21	0.95
SiO2	64.02	63.16	64.39	63.3
K2O	16.27	16.6	16.6	15.82
CaO	0	0	0	0
Na2O	0.11	0.04	0.09	0.16
MgO	0	0.11	0.03	0
Al2O3	19.28	18.83	17.68	18.28
Total	99.8	99.12	99	98.51
	Cations-based on 8 oxygen			
Si	2.965	2.959	3.012	2.974
Al	1.052	1.039	0.975	1.012
Total	4.017	3.998	3.987	3.986
Ti	0	0	0	0
Mg	0	0.007	0.001	0
Fe	0.004	0.014	0.008	0.036
Na	0.009	0.002	0.007	0.014
Ca	0	0	0	0
K	0.96	0.991	0.99	0.947
Total	0.973	1.014	1.006	0.997

APPENDIX III: MICROPROBE ANALYSES - PYROXENE

UNIT	(MB)	(MB)	(MB)	(MB)	(MB)	(MB)	(MGA)	(MGA)	(MGA)	(MGA)	(MGA)
SAMPLE	EM19	EM19	EM19	EM19	EM19	EM19	EM30	EM30	EM30	EM30	EM30
TiO2	0.64	0.41	0.52	0.46	0.56	0.05	0.48	0.7	0.87	1.07	1.17
Cr2O3	0.84	0.72	0.64	0.23	0.22	0.06	0.08	0.07	0	0.08	0.07
MnO	0.14	0.13	0.2	0.16	0.2	0.2	0.27	0.35	0.25	0.24	0.25
FeO	5.91	5.83	6.07	6.91	7.65	5.27	10.13	11.65	10.02	10.26	9.79
SiO2	52.75	52.18	53.18	52.93	52.05	54.34	49.79	49.32	50.07	48.54	49.11
K2O	0.06	0.01	0.04	0.04	0.05	0.02	0.41	0	0	0.04	0
CaO	20.82	20.74	19.46	19.68	19.44	23.53	20.58	16.96	19.63	20.32	19.93
Na2O	0.17	0.19	0.46	0.07	0.07	0.18	0.29	0.34	0.37	0.34	0.3
MgO	17.26	17.44	16.77	17.79	17.72	16.38	14.4	16.94	15.09	15.07	15.04
Al2O3	2.72	2.61	1.73	1.5	2.01	0.88	1.8	1.89	1.84	2.39	2.79
Total	101.3	100.27	99.06	99.76	99.99	100.9	98.23	98.23	98.13	98.36	98.46
	Cations - based on 6 oxygen										
Si	1.911	1.911	1.962	1.948	1.92	1.978	1.91	1.885	1.911	1.862	1.869
Al	0.116	0.111	0.075	0.064	0.086	0.037	0.081	0.085	0.082	0.108	0.125
Total	2.027	2.022	2.037	2.012	2.006	2.015	1.991	1.97	1.993	1.97	1.994
Ti	0.017	0.011	0.014	0.012	0.015	0.001	0.013	0.019	0.024	0.03	0.033
Cr	0.023	0.02	0.018	0.006	0.005	0.001	0.002	0.001	0	0.002	0.002
Mg	0.932	0.951	0.921	0.975	0.974	0.887	0.823	0.964	0.858	0.861	0.854
Fe	0.178	0.178	0.019	0.211	0.236	0.16	0.324	0.372	0.319	0.329	0.312
Mn	0.004	0.003	0.005	0.004	0.005	0.005	0.008	0.011	0.008	0.006	0.008
Ca	0.808	0.813	0.769	0.775	0.768	0.917	0.845	0.694	0.802	0.835	0.812
Na	0.011	0.013	0.032	0.004	0.004	0.013	0.021	0.024	0.027	0.024	0.022
K	0.002	0	0.001	0.001	0.002	0	0.02	0	0	0.001	0
Total	1.975	1.989	1.779	1.988	2.009	1.984	2.056	2.085	2.038	2.088	2.043

APPENDIX III: MICROPROBE ANALYSES - PYROXENE

UNIT	(MGA)	(MGA)	(OD)	(OD)	(OD)	(OD)	(OD)	(SG)	(SG)	(SG)	(SG)
SAMPLE	EM30	EM30	EM64	EM64	EM64	EM64	EM64	EM80	EM80	EM80	EM80
TiO2	1.02	1.3	1.14	0.84	1.14	0.65	0.89	0.84	0.83	0.67	0.7
Cr2O3	0.06	0.11	0.14	0.24	0.06	0.34	0.3	0	0	0	0
MnO	0.3	0.28	0.22	0.13	0.25	0.21	0.2	0.56	0.63	0.56	0.34
FeO	9.91	9.89	10.48	10.26	12.03	9.9	9.33	20.34	16.6	22.46	15.12
SiO2	49.66	48.93	49.76	50.48	50.5	51.05	50.12	50.29	49.69	49.55	49.66
K2O	0.01	0	0.09	0	0.01	0	0	0.03	0.04	0.01	0.05
CaO	19.6	20.14	18.91	19.77	18.75	17.69	19.63	14.53	20.54	14.24	18.78
Na2O	0.42	0.33	0.46	0.32	0.35	0.29	0.32	0	0.15	0.11	0.16
MgO	15.24	14.96	14.85	14.92	14.08	16.02	14.95	12.53	9.83	11.95	12.13
Al2O3	1.96	2.68	2.91	3.08	2.83	1.94	2.95	1.02	1.21	1	2.22
Total	98.19	98.63	98.96	100.03	99.98	98.09	98.67	100.14	99.54	100.56	99.14
	Cations - based on 6 oxygen										
Si	1.897	1.863	1.885	1.888	1.898	1.933	1.895	1.941	1.934	1.926	1.914
Al	0.087	0.119	0.129	0.135	0.125	0.085	0.131	0.046	0.055	0.045	0.101
Total	1.984	1.982	2.014	2.023	2.023	2.018	2.026	1.987	1.989	1.971	2.015
Ti	0.029	0.037	0.032	0.023	0.032	0.018	0.024	0.023	0.024	0.019	0.02
Cr	0.001	0.003	0.003	0.006	0.001	0.01	0.009	0	0	0	0
Mg	0.868	0.849	0.838	0.831	0.789	0.903	0.842	0.72	0.57	0.692	0.697
Fe	0.316	0.315	0.331	0.32	0.377	0.313	0.294	0.655	0.54	0.73	0.486
Mn	0.009	0.009	0.006	0.003	0.007	0.006	0.005	0.018	0.021	0.018	0.01
Ca	0.802	0.821	0.767	0.792	0.754	0.717	0.794	0.6	0.856	0.593	0.775
Na	0.03	0.023	0.033	0.021	0.024	0.02	0.022	0	0.011	0.007	0.011
K	0	0	0.004	0	0	0	0	0.001	0.001	0	0.002
Total	2.055	2.057	2.014	1.996	1.984	1.987	1.99	2.017	2.023	2.059	2.001

APPENDIX III: MICROPROBE ANALYSES - PYROXENE

UNIT	(SG)	(SG)	(SG)	(SG)	(SG)	(FD)	(FD)	(FD)	(FD)	(FD)	(FD)
SAMPLE	EM80	EM80	EM80	EM80	EM80	EM63	EM63	EM63	EM63	EM63	EM63
TiO2	0.93	0.84	0.5	0.56	0.59	0.79	0.61	0.57	0.57	0.64	0.58
Cr2O3	0	0	0	0	0.09	0.06	0.07	0.04	0.06	0.07	0.05
MnO	0.3	0.52	0.54	0.48	0.32	0.5	0.45	0.51	0.55	0.42	0.47
FeO	17.19	19.41	23.4	19.34	19.15	24.82	23.53	23.12	24.18	24.69	22.96
SiO2	48.41	50.67	49.82	49.89	47.11	47.49	47.96	49.43	48.28	49.2	49.17
K2O	0.09	0	0	0	0.25	0	0	0	0	0	0
CaO	17.95	15.68	12.93	18.58	17.32	18.11	19.74	18.74	18.3	18.19	18.96
Na2O	0.09	0	0.13	0.12	0.14	0.22	0.37	0.22	0.3	0.04	0.13
MgO	11.77	13.32	11.91	10.28	10.21	5.93	5.74	6.74	5.64	5.3	6.46
Al2O3	2.46	1.27	0.98	1.42	3.34	0.9	0.51	0.75	0.92	0.93	0.78
Total	99.18	101.71	100.21	100.68	98.5	98.81	98.99	100.13	98.79	99.47	99.55
	Cations - based on 6 oxygen										
Si	1.885	1.921	1.943	1.93	1.865	1.932	1.945	1.962	1.956	1.974	1.962
Al	0.112	0.057	0.044	0.064	0.155	0.043	0.024	0.035	0.043	0.044	0.036
Total	1.997	1.978	1.987	1.994	2.02	1.975	1.969	1.997	1.999	2.018	1.998
Ti	0.026	0.023	0.014	0.016	0.017	0.024	0.018	0.016	0.016	0.188	0.016
Cr	0	0	0	0	0.002	0.001	0.002	0.001	0.001	0.001	0.001
Mg	0.682	0.751	0.691	0.592	0.602	0.359	0.346	0.398	0.34	0.317	0.384
Fe	0.559	0.615	0.762	0.625	0.633	0.844	0.797	0.768	0.819	0.828	0.766
Mn	0.009	0.015	0.017	0.015	0.01	0.017	0.016	0.016	0.019	0.014	0.015
Ca	0.748	0.636	0.54	0.77	0.734	0.789	0.857	0.797	0.794	0.782	0.811
Na	0.005	0	0.009	0.008	0.01	0.017	0.029	0.016	0.023	0.002	0.009
K	0.004	0	0	0	0.011	0	0	0	0	0	0
Total	2.033	2.04	2.033	2.026	2.019	2.051	2.065	2.012	2.012	2.132	2.002

APPENDIX III: MICROPROBE ANALYSES - PYROXENE

UNIT	(FD)	(FD)	(EMG)	(EMG)	(EMG)	(EMG)	(EMG)	(EMG)	(EMG)	(EMG)	(EMG)
SAMPLE	EM63	EM63	EM21	EM21	EM21	EM21	EM21	EM21	EM34	EM34	EM34
TiO2	0.78	0.54	0.39	0.3	0.2	0.22	0.28	0.39	0.27	0.39	0.46
Cr2O3	0.07	0.1	0	0	0.01	0	0.02	0	0.03	0.05	0
MnO	0.56	0.48	0.98	0.99	0.94	1.04	1.04	1.11	0.91	0.96	0.93
FeO	23.46	24.94	19.06	18.67	19.88	19.32	18.31	18.8	22.57	22.86	22.06
SiO2	48.81	48.3	50.71	49.74	50.33	50.8	49.66	50.29	49.18	49.56	50.02
K2O	0	0	0	0.06	0	0.03	0	0	0.16	0.02	0.08
CaO	18.62	18.21	20.25	20.68	20.05	19.91	20.2	20.69	18.42	18.63	18.51
Na2O	0.13	0.17	0.45	0.44	0.55	0.39	0.38	0.46	0.3	0.38	0.24
MgO	5.65	6.14	8.25	7.99	7.51	7.77	8.21	8.34	8.18	7.94	8.32
Al2O3	0.76	0.95	0.66	0.81	0.76	0.78	0.76	0.74	0.71	0.79	0.74
Total	98.85	99.82	100.75	99.67	100.24	100.25	98.86	100.82	100.73	101.57	101.38
	Cations - based on 6 oxygen										
Si	1.967	1.941	1.97	1.958	1.973	1.982	1.965	1.957	1.941	1.938	1.951
Al	0.036	0.044	0.029	0.037	0.034	0.035	0.035	0.033	0.032	0.036	0.033
Total	2.003	1.985	1.999	1.995	2.007	2.017	2	1.99	1.973	1.974	1.984
Ti	0.024	0.015	0.01	0.008	0.005	0.005	0.008	0.01	0.008	0.012	0.013
Cr	0.001	0.002	0	0	0	0	0	0	0	0.001	0
Mg	0.339	0.367	0.478	0.468	0.438	0.451	0.484	0.482	0.481	0.463	0.483
Fe	0.79	0.837	0.619	0.614	0.651	0.629	0.605	0.61	0.745	0.747	0.719
Mn	0.019	0.015	0.032	0.032	0.031	0.033	0.033	0.036	0.03	0.031	0.029
Ca	0.803	0.784	0.842	0.872	0.842	0.832	0.856	0.862	0.778	0.781	0.772
Na	0.009	0.013	0.033	0.032	0.041	0.028	0.028	0.034	0.023	0.028	0.017
K	0	0	0	0.002	0	0.001	0	0	0.006	0.001	0.004
Total	1.985	2.033	2.014	2.028	2.008	1.979	2.014	2.034	2.071	2.064	2.037

APPENDIX III: MICROPROBE ANALYSES - PYROXENE

UNIT	(EMG)	(EMG)	(EMG)	(EMG)	(EMG)	(EMG)
SAMPLE	EM34	EM34	EM34	EM34	EM34	EM34
TiO2	0.37	0.31	0.21	0.26	0.14	0.29
Cr2O3	0	0	0.03	0.04	0	0.05
MnO	1.04	0.92	0.82	1.02	0.98	1.13
FeO	23.18	23.78	23.7	22.77	22.51	23.47
SiO2	48.96	47.86	48.23	47.31	49.5	47.61
K2O	0.02	0.27	0	0.03	0.02	0.03
CaO	18.32	18.26	17.74	18.73	18.34	17.56
Na2O	0.3	0.29	0.29	0.23	0.23	0.14
MgO	7.36	7.48	7.77	7.44	7.67	7.63
Al2O3	0.84	0.84	0.87	0.75	0.78	0.8
Total	100.39	100	99.65	98.58	100.16	98.71
	Cations - based on 6 oxygen					
Si	1.943	1.92	1.932	1.921	1.958	1.928
Al	0.038	0.039	0.04	0.036	0.036	0.038
Total	1.981	1.959	1.972	1.957	1.994	1.966
Ti	0.011	0.009	0.006	0.007	0.004	0.008
Cr	0	0	0	0.001	0	0.001
Mg	0.434	0.446	0.463	0.451	0.452	0.459
Fe	0.769	0.797	0.794	0.773	0.744	0.795
Mn	0.034	0.031	0.027	0.035	0.033	0.038
Ca	0.779	0.784	0.761	0.814	0.776	0.762
Na	0.022	0.022	0.021	0.018	0.016	0.011
K	0.001	0.013	0	0.001	0.001	0.001
Total	2.05	2.102	2.072	2.1	2.026	2.075

APPENDIX III: MICROPROBE ANALYSES - OLIVINE

UNIT	(MGA)	(MGA)	(MGA)	(MGA)	(MGA)	(MGA)	(MGA)	(OD)	(OD)	(OD)
SAMPLE	EM30	EM30	EM30	EM30	EM30	EM30	EM30	EM64	EM64	EM64
MnO	0.39	0.3	0.55	0.37	0.33	0.43	0.43	0.43	0.48	0.57
FeO	27.34	27.63	27.18	26.39	26.67	27.65	26.45	41.62	41.29	43.41
SiO2	38.11	38.73	37.74	38.93	38.33	38.42	38.13	33.06	32.76	32.05
CaO	0.56	0.09	0.06	0.2	0.05	0.02	0.07	0.27	0.23	0.21
MgO	35.51	34.82	35.13	35.76	36.34	34.3	36.01	22.91	23.53	22.22
Total	101.91	101.57	100.65	101.65	101.71	100.83	101.11	98.29	98.29	98.46
	Cations - based on 4 oxygen									
Si	0.996	1.014	0.999	1.012	0.999	1.014	1	0.974	0.965	0.954
Mg	1.383	1.357	1.386	1.385	1.412	1.35	1.407	1.006	1.033	0.987
Fe	0.597	0.604	0.601	0.574	0.581	0.61	0.58	1.026	1.017	1.081
Mn	0.008	0.006	0.011	0.007	0.007	0.009	0.009	0.01	0.011	0.014
Ca	0.015	0.002	0.001	0.005	0	0	0.001	0.007	0.007	0.006
Total	2.003	1.969	1.999	1.971	2	1.969	1.997	2.049	2.068	2.088

APPENDIX III: MICROPROBE ANALYSES - OLIVINE

UNIT	(OD)	(OD)	(OD)	(OD)	(OD)	(OD)	(FD)	(FD)	(FD)	(FD)
SAMPLE	EM64	EM64	EM64	EM64	EM64	EM64	EM38	EM38	EM38	EM38
MnO	0.6	0.61	0.63	0.6	0.55	0.51	1.35	1.38	1.29	1.32
FeO	43.86	41.41	43.02	41.26	41.85	43.47	63.87	62.14	61.69	62.95
SiO2	32.53	35.05	34.75	34.64	34.73	35.2	31.33	31.56	31.3	31.81
CaO	0.27	0.41	0.42	0.35	0.36	0.4	0.27	0.27	0.34	0.32
MgO	24.02	21.49	21.98	22.91	23.14	20.96	4.17	4.18	3.77	4.08
Total	101.27	98.96	100.8	99.76	100.64	100.55	100.99	99.53	98.39	100.48
	Cations - based on 4 oxygen									
Si	0.94	1.018	0.998	0.998	0.993	1.013	1.012	1.027	1.032	1.028
Mg	1.035	0.93	0.941	0.983	0.986	0.899	0.2	0.203	0.185	0.196
Fe	1.061	1.006	1.034	0.994	1	1.047	1.727	1.692	1.7	1.701
Mn	0.014	0.014	0.015	0.014	0.012	0.012	0.036	0.037	0.036	0.036
Ca	0.007	0.012	0.012	0.01	0.011	0.012	0.009	0.009	0.012	0.011
Total	2.117	1.962	2.002	2.001	2.009	1.97	1.972	1.941	1.933	1.944

APPENDIX III: MICROPROBE ANALYSES - OLIVINE

UNIT	(FD)	(FD)	(FD)	(FD)
SAMPLE	EM38	EM38	EM38	EM38
MnO	1.35	1.49	1.27	1.47
FeO	61.55	63.22	62.43	61.68
SiO2	31.25	31.95	31.04	31.31
CaO	0.33	0.34	0.33	0.32
MgO	3.79	4.03	3.94	4.05
Total	98.27	101.03	99.01	98.83
	Cations - based on 4 oxygen			
Si	1.031	1.027	1.02	1.028
Mg	0.186	0.193	0.193	0.197
Fe	1.699	1.701	1.717	1.693
Mn	0.038	0.041	0.035	0.04
Ca	0.011	0.011	0.012	0.011
Total	1.934	1.946	1.957	1.941

APPENDIX III: MICROPROBE ANALYSES - FE-TI OXIDES

UNIT	(MB)	(MB)	(MB)	(MB)	(MB)	(MB)	(MB)	(MB)	(MB)	(MGA)	(MGA)
SAMPLE	EM19	EM19	EM19	EM19	EM19	EM19	EM19	EM19	EM19	EM30	EM30
TiO2	46.49	42.26	47.17	47.54	48.29	46.88	8.1	9.29	9.34	46.8	47.3
Cr2O3	0	0	0.03	0.04	0	0.05	0.04	0.02	0.07	0.02	0.07
MnO	2.77	2.43	0.47	0.74	2.36	3.84	0.46	1.23	1.04	0.53	0.42
FeO	37.27	35.7	34.35	34.41	37.22	36.72	36.17	38.31	38.68	31.78	31.84
Fe2O3	11.15	12.27	12.21	12.78	9.58	10.64	49.16	46.52	46.58	14.06	13.94
SiO2	0.31	0.19	0.23	0.3	0.27	0.17	0.32	0.35	0.3	0.02	0
MgO	0.97	1.93	4.26	4.26	2.14	0.87	1.31	0.12	0.08	5.48	5.76
Al2O3	0.232	0.24	0.25	0.29	0.23	0.23	3.3	3.08	3.06	0.19	0.19
Total	98.97	98.83	98.7	100.01	99.82	99.17	98.5	98.55	98.78	98.84	99.45
	Cations - based on 12 oxygen										
Si	0.007	0.004	0.005	0.007	0.007	0.004	0.014	0.014	0.013	0	0
Al	0.009	0.007	0.007	0.008	0.007	0.007	0.175	0.163	0.162	0.005	0.005
Cr	0	0	0	0	0	0	0.001	0	0.003	0	0
Fe3+	0.219	0.242	0.236	0.244	0.184	0.209	1.672	1.583	1.582	0.272	0.267
Ti	0.916	0.912	0.913	0.908	0.929	0.922	0.275	0.316	0.317	0.905	0.907
Total	1.151	1.165	1.161	1.167	1.127	1.142	2.137	2.076	2.077	1.182	1.179
Mg	0.037	0.007	0.163	0.161	0.081	0.034	0.088	0.008	0.005	0.21	0.218
Fe2+	0.817	0.782	0.739	0.731	0.797	0.803	1.369	1.45	1.462	0.683	0.679
Mn	0.061	0.054	0.009	0.016	0.051	0.085	0.017	0.046	0.038	0.011	0.009
Total	0.915	0.843	0.911	0.908	0.929	0.922	1.474	1.504	1.505	0.904	0.906

APPENDIX III: MICROPROBE ANALYSES - FE-TI OXIDES

UNIT	(MGA)	(MGA)	(MGA)	(MGA)	(MGA)	(MGA)	(MGA)	(MGA)	(MGA)	(MGA)	(MGA)
SAMPLE	EM30	EM30	EM30	EM30	EM30	EM30	EM30	EM30	EM30	EM30	EM30
TiO2	46.03	44.95	46.58	47.63	47.78	48.73	47.43	8.82	9.28	9.28	11.56
Cr2O3	0.04	0.03	0.04	0.07	0.11	0.05	0	0.25	0.21	0.18	0.13
MnO	0.38	0.5	0.44	0.41	0.47	0.57	0.45	0.2	0.25	0.21	0.23
FeO	32.68	31.29	31.99	33.57	33.7	34.08	33.35	35.52	35.92	35.9	35.92
Fe2O3	16.09	16.58	13.59	14.21	13.7	12.01	13.12	50.45	48.4	49.09	44.59
SiO2	0	0.07	0.16	0	0.04	0.14	0.15	0.45	0	0	0.87
MgO	4.67	4.84	5.3	4.96	4.93	5.14	4.96	2.77	2.43	2.6	3.76
Al2O3	0.26	0.25	0.25	0.18	0.19	0.21	0.2	3.04	2.95	2.86	2.9
Total	100.11	98.41	98.16	100.97	100.78	100.74	99.52	100.8	99.23	99.94	98.96
	Cations - based on 12 oxygen										
Si	0	0.001	0.004	0	0	0.003	0.004	0.019	0	0	0.036
Al	0.007	0.007	0.007	0.005	0.005	0.006	0.006	0.156	0.154	0.148	0.145
Cr	0	0	0	0	0.002	0	0	0.008	0.007	0.005	0.004
Fe3+	0.311	0.326	0.264	0.271	0.26	0.226	0.252	1.653	1.622	1.636	1.429
Ti	0.891	0.886	0.904	0.906	0.908	0.918	0.909	0.289	0.31	0.309	0.371
Total	1.209	1.22	1.179	1.182	1.175	1.153	1.171	2.125	2.093	2.098	1.985
Mg	0.179	0.188	0.204	0.186	0.185	0.191	0.188	0.179	0.161	0.171	0.238
Fe2+	0.704	0.686	0.69	0.709	0.713	0.715	0.711	1.295	1.339	1.332	1.282
Mn	0.007	0.011	0.009	0.008	0.01	0.012	0.009	0.006	0.009	0.007	0.007
Total	0.89	0.885	0.903	0.903	0.908	0.918	0.908	1.48	1.509	1.51	1.527

APPENDIX III: MICROPROBE ANALYSES - FE-TI OXIDES

UNIT	(MGA)	(MGA)	(MGA)	(MGA)	(MGA)	(MGA)	(OD)	(OD)	(OD)	(OD)	(OD)
SAMPLE	EM30	EM30	EM30	EM30	EM30	EM30	EM64	EM64	EM64	EM64	EM64
TiO2	9.58	10.2	9.02	7.79	10.1	9.71	48.94	49.54	48.88	49.45	49.78
Cr2O3	0.19	0.09	0.12	0.22	0.11	0.13	0	0	0	0	0
MnO	0.29	0.3	0.46	0.2	0.34	0.35	0.36	0.52	0.45	0.39	0.37
FeO	36.91	37.22	36.16	35.53	36.92	36.23	39.56	40.33	39.77	40.63	43.12
Fe2O3	49.47	47.77	47.86	51.71	46.72	48.15	8	7.6	8.66	6.52	6.03
SiO2	0.11	0.13	0.14	0.19	0.17	0.07	0.04	0.79	0.94	0	0
MgO	2.46	2.47	1.76	2.02	2.25	2.55	2.29	2.07	2.09	1.93	0.71
Al2O3	3.04	3.02	2.9	2.98	3.03	2.9	0.09	0.13	0.12	0.18	0.09
Total	101.75	100.98	98.16	100.22	99.36	99.89	99.25	100.2	99.97	99.1	100.1
	Cations - based on 12 oxygen										
Si	0.004	0.005	0.005	0.008	0.006	0.002	0	0.02	0.023	0	0
Al	0.155	0.154	0.154	0.156	0.157	0.15	0.002	0.004	0.003	0.005	0.002
Cr	0.006	0.002	0.004	0.008	0.002	0.004	0	0	0	0	0
Fe3+	1.611	1.559	1.627	1.739	1.55	1.598	0.155	0.144	0.164	0.126	0.107
Ti	0.312	0.333	0.307	0.261	0.334	0.321	0.946	0.935	0.928	0.954	0.96
Total	2.088	2.053	2.097	2.172	2.049	2.075	1.103	1.103	1.118	1.085	1.069
Mg	0.159	0.159	0.118	0.134	0.148	0.167	0.087	0.077	0.077	0.074	0.027
Fe2+	1.338	1.353	1.368	1.33	1.364	1.338	0.85	0.847	0.84	0.872	0.933
Mn	0.01	0.01	0.017	0.007	0.012	0.013	0.007	0.01	0.009	0.008	0.007
Total	1.507	1.522	1.503	1.471	1.524	1.518	0.944	0.934	0.926	0.954	0.967

APPENDIX III: MICROPROBE ANALYSES - FE-TI OXIDES

UNIT	(OD)	(OD)	(OD)	(OD)	(OD)	(OD)	(OD)	(SG)	(SG)	(SG)	(SG)
SAMPLE	EM64	EM64	EM64	EM64	EM64	EM64	EM64	EM80	EM80	EM80	EM80
TiO2	48.97	49.13	48.81	48.36	19.32	20.85	17.82	50.31	51.52	50.67	50.93
Cr2O3	0	0	0.05	0	0.05	0	0	0.04	0.05	0.02	0.04
MnO	0.49	0.38	0.46	0.5	2	2.75	1.17	0.61	0.53	0.65	0.53
FeO	40.6	40.71	40.22	41.52	45.96	46.97	45.88	43.98	45.26	44.14	44.83
Fe2O3	8.3	7.95	9.39	8.06	29.47	26.68	31.4	5.65	3.7	5.31	4.46
SiO2	0.04	0.02	0	0.07	0.1	0.02	0	0	0.02	0.02	0
MgO	1.65	1.73	1.8	0.82	0.67	0.36	0.17	0.36	0.3	0.43	0.24
Al2O3	0.1	0.11	0.1	0.09	1.71	1.3	1.73	0.14	0.1	0.07	0
Total	100.11	100.01	100.77	99.35	99.13	98.91	98.17	101.05	101.41	101.27	100.99
	Cations - based on 12 oxygen										
Si	0.007	0	0	0.001	0.004	0	0	0	0	0	0
Al	0.003	0.003	0.003	0.002	0.083	0.064	0.087	0.004	0.003	0.001	0
Cr	0	0	0.007	0	0.001	0	0	0	0	0	0
Fe3+	0.16	0.153	0.18	0.157	0.925	0.836	1.014	0.108	0.07	0.101	0.085
Ti	0.943	0.947	0.937	0.944	0.607	0.654	0.575	0.96	0.974	0.965	0.97
Total	1.113	1.103	1.127	1.104	1.62	1.554	1.676	1.072	1.047	1.067	1.055
Mg	0.062	0.065	0.068	0.031	0.042	0.022	0.01	0.013	0.011	0.016	0.009
Fe2+	0.869	0.872	0.858	0.901	1.607	1.639	1.649	0.934	0.951	0.936	0.95
Mn	0.01	0.007	0.01	0.01	0.07	0.097	0.042	0.013	0.011	0.013	0.011
Total	0.941	0.944	0.936	0.942	1.719	1.758	1.701	0.96	0.973	0.965	0.97

APPENDIX III: MICROPROBE ANALYSES - FE-TI OXIDES

UNIT	(SG)	(SG)	(SG)	(SG)	(SG)	(SG)	(SG)	(SG)	(SG)	(SG)	(SG)
SAMPLE	EM80	EM80	EM80	EM80	EM80	EM80	EM80	EM80	EM80	EM80	EM80
TiO2	50.63	52.69	51.56	15.54	17.35	15.73	17.34	18.41	20.03	18.93	16.85
Cr2O3	0.02	0	0.07	0.09	0.04	0.02	0.02	0.04	0.06	0.03	0
MnO	0.61	0.66	0.61	0.39	0.48	0.53	0.42	0.59	0.72	0.57	0.63
FeO	44.5	46.27	45.26	45.27	46.83	45.13	47.02	47.6	49.41	47.76	46.28
Fe2O3	5.09	1.31	2.39	37.86	33.93	37.52	34.37	31.43	26.69	29.31	35.19
SiO2	0	0	0	0.08	0.04	0.03	0.07	0.04	0.09	0	0.05
MgO	0.23	0.25	0.27	0.19	0.04	0.19	0.08	0.04	0.06	0.04	0.15
Al2O3	0.02	0.1	0.12	1.5	1.34	1.23	1.38	1.49	1.27	1.71	1.53
Total	101.08	101.27	100.21	100.75	99.97	100.32	100.61	99.56	101.19	98.33	100.63
	Cations - based on 12 oxygen										
Si	0	0	0	0.002	0.001	0	0.002	0.001	0.002	0	0.001
Al	0	0.003	0.003	0.075	0.066	0.062	0.068	0.073	0.062	0.085	0.076
Cr	0	0	0	0.002	0	0	0	0	0.001	0	0
Fe3+	0.097	0.025	0.046	1.221	1.088	1.217	1.096	0.999	0.92	0.937	1.123
Ti	0.967	0.991	0.982	0.501	0.556	0.511	0.553	0.585	0.621	0.605	0.537
Total	1.064	1.019	1.031	1.801	1.711	1.79	1.719	1.658	1.606	1.627	1.737
Mg	0.008	0.009	0.01	0.011	0.002	0.011	0.005	0.002	0.002	0.002	0.009
Fe2+	0.945	0.967	0.958	1.625	1.672	1.63	1.668	1.685	1.705	1.698	1.645
Mn	0.013	0.013	0.013	0.014	0.016	0.019	0.015	0.021	0.024	0.02	0.022
Total	0.966	0.989	0.981	1.65	1.69	1.66	1.688	1.708	1.731	1.72	1.676

APPENDIX III: MICROPROBE ANALYSES - FE-TI OXIDES

UNIT	(SG)	(FD)	(FD)	(FD)	(FD)	(FD)	(FD)	(FD)	(FD)	(FD)	(FD)
SAMPLE	EM80	EM63	EM63	EM63	EM63	EM63	EM63	EM63	EM63	EM63	EM63
TiO2	18.91	49.79	49.84	50.39	50.41	49.35	49.95	47.09	49.28	50.51	8.29
Cr2O3	0.07	0.03	0	0.02	0	0.11	0	0.05	0	0.05	0.02
MnO	0.53	0.78	0.74	0.73	0.75	1.28	0.64	0.78	0.67	0.66	0.37
FeO	48.31	43.45	45.43	44	44.27	42.6	44.04	41.43	43.4	44.43	38.28
Fe2O3	31.35	4.57	4.9	4.89	5.09	4.53	4.95	4.08	4.67	4.03	51.27
SiO2	0.03	0	0	0	0	6.17	0	0	0.16	0.38	0
MgO	0.06	0.3	0.36	0.32	0.17	0.27	0.13	0.07	0.13	0.18	0.09
Al2O3	1.23	0.04	0.02	0.04	0	0.13	0.2	5.61	0.05	0.09	1.25
Total	100.38	98.93	99.29	100.37	100.69	98.16	99.9	99.06	98.21	99.9	99.55
	Cations - based on 12 oxygen										
Si	0	0	0	0	0	0.145	0	0	0.004	0.009	0
Al	0.06	0	0	0	0	0.003	0.005	0.166	0.001	0.002	0.069
Cr	0.001	0	0	0	0	0.001	0	0	0	0	0
Fe3+	0.989	0.089	0.095	0.094	0.097	0.08	0.095	0.077	0.091	0.077	1.8
Ti	0.597	0.969	0.967	0.967	0.967	0.874	0.965	0.889	0.965	0.966	0.291
Total	1.647	1.058	1.062	1.061	1.064	1.103	1.065	1.132	1.061	1.054	2.16
Mg	0.002	0.011	0.013	0.012	0.006	0.009	0.005	0.002	0.004	0.006	0.005
Fe2+	1.698	0.94	0.938	0.939	0.944	0.839	0.946	0.871	0.945	0.945	1.495
Mn	0.018	0.016	0.016	0.016	0.016	0.025	0.025	0.016	0.014	0.014	0.014
Total	1.718	0.957	0.967	0.967	0.966	0.873	0.976	0.889	0.963	0.965	1.514

APPENDIX III: MICROPROBE ANALYSES - FE-TI OXIDES

UNIT	(FD)	(FD)	(FD)	(FD)	(FD)	(FD)	(FD)	(FD)
SAMPLE	EM63	EM63	EM63	EM63	EM63	EM63	EM63	EM63
TiO2	7.49	9.67	9.88	11.47	8.87	9.62	10.84	10.31
Cr2O3	0	0	0	0	0	0	0	0.03
MnO	0.44	0.41	0.28	0.54	0.32	0.45	0.39	0.67
FeO	37.02	39.74	39.62	40.96	38.68	39.23	40.78	39.53
Fe2O3	51.82	49.3	47.3	44.71	49.85	48.82	46.51	46.73
SiO2	0.14	0.39	0.09	0.18	0.3	0.29	0.28	0.19
MgO	0.08	0.03	0	0	0.07	0.09	0.02	0.13
Al2O3	1.24	0.97	1.28	1.14	1.13	0.88	1.18	1.3
Total	98.09	100.12	98.36	98.82	98.92	99.1	99.72	98.67
	Cations - based on 12 oxygen							
Si	0.006	0.017	0.004	0.007	0.014	0.012	0.012	0.008
Al	0.068	0.052	0.069	0.06	0.061	0.047	0.062	0.07
Cr	0	0	0	0	0	0	0	0
Fe3+	1.851	1.687	1.646	1.527	1.738	1.694	1.579	1.612
Ti	0.267	0.33	0.344	0.391	0.309	0.333	0.367	0.356
Total	2.192	2.086	2.063	1.985	2.122	2.086	2.02	2.046
Mg	0.004	0.001	0	0	0.004	0.005	0.001	0.008
Fe2+	1.473	1.514	1.535	1.557	1.501	1.515	1.542	1.519
Mn	0.017	0.015	0.011	0.02	0.012	0.018	0.014	0.026
Total	1.494	1.53	1.546	1.577	1.517	1.538	1.557	1.553

APPENDIX IV

Results of Mass Balance Calculations

Mass balance calculations were carried out using the computer program GPP by Geist, Baker, and McBirney (1985). The following printouts show the chemical analyses used for the parent, daughter, and any minerals subtracted in the calculations. R squared represents the sum of the squares of the residuals and is a measure of the fit of the solution.

APPENDIX IV: Mass Balance Calculations

UNWEIGHTED INPUT DATA:

	PARENT	OL63	CPX63	PLAG63	MAG63	ILM63	AP	DAUGHTER
SIO2	60.00	31.00	48.88	58.49	0.29	0.00	0.00	70.64
TIO2	1.70	0.11	0.59	0.10	9.62	49.79	0.00	0.49
AL2O3	13.00	0.00	0.87	25.96	0.88	0.04	0.00	12.50
FE2O3	0.00	0.00	0.00	0.00	0.00	0.00	0.00	0.00
FEO	15.00	64.26	23.94	0.30	83.16	47.56	0.21	4.11
MNO	0.25	1.13	0.48	0.00	0.45	0.78	1.52	0.07
MGO	0.90	4.05	5.80	0.00	0.09	0.30	0.54	0.35
CAO	5.00	0.00	18.48	6.87	0.00	0.00	52.40	1.37
NA2O	3.75	0.00	0.15	7.25	0.00	0.00	0.00	3.37
K2O	3.10	0.00	0.00	0.64	0.00	0.00	0.00	4.71
H2O+	0.90	0.00	0.00	0.00	0.00	0.00	0.06	0.30
H2O-	0.00	0.00	0.00	0.00	0.00	0.00	0.00	0.00
P2O5	0.69	0.00	0.00	0.00	0.00	0.00	40.98	0.04

(PARENT-MINERALS=DAUGHTER)

PARENT: EM63 (Ferrodiorite)
DAUGHTER: EM21 (Eagle Mt. Granophyre)

	SOL'N	% CUMULATE
EM63	1.000	
OL63	-0.015	3.481
CPX63	-0.100	22.841
PLAG63	-0.202	46.286
MAG63	-0.098	22.419
ILM63	-0.006	1.400
AP	-0.016	3.572
EM21	0.564	

R SQUARED = 0.331

	PARENT ANALYSIS	DAUGHTER ANALYSIS	DAUGHTER CALC	WEIGHTED RESID
SIO2	58.92	74.13	73.73	0.40
TIO2	1.67	0.51	0.51	0.01
AL2O3	12.77	13.12	12.96	0.16
FEO	14.73	4.31	4.29	0.02
MNO	0.25	0.07	0.18	-0.11
MGO	0.88	0.37	0.39	-0.03
CAO	4.91	1.44	1.44	-0.01
NA2O	3.68	3.54	3.89	-0.35
K2O	3.04	4.94	5.16	-0.11
P2O5	0.68	0.04	0.02	0.02

APPENDIX IV: Mass Balance Calculations

UNWEIGHTED INPUT DATA:

	PARENT	KSP68	QZ	PLAG68	DAUGHTER
SIO2	70.64	63.77	%100.00	66.94	73.64
TIO2	0.49	0.00	0.00	0.09	0.28
AL2O3	12.50	18.25	0.00	20.01	11.75
FE2O3	0.00	0.00	0.00	0.00	0.00
FEO	4.11	0.30	0.00	0.93	2.94
MNO	0.07	0.06	0.00	0.00	0.03
MGO	0.35	0.07	0.00	0.05	0.25
CAO	1.37	0.00	0.00	0.29	0.16
NA2O	3.37	0.07	0.00	11.25	2.08
K2O	4.71	16.59	0.00	0.25	6.34
H2O+	0.30	0.00	0.00	0.00	0.60
H2O-	0.00	0.00	0.00	0.00	0.00
P2O5	0.04	0.00	0.00	0.00	0.00

(PARENT-MINERALS=DAUGHTER)

PARENT: EM21 (Eagle Mt. Granophyre)
DAUGHTER: EM68 (Miarolitic Granophyre)

	SOL'N	% CUMULATE
EM21	1.000	
KSP68	0.322	57.005
QZ	0.247	43.633
PLAG68	-0.004	-0.638
EM68	1.566	

R SQUARED = 0.863

	PARENT ANALYSIS	DAUGHTER ANALYSIS	DAUGHTER CALC	WEIGHTED RESID
SIO2	72.37	75.55	75.07	0.48
TIO2	0.50	0.29	0.32	-0.03
AL2O3	12.81	12.05	11.93	0.12
FEO	4.21	3.02	2.76	0.26
MNO	0.07	0.03	0.06	-0.03
MGO	0.36	0.26	0.24	0.01
CAO	1.40	0.16	0.90	-0.73
NA2O	3.45	2.13	2.20	-0.07
K2O	4.83	6.50	6.52	-0.01

APPENDIX IV: Mass Balance Calculations

UNWEIGHTED INPUT DATA:

	PARENT	KSP68	QZ	PLAG68	DAUGHTER
SIO2	60.00	63.77	%100.00	66.94	73.64
TIO2	1.70	0.00	0.00	0.09	0.28
AL2O3	13.00	18.25	0.00	20.01	11.75
FE2O3	0.00	0.00	0.00	0.00	0.00
FEO	16.00	0.30	0.00	0.93	2.94
MNO	0.25	0.06	0.00	0.00	0.03
MGO	0.90	0.07	0.00	0.05	0.25
CAO	5.00	0.00	0.00	0.29	0.16
NA2O	3.75	0.07	0.00	11.25	2.08
K2O	3.10	16.59	0.00	0.25	6.34
H2O+	0.90	0.00	0.00	0.00	0.60
H2O-	0.00	0.00	0.00	0.00	0.00
P2O5	0.69	0.00	0.00	0.00	0.00

(PARENT-MINERALS=DAUGHTER)

PARENT: EM63 (Ferrodiorite)
DAUGHTER: EM68 (Miarolitic Granophyre)

	SOL'N	% CUMULATE
EM63	1.000	
KSP68	2.285	43.513
QZ	2.001	38.113
PLAG68	0.965	18.375
EM68	6.250	

R SQUARED = 0.901

	PARENT ANALYSIS	DAUGHTER ANALYSIS	DAUGHTER CALC	WEIGHTED RESID
SIO2	57.86	75.55	75.02	0.53
TIO2	1.64	0.29	0.29	0.00
AL2O3	12.54	12.05	11.84	0.22
FEO	15.43	3.02	2.81	0.20
MNO	0.24	0.03	0.06	-0.03
MGO	0.87	0.26	0.18	0.08
CAO	4.82	0.16	0.84	-0.68
NA2O	3.62	2.13	2.35	-0.22
K2O	2.99	6.50	6.61	-0.11

APPENDIX IV: Mass Balance Calculations

UNWEIGHTED INPUT DATA:

	PARENT	KSP68	QZ	PLAG68	DAUGHTER
SIO2	76.36	63.77	%100.00	66.94	73.64
TIO2	0.25	0.00	0.00	0.09	0.28
AL2O3	11.02	18.25	0.00	20.01	11.75
FE2O3	0.00	0.00	0.00	0.00	0.00
FEO	2.69	0.30	0.00	0.93	2.94
MNO	0.04	0.06	0.00	0.00	0.03
MGO	0.34	0.07	0.00	0.05	0.25
CAO	0.47	0.00	0.00	0.29	0.16
NA2O	2.20	0.07	0.00	11.25	2.08
K2O	5.57	16.59	0.00	0.25	6.34
H2O+	0.40	0.00	0.00	0.00	0.60
H2O-	0.00	0.00	0.00	0.00	0.00
P2O5	0.01	0.00	0.00	0.00	0.00

(PARENT-MINERALS=DAUGHTER)

PARENT: EM54 (Rhyolite)
DAUGHTER: EM68 (Miarolitic Granophyre)

	SOL'N	% CUMULATE
EM54	1.000	
KSP68	0.021	%-26.880
QZ	-0.077	97.303
PLAG68	-0.023	29.577
EM68	0.921	

R SQUARED = 0.233

	PARENT ANALYSIS	DAUGHTER ANALYSIS	DAUGHTER CALC	WEIGHTED RESID
SIO2	77.18	75.55	75.25	0.30
TIO2	0.25	0.29	0.27	0.02
AL2O3	11.14	12.05	12.00	0.05
FEO	2.72	3.02	2.93	0.08
MNO	0.04	0.03	0.05	-0.01
MGO	0.34	0.26	0.37	-0.12
CAO	0.48	0.16	0.51	-0.34
NA2O	2.22	2.13	2.13	0.00
K2O	5.63	6.50	6.48	0.02

APPENDIX IV: Mass Balance Calculations

UNWEIGHTED INPUT DATA:

	PARENT	KSP68	QZ	PLAG68	DAUGHTER
SIO2	45.76	63.77	%100.00	66.94	73.64
TIO2	1.68	0.00	0.00	0.09	0.28
AL2O3	15.49	18.25	0.00	20.01	11.75
FE2O3	0.00	0.00	0.00	0.00	0.00
FEO	13.81	0.30	0.00	0.93	2.94
MNO	0.18	0.06	0.00	0.00	0.03
MGO	8.48	0.07	0.00	0.05	0.25
CAO	9.34	0.00	0.00	0.29	0.16
NA2O	2.25	0.07	0.00	11.25	2.08
K2O	0.51	16.59	0.00	0.25	6.34
H2O+	0.60	0.00	0.00	0.00	0.60
H2O-	0.00	0.00	0.00	0.00	0.00
P2O5	0.10	0.00	0.00	0.00	0.00

(PARENT-MINERALS=DAUGHTER)

PARENT: EM30 (Metagabbro)
DAUGHTER: EM68 (Miarolitic Granophyre)

	SOL'N	% CUMULATE
EM30	1.000	
KSP68	3.542	42.709
QZ	3.229	38.941
PLAG68	1.522	18.350
EM68	9.293	

R SQUARED = 2.999

	PARENT ANALYSIS	DAUGHTER ANALYSIS	DAUGHTER CALC	WEIGHTED RESID
SIO2	46.93	75.55	75.16	0.39
TIO2	1.72	0.29	0.21	0.08
AL2O3	15.89	12.05	12.03	0.02
FEO	14.16	3.02	1.86	1.16
MNO	0.18	0.03	0.04	-0.01
MGO	8.70	0.26	1.01	-0.75
CAO	9.58	0.16	1.12	-0.96
NA2O	2.31	2.13	2.12	0.01
K2O	0.52	6.50	6.45	0.06

APPENDIX V

Distribution Coefficients Used for Trace Element Modeling

Superscripts refer to the following references:

(1) Arth, 1976
(2) Arth & Barker, 1976
(3) Cox, Bell, & Pankhurst, 1984
(4) Geist, Baker, & McBirney, 1985
(5) Nagasawa & Schnetzler, 1971
(6) Paster et al., 1974
(7) Schnetzler & Philpotts, 1970

Eagle Mountain Granophyre

Element	Plagioclase	Pyroxene	Mag
Rb	0.04 (5)	0.02 (4)	----
Sr	4.4 (5)	0.10 (4)	0.06 (4)
Zr	0.27 (4)	0.16 (4)	0.22 (4)
Ba	0.31 (5)	0.03 (4)	0.09 (4)
La	0.19 (4)	0.16 (4)	0.28 (4)
Sm	0.04 (7)	0.68 (7)	0.56 (4)
Eu	0.39 (7)	0.64 (7)	0.36 (4)
Yb	0.01 (7)	0.90 (7)	----

APPENDIX V: Distribution Coefficients

Miarolitic Granophyre

Element	Albite	Orthoclase	Zircon
Rb	0.04 [1]	0.34 [1]	----
Sr	4.4 [1]	3.87 [1]	----
Ba	0.31 [1]	6.12 [1]	----
Nd	0.21 [1]	0.03 [1]	2.20 [1]
Sm	0.13 [1]	0.02 [1]	3.14 [1]
Eu	2.15 [1]	1.13 [1]	3.14 [1]
Yb	0.05 [1]	0.01 [1]	270 [1]

Rhyolite

Element	K-feldspar	Albite	Mag
Rb	0.4 [3]	0.04 [3]	----
Sr	4 [3]	4.4 [3]	----
Zr	----	0.12 [4]	----
Ba	6 [3]	0.3 [3]	----
La	----	0.34 [4]	8.3 [4]
Nd	0.03 [1]	0.21 [1]	----
Sm	0.02 [1]	0.13 [1]	6.71 [4]
Eu	1.13 [1]	2.15 [1]	2.96 [4]
Yb	0.01 [1]	0.05 [1]	----

APPENDIX V: Distribution Coefficients

Metagabbro

Element	Plag	Cpx	Olivine	Mag	Ilm
Rb	0.07 [1]	0.03 [1]	0.01 [1]	----	----
Sr	1.83 [1]	0.12 [1]	0.01 [1]	----	----
Zr	0.08 [4]	0.28 [4]	0.03 [4]	0.24 [4]	0.79 [4]
Ba	0.23 [1]	0.03 [1]	0.01 [1]	----	----
La	0.06 [1]	0.56 [1]	0.02 [1]	1.57 [4]	0.1 [4]
Sm	0.07 [1]	0.50 [1]	0.01 [1]	1.27 [4]	0.15 [4]
Eu	0.34 [1]	0.51 [1]	0.01 [1]	0.88 [4]	0.1 [4]
Yb	0.07 [1]	0.62 [1]	0.01 [1]	----	----

Ferrodiorite

Element	Plag	Ol	Cpx	Ilm	Mag	Ap
Rb	0.05 [1]	0.02 [4]	0.02 [4]	----	----	----
Sr	2.84 [1]	0.05 [4]	0.10 [4]	0.28 [4]	0.06 [4]	----
Zr	0.27 [4]	0.05 [4]	0.16 [4]	0.81 [4]	0.22 [4]	----
Ba	0.36 [1]	0.03 [4]	0.03 [4]	----	----	0.03 [6]
La	0.19 [4]	0.01 [4]	0.06 [6]	0.10 [6]	0.02 [6]	8.6 [6]
Zn	0.13 [6]	1.8 [6]	0.49 [6]	0.38 [6]	2.6 [6]	0.1 [6]

APPENDIX V: Distribution Coefficients

Giants Range Granodiorite

Element	K-spar	Plag	Biotite	Hnbld	Cpx
Rb	0.34 [1]	0.04 [1]	2.24 [1]	0.01 [1]	0.03 [1]
Sr	3.87 [1]	4.4 [1]	----	0.02 [1]	0.52 [1]
Zr	----	0.12 [4]	4.12 [4]	----	----
Ba	6.12 [1]	0.31 [1]	9.7 [1]	0.04 [1]	0.13 [1]
Sm	0.02 [1]	0.13 [1]	0.26 [1]	7.77 [1]	1.67 [1]
Eu	1.13 [1]	2.15 [1]	0.24 [1]	5.14 [1]	1.56 [1]
Yb	0.01 [1]	0.05 [1]	0.44 [1]	8.38 [1]	1.58 [1]